UNIVERSITÀ DEGLI STUDI DI PADOVA

TÉCNICO LISBOA

UNIVERSITÀ DEGLI STUDI DI NAPOLI FEDERICO II

Università degli Studi di Padova

Centro Ricerche Fusione (**CRF**)

Università degli studi di Napoli Federico II

Universidade de Lisboa

Instituto Superior Técnico (**IST**)

JOINT RESEARCH DOCTORATE IN FUSION SCIENCE AND ENGINEERING

Cycle XXX

MODELLING AND CONTROL OF RFX-MOD TOKAMAK EQUILIBRIA

Coordinator: Prof. Paolo Bettini

Supervisor: Prof. Fabio Villone

Co-Supervisor: Dr.Ing. Giuseppe Marchiori

Ph.D. student: Domenico Abate

Padova, January 2018

UNIVERSITÀ DEGLI STUDI DI PADOVA

LMU LUDWIG-MAXIMILIANS-UNIVERSITÄT MÜNCHEN

TÉCNICO LISBOA

JOINT Doctorate and NETWORK in Fusion Science and Engineering

Network Partners:

- Instituto Superior Técnico (IST) Lisboa, Portugal
- Università degli studi di Padova, Italy
- Ludwig Maximilians University Munich, Germany

In collaboration with:

Consorzio RFX
IPP Garching, Germany

Abstract

The subject that concerns this thesis is the modelling and control of plasma equilibria in the RFX-mod device operating as shaped tokamak. The aim was to develop an overall model of the plasma-conductors-controller system of RFX-mod shaped tokamak configuration for electromagnetic control purposes, with particular focus on vertical stability. Thus, the RFX-mod device is described by models of increasing complexity and involving both theoretical and experimental data. The CREATE-L code is used to develop 2D linearized plasma response models, with simplifying assumptions on the conducting structures (axisymmetric approximations). Such models, thanks to their simplicity, have been used for feedback controller design. The CarMa0 code is used to develop linearized plasma response models, but considering a detailed 3D description of the conducting structures. These models provide useful hints on the accuracy of the simplified models and on the importance of 3D structures in the plasma dynamics. The CarMa0NL code is used to model the time evolution of plasma equilibria, by taking into account also nonlinear effects which can come into play during specific phases (e.g. disruptions, limiter-to-divertor transitions, L-H transition etc.). The activity can be divided into two main parts: the first one involves the modelling of numerically generated low-β plasmas, which are used as a reference for the design and implementation of the plasma shape and position control system; the second part is related to the results of the experimental campaigns on shaped plasmas from low-β to H-mode regime, with particular efforts on the development of a novel plasma response model for the new equilibrium regimes achieved. Several challenges and peculiarities characterize the project in both the modelling and control frameworks. Strong plasma shape and different plasma regimes (i.e. low-β to H-mode plasmas), deeply affect the modelling activity and require the development of several numerical tools and methods of analysis. From the control system point of view, non-totally observable dynamic and model order reduction requirements allowed a full application of the model based approach in order to successfully design the plasma shape and vertical stability control system.

The first part is based on theoretical data generated by the MAXFEA equilibrium

code and used to derive the linearized model through the CREATE-L code. Two reference models have been produced for the magnetic configurations interested in shaped operations: the lower single null (LSN) and the upper single null (USN). The CREATE-L models are the most simple in terms of modelling complexity, because the conducting structures are described within the axisymmetric approximation. On the other hand, the simple but reliable properties of the CREATE-L model led to the successful design of the RFX-mod plasma shape and control system, which has been successfully tested and used to increase plasma performances involved in the second part of the thesis. Then, an investigation on the possible 3D effects of the conducting structures on these numerically generated plasma configurations has been carried out by producing plasma linearized models with an increased level of complexity. A detailed 3D volumetric description of the conducting structures of RFX-mod has been carried out and included in the plasma linearized models through the CarMa0 code. A comparison between the accuracy of this model and the previous 2D one has been performed. The different assumptions and approximations of the various models allow a clear identification of the key phenomena ruling the evolution of the n=0 vertical instability in RFX-mod tokamak discharges, and hence, provide fundamental information in the planning and the execution of related experiments and in refining the control system design. Finally, the nonlinear evolutionary equilibrium model including 3D volumetric structures CarMa0NL has been used to model nonlinear effects by simulating a "fictitious" linear current quench.

The second part involves a modelling activity strictly related to the results of the experimental campaigns. In particular, new linearized models for the experimental plasmas in USN configuration have been carried out for all the plasma regimes involved in the experimental campaign, i.e. from low-β to H-mode. An iterative procedure for the production of accurate linearized plasma response models has been realized in order to handle the experimental data. The new plasma linearized models allowed further investigations on vertical stability, including 3D wall effects, in the three different plasma regimes (i.e. low-β, intermediate-β, H-mode). Furthermore, the axisymmetric plasma linearized models (CREATE-L) have been analyzed in the framework of the control theory revealing peculiar features in terms of associated SISO transfer function for vertical stability control and in terms of full MIMO model for shaping control. The MIMO model has been used to investigate the plasma wall-gaps oscillations experimentally observed in some intermediate-β plasma shots. A non-linear time evolution of the plasma discharge for a low-β plasma has been carried out by using the evolutionary equilibrium code CarMa0NL. Finally, it was investigated the vertical instability for the experimental plasmas in

terms of a possible relation between plasma parameters and the occurrence of it; for these purposes, the solution of the inverse plasma equilibrium problem for the production of numerically generated plasma equilibria with variations on the plasma parameters observed experimentally was performed. This involves a wide class of numerical methods that will be described in details. Then, statistical hypothesis test has been adopted to compare the mean values of the parameters of both experimental and numerically generated plasmas showing different behaviours in terms of vertical stability.

Sommario

La presente tesi tratta la modellazione e il controllo di plasmi in equilibrio, a sezione non circolare e relativi all'esperimento RFX-mod operante come tokamak. L'obiettivo è di sviluppare un modello complessivo di RFX-mod (includendo plasma-conduttori-controllore) con finalità di controllo elettromagnetico del plasma. L'esperimento RFX-mod è stato descritto con modelli caratterizzati da un crescente livello di complessità, coinvolgendo sia dati teorici che sperimentali. Il codice CREATE-L è stato usato per lo sviluppo di modelli linearizzati di risposta di plasma, con ipotesi semplificative sulla rappresentazione delle strutture conduttrici (approssimazione assialsimmetrica). Questi modelli, grazie alla loro semplicità, sono stati utilizzati per la progettazione del sistema di controllo. Il codice CarMa0 è stato usato per sviluppare modelli analoghi ma con una rappresentazione tridimensionale delle strutture conduttrici; questi permettono di verificare l'accuratezza dei modelli semplificati e indagare l'importanza delle strutture tridimensionali sulla dinamica del sistema. Il codice CarMa0NL ha permesso la trattazione di fenomeni evolutivi nel tempo e non-lineari (e.g. disruzioni, transizioni limiter-divertor, transizioni L-H etc.). L'attività può essere suddivisa in due parti: la prima riguarda la modellizzazione di plasmi a basso β teorici, non ottenuti sperimentalmente, usati come riferimento per la progettazione e l'implementazione del sistema di controllo della forma e della posizione verticale del plasma; la seconda parte, è legata ai risultati delle campagne sperimentali sui plasmi a sezione non circolari in diversi regimi, dal basso β al modo H, con particolare attenzione allo sviluppo di un nuovo modello linearizzato di risposta di plasma per i nuovi regimi di equilibrio raggiunti. L'attività di ricerca è caratterizzata da molteplici problematiche e peculiarità sia in termini di modellazione che di controllo. La pronunciata non circolarità della forma di plasma e i diversi regimi coinvolti hanno influenzato fortemente l'attività di modellazione che ha richiesto, infatti, lo sviluppo di molteplici strumenti computazionali e di analisi dati. Per quanto concerne il controllo, la non completa osservabilità della dinamica del sistema e la necessità di ridurre l'ordine del modello sono solo alcuni degli aspetti che hanno determinato la progettazione del sistema di controllo di forma e di posizione

verticale.

La prima parte è basata su dati teorici generati dal codice di equilibrio MAXFEA e poi utilizzati per derivare il modello linearizzato attraverso il codice CREATE-L. In questo contesto, sono stati prodotti due modelli di riferimento per le configurazioni magnetiche relative a plasmi non circolari: il singolo nullo inferiore (LSN) e il singolo nullo superiore (USN). I modelli CREATE-L sono i più semplici in termini di complessità di modellazione, in quanto le strutture conduttive della macchina sono descritte nell'approssimazione assialsimmetrica. D'altro canto, le proprietà semplici ma affidabili del modello CREATE-L hanno portato alla progettazione del sistema di controllo di forma e posizione verticale del plasma di RFX-mod, che è stato in seguito testato e utilizzato con successo per aumentare le prestazioni del plasma. Successivamente, è stata condotta un'analisi sui possibili effetti 3D delle strutture conduttrici sulle due configurazioni di plasma di riferimento, producendo dunque modelli linearizzati caratterizzati da un sempre maggiore livello di complessità. Una dettagliata descrizione volumetrica (3D) delle strutture conduttrici di RFX-mod è stata eseguita e inclusa nei modelli linearizzati di plasma attraverso il codice CarMa0. Successivamente, è stato eseguito un confronto tra l'accuratezza di questo modello e quello precedente 2D. Le diverse ipotesi e approssimazioni dei vari modelli consentono una chiara identificazione dei fenomeni chiave che governano l'evoluzione dell'instabilità verticale $n = 0$ in scariche RFX-mod tokamak e quindi forniscono informazioni fondamentali nella pianificazione ed esecuzione di esperimenti correlati oltre che nella raffinazione del progetto del sistema di controllo. Infine, il modello di equilibrio evolutivo non lineare CarMa0NL, che comprende le strutture volumetriche 3D, è stato utilizzato per modellare gli effetti non lineari simulando una variazione di corrente lineare "fittizia". La seconda parte è costituita da un'attività di modellazione strettamente correlata ai risultati delle campagne sperimentali. In particolare, sono stati eseguiti nuovi modelli linearizzati per i plasmi sperimentali nella configurazione USN per tutti i regimi di plasma coinvolti, cioè dal basso β fino al modo H. È stata ideata e sviluppata una procedura iterativa per la produzione di modelli linearizzati di risposta di plasma estremamente accurati, al fine di riprodurre al meglio i dati sperimentali. I nuovi modelli hanno consentito ulteriori studi sulla stabilità verticale, inclusi gli effetti della parete 3D, nei tre diversi regimi studiati (basso β, β intermedio, modo H). I modelli linearizzati assialsimmetrici (CREATE-L) sono stati analizzati dal punto di vista della teoria dei controlli, rilevando caratteristiche peculiari in termini di funzione di trasferimento SISO associata al controllo della stabilità verticale e in termini di modello completo MIMO relativo al controllo di forma. Il modello MIMO è stato utilizzato per in-

dagare le oscillazioni nella forma del plasma osservate sperimentalmente in alcune scariche a β intermedio. L'evoluzione temporale non lineare della scarica di plasma, per plasmi sperimentali a regimi a basso β, è stata effettuata usando il codice di equilibrio evolutivo CarMa0NL. Infine, è stata studiata l'instabilità verticale per i plasmi sperimentali in termini di un possibile rapporto tra i parametri del plasma e il suo verificarsi; a tal fine è stata eseguita la soluzione del problema inverso per la produzione di equilibri di plasma teorici di riferimento, prodotti come variazioni sui parametri dei plasmi osservati sperimentalmente, il che comporta una vasta gamma di metodi numerici descritti in dettaglio. Successivamente, è stato adottato un test di ipotesi statistica per confrontare i valori medi dei parametri di plasma, sia sperimentali che teorici, associati a due diversi comportamenti in termini di stabilità verticale.

Sumário

Translated from English to Portuguese by Google

O assunto que diz respeito a esta tese é a modelagem e controle dos equilíbrios de plasma no dispositivo RFX-mod que opera como tokamak moldado. O objetivo era desenvolver um modelo geral do sistema de controle de plasma-controlador de tokamak em forma de modificação RFX para fins de controle eletromagnético. A atividade pode ser subdividida em duas partes principais: a primeira envolve a modelagem da referência teórica - β plasmas para o projeto e implementação do sistema de controle de posição e forma de plasma; o segundo, está relacionado aos resultados das campanhas experimentais em plasmas moldados do regime de baixa taxa de US β para H, com esforços particulares no desenvolvimento de um novo modelo de resposta ao plasma para os novos regimes de equilíbrio alcançados. A primeira parte é baseada em dados teóricos gerados pelo código de equilíbrio MAXFEA e, em seguida, usado para derivar o modelo linearizado através do código CREATE-L. Dois modelos de referência foram produzidos para as configurações magnéticas interessadas em operações moldadas: o menor nulo único (LSN) e o nulo único superior (USN). Os modelos CREATE-L são os mais simples em termos de complexidade de modelagem, porque as estruturas condutoras são descritas dentro da aproximação axisymmetric. Por outro lado, as propriedades simples mas confiáveis do modelo CREATE-L levaram ao design bem sucedido do sistema de controle e forma de plasma RFX-mod, que foi testado com sucesso e usado para aumentar os desempenhos plasmáticos envolvidos na segunda parte do tese. Então, uma investigação sobre os possíveis efeitos em 3D das estruturas condutoras nessas configurações teóricas de plasma de referência foi realizada através da produção de modelos linearizados com um aumento de nível de complexidade. Uma detalhada descrição volumétrica em 3D das estruturas condutoras do RFX-mod foi realizada e incluída nos modelos plasmados por plasma através do código CarMa0. Foi realizada uma comparação entre a precisão desse modelo e o 2D anterior. As diferentes hipóteses e aproximações dos vários modelos permitem uma identificação clara dos fenômenos-chave que governam a evolução da instabilidade vertical $n = 0$

nas descargas de tokamak de RFX-mod e, portanto, fornecem informações fundamentais no planejamento e execução de experimentos relacionados e na refinação do design do sistema de controle. Finalmente, o modelo de equilíbrio evolutivo não linear, incluindo as estruturas volumétricas 3D CarMa0NL, tem sido usado para modelar efeitos não-lineares, simulando uma saturação de corrente linear "fictícia". A segunda parte envolve uma atividade de modelagem estritamente relacionada aos resultados das campanhas experimentais. Em particular, novos modelos linearizados para os plasmas experimentais na configuração USN foram realizados para todos os regimes de plasma envolvidos na campanha experimental, isto é, do modo baixo$-\beta$ ao modo H. Um procedimento iterativo para a produção de modelos de resposta de plasma linearizados precisos foi realizado para lidar com os dados experimentais. Os novos modelos linearizados em plasma permitiram investigações adicionais sobre estabilidade vertical, incluindo efeitos de parede 3D, nos três regimes de plasma diferentes (i.e. β baixo, intermediário$-\beta$, modo H). Além disso, os modelos linearizados de plasma assimétrico (CREATE-L) foram analisados no âmbito da teoria do controle, revelando características peculiares em termos de função de transferência SISO associada ao controle de estabilidade vertical e em termos de modelo MIMO completo para controle de moldagem. O modelo MIMO tem sido usado para investigar as oscilações de paredes plasmáticas observadas experimentalmente em alguns tiros plasmáticos intermediários$-\beta$. Uma evolução do tempo não linear da descarga plasmática para um plasma β baixo foi realizada utilizando o código de equilíbrio evolutivo CarMa0NL. Finalmente, investigou-se a instabilidade vertical dos plasmas experimentais em termos de uma possível relação entre os parâmetros plasmáticos ea sua ocorrência; Para este efeito, foi realizada a solução do problema inverso do equilíbrio plasmático para a produção de equilíbrios teóricos de referência plasmática com variações nos parâmetros plasmáticos observados experimentalmente. Isso envolve uma ampla classe de métodos numéricos que serão descritos em detalhes. Em seguida, teste de hipóteses estatísticas foi adotado para comparar os valores médios dos parâmetros de plasmas experimentais e teóricos mostrando comportamento diferente em termos de estabilidade vertical.

Contents

List of Figures

List of Tables

Chapter 1

Overview

The achievement of H-mode regime was the final aim of executing shaped tokamak plasma discharges in RFX-mod. Thus, non-circular equilibrium configurations have been developed, both in double null (DN) and single null (SN) geometries, leading to the design and implementation of plasma shape feedback control system [1]. Such elongated plasma configurations exhibit the well-known vertical instability (n= 0, resistive wall mode RWM) which must be suitably controlled. The shaped operations in different regimes, from low-β plasma to H-mode regime, give a unique opportunity of a test-bed of the modelling activity. The present thesis aims to develop an overall model of the plasma-conductors-controller system of RFX-mod shaped tokamak for electromagnetic control purposes. The activity can be subdivided into two main parts: the first involves the modelling of theoretical reference low-β plasmas for the design of the previously mentioned plasma shape and position control system; the second, is related to the results of the experimental campaigns on shaped plasmas from low-β to H-mode regime, with particular efforts on the development of a novel plasma response model for the new equilibrium regimes achieved.

Before going into the main topic, an introduction to Controlled Nuclear Fusion (CNF) science is given in Chap. 2, including general principles and an historical overview of its progress. The electromagnetic modelling and control of fusion plasmas are described in Chap. 3, including the mathematical formulation of the problem and some literature review. Then, the RFX-mod device is described in Chap. 4, with particular effort on its tokamak operations. The last three chapters deal with the research activity related to the development of this thesis; the two previously mentioned main parts of the thesis are described in Chap. 5. The methodology is proposed in Chap. 6. Finally, results and conclusions are presented in Chap. 7 and Chap. 8.

Chapter 2

Controlled Nuclear Fusion

In this chapter a brief introduction on the controlled nuclear fusion (CNF) research field, as a scientific discipline, is given in terms of historical dynamics and scientific principles. The historical analysis aims to highlight the causes of CNF evolution; the effort is to stress the differences between the research lines developed inside the magnetically confinement community, not just formally because of historical reasons but also scientifically in terms of different views of the same discipline. The developments caused by the dominant design concept have been analyzed in terms of experimental progress in one of the greatest effort in modern science. Then, the principles of nuclear fusion reactions are described including a brief description of the magnetic confinement configurations. Finally, the fundamental problem of plasma equilibrium in a magnetic field is proposed in relation to the electromagnetic control of fusion plasmas.

2.1 Prologue

Fusion. From Latin word *fusio*, "an outpouring, effusion". From c. 1550 Middle French language, *fusion*, "act of melting by heat". Meaning "union or blending of different things; state of being united or blended" is by 1776; used especially in 19c, of politics, in early 20c. of psychology, atoms, and jazz (in nuclear physics sense, first recorded 1947; in musical sense, by 1972). And one more. This one is a non-definition of Fusion as a noun, more generally as a depicted feeling which eyes may recognize as a lighthouse in the foggy sea: "A cozy waste land to mold human knowledge".

2.2 General remarks

The research on controlled nuclear fusion (CNF) saw its dawn in the face of the most obscure wishes: the development of the most powerful weapon ever built by human being. This gruesome competition involved countries with accumulated knowledge and experience of managing and implementing the high-cost projects required for this type of research, as building hydrogen bomb weaponry required. The research work was superbly organized since it would demonstrate the determination of not being left behind by the opposition in the anguishing run to be armed with the most powerful weapons. At its early stages, the controlled nuclear fusion was strictly classified since it was a support of military programs, but even when it switched to peaceful uses of atomic energy, it preserved an inertial secrecy. This led to an infrequent phenomena in scientific development: the misalignment between signifier and meaning; let me explain what it means. The phrase 'high-altitude goo in a jet' naturally refers to something related to the field of aerospace or aeronautical engineering. Well it would not surprise that, at early 1950s, this could mean 'high-temperature plasma in a magnetic field'. In fact, the top secret protocols required to use such misleading terms as 'goo', 'altitude' and 'jet' to code respectively the words 'plasma', 'temperature' and 'magnetic field' [2]. Even without going deeply in the historical analysis of nuclear fusion development, it can be easily deduced by the reader that this secrecy would lead just to problems such as a non-uniform level of knowledge between different nations. These readers would be wrong. In fact, from the First International Conference on Peaceful Uses of Atomic Energy held in Geneva in 1955, characterized by a religious silence on the CNF, to the Second Geneva Conference on the nuclear fusion problem, just two years later the declassifying initiative of USSR scientists in April 1956, it was possible to see 105 papers presented, with detailed work performed in all the countries of the world. Thus it shows that, despite the regime of classification, and apparently without any leakage of information, research had been conducted in practically identical directions, which means by looking the same horizon but walking different paths. Considering the magnetically confined nuclear fusion, it will be shown that these paths would determine the discovery of the three main approaches to magnetically confinement of a plasma in a closed toroidal system. In addition, the open magnetic system concepts were also achieved independently. The original purpose of designing nuclear fusion reactors with deuterium plasma was primarily the generation of bomb-grade materials (charges) for thermonuclear weapons. Successes in designing thermonuclear bombs led to confidence in a similarly fast solution to the problem of designing a nuclear fusion reactor. This change in the final purposes of a scientific research

field as CNF, shows how much good and bad are firmly bound to the same step, so firmly that anyone who wants as much as possible of one of them must necessarily have as much as possible of the other. This stoic vision leads to the vision of Science as a promoter of progress in the life of human being, corresponding to the slightest displeasure for humanity in the research of the least possible displeasure. This is the reason why it cannot surprise that from the production of the most powerful weapon, scientists in all the world took pride in advancing to the magnificent goal of CNF: the generation of energy 'out of water' (the potential resources of energy inherent in deuterons in 1 litre of water is three hundred times greater than in 1 litre of petrol) [2]. I should now like to ask: where are we going?

2.3 Before 1958 conference: the beginnings

The early history of fusion represents the history of Science as an isolated process independent from the methodologies adopted by each scientific community, which in our case are represented by the nations involved in CNF research; as we have seen, until the 2nd Geneva Conference on Peaceful Uses of Atomic Energy (1958), all CNF research was strictly classified. Nevertheless, this scientific area developed independently in each scientific community, without needed influences or shared basic knowledge. It is not easy to choose a single history of fusion path to follow but if the reader wants to find the dawn of CNF research, then he or she has to move in the early years of 1930. As it is suggested in the G. A. Gamow's book, one of the first attempts at CNF research is in connection with reminiscences of a meeting with one of the leaders of the country, N. I. Bukharin:

"*Nikolai Bukharin is a veteran revolutionary and a close friend of the late Lenin; furthermore, he is the only one among the leading communists (with the exception of Lenin himself, of course) who was born into an old Russian family. I encountered him when his rank in the hierarchy was lowered and he occupied a relatively modest position as a Committee chairman, the Supreme Council of National Economy (VSNKh). His responsibilities covered monitoring the progress of Soviet science and technology; there can be no doubt that this position was of no political importance (Bukharin fell victim to Stalin's purges and was executed five years after I left Russia). He was once present at my lecture at the Academy of Sciences (which at that time was based in Leningrad) on thermonuclear reactions and their role as the energy source of the Sun and other stars. When the lecture ended, he suggested that I take the post of the head of project on developing controlled nuclear fusion reactions (this proposal was made in 1932!). I could have at my disposal, for several minutes*

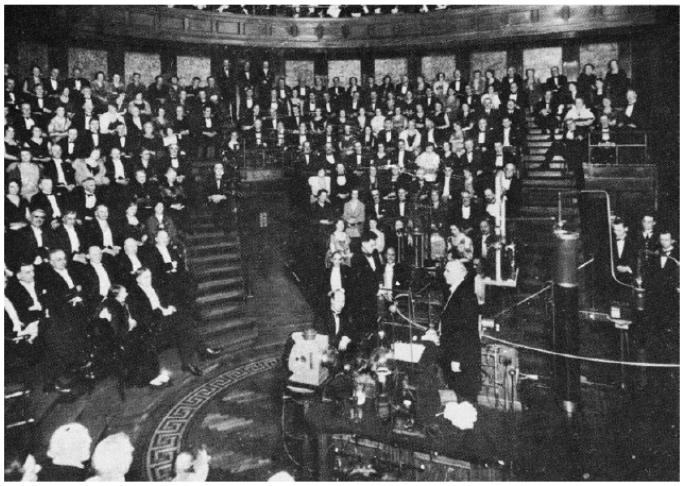

Figure 2.1: Royal Institution, 1934, Rutherford demonstration of deuterium atoms fusion.

one night every week, the entire electric power of the Moscow industrial region in order to send it through a very thick copper wire saturated with small 'bubbles' of lithium - hydrogen mixture. I declined the proposal and I am glad that I took this decision, because at that time it would definitely not have worked" [3].

In Europe it was the 1932 when the path of history of fusion started with Rutherford and his team in Cambridge, UK; their public scientific experiment at the Royal Institution in 1934, without any concerns on safety conditions as visible in Fig. 2.1, showed the first man-produced fusion reactions of deuterium atoms. During the experiment they observed the fusion of deuterium atoms and also discovered two new fusion born nuclei, ^3He and tritium. During his demonstration, Rutherford did mention that each fusion reaction produced a large amount of energy, but there was overall a net loss of energy because of the low fusion probability of the deuterium ions accelerated against the deuterium target. In his talk, Rutherford dismissed nuclear energy as 'moonshine'! [4]. In the following ten years, the H. Bethe work on the theory of nucleus of deuteron and the prediction of many nuclear reactions cross-sections, allowed to establish that the stars were powered by fusion processes. In the enormous ball of gas which constitutes a star, initially mainly hydrogen, a complex fusion cascade is taking place transforming, over billions of years, first hydrogen into helium then into progressively heavier nuclei. By the early 1950s, the basic properties of fusion of light atoms were sufficiently well known for John Lawson to establish the fundamental conditions needed to achieve net power output from fusion reactions in his famous necessary criterion [5]. His elegant power balance analysis showed that the product of fuel density (n) and plasma energy confinement time (τ_E) was a function of only plasma temperature (T), impurity content and fusion power gain (Q). The criterion was based on confinement $n\tau_E \geq 1.5\ 10^{20} m^{-3} s$ - where n is the ion

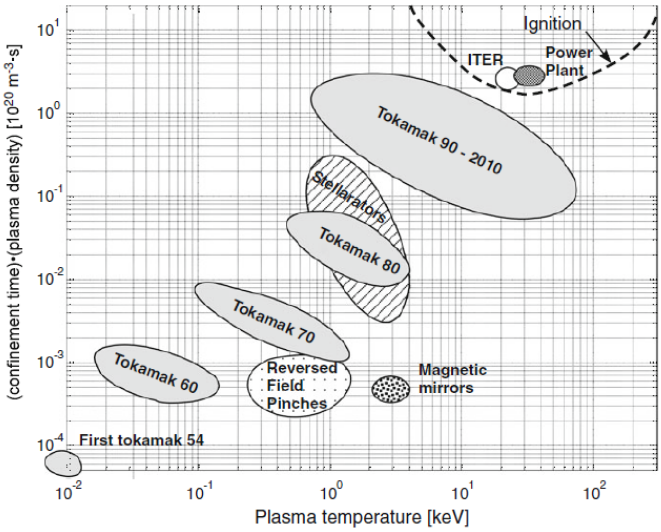

Figure 2.2: Lawson diagram for magnetic fusion.

density and τ_E is the energy confinement time of the fuel ions. Lawson also stated that the temperature needed to be about 10 keV (100 millions degrees). Typically, the conditions to be reached are $n \sim 10^{20} m^{-3}, \tau_E > 1.5s, T > 10keV$. Achieving the density was relatively easy. The temperature seemed to be a daunting task but several methods have now successfully reached and even exceeded this value. However, the real challenge was to be the energy confinement time; it is indeed the main objective of ITER to exceed for the first time in a magnetic confinement device the value required for net energy production [5]. The Lawson diagram ($n\tau_E$ vs T, as shown in Fig. 2.2) was developed from this analysis and, with various refinements through the decades, still is the standard for measuring progress towards fusion energy[4].

In the USSR, the story followed another road, a road more close to a novel than to a historical behavior; it started a long, but not so far, time ago, in the fall of the summer of 1950, by the hand of a signal man on Sakhalin Island, which was a real waste land, named Oleg Aleksantdrovich Lavrent'ev. This guy was still doing his service in the army, even if the war sunset was left behind several years ago, and despite the fact that his personal interest for physics had not sunset in each single day of war. He became interested in nuclear physics in his youth, around the seventh grade, after reading a book titled "An introduction to Nuclear Physics", but his quest to learn more was put on hold after the outbreak of War World II. In 1944, with only an eighth-grade education, he crossed the front line and volunteered in the Soviet army as an artilleryman. He was serving in one of the Baltic states when the V-Day came in. Then he continued his army service in Poronaisk, a small town in the Sakhalin, which revealed itself to be a peace-full place, with an army's library

providing him technical books and higher education manuals. It all appeared as first rays of a new rising sun, a step beyond the war and towards the future. The most relevant informations he could get came from a journal, "The achievements on Physical Sciences", which he paid for the subscription out of his monthly allowance. In 1948 Lavrent'ev was charged with preparing a lecture on a nuclear issue by his commanding officers who were well aware of the clever sergeant. "I had a few free days to prepare a lecture. During that period I rethought all the knowledge I'd gained so far. As a result, I've found solutions to the problems I had been battling with for years" [6]. The island was an empty space, no specialists in that field, no one to share knowledge and discuss; how to advise the authorities of his scientific findings? The island was recently liberated from the Japanese when he decided to send a letter to the Central Committee of the Communist Party of the Soviet Union, reporting the following statement "I know the secret of the hydrogen bomb". Soon, an officer sent by the Kremlin to interrogate Lavrent'ev gave him also the work conditions, a safe room and two weeks, to put his ideas in writing. In the following two weeks of July he secretly wrote the report, consisted of two parts: one involving the production of a H-bomb and the other devoted to the non-military use of nuclear power. The first part of Lavren'ev's report described, confidently, the functional principles of an hydrogen bomb possibly made with solid lithium-6 deuteride, used as fuel, and initiated by a huge pulse of neutrons from a nuclear fission bomb to create tritium and facilitate deuterium-tritium thermonuclear fusion reactions. In the second part, he proposed to use controlled thermonuclear fusion to produce electricity. In his idea, a chain reaction in the fusion of light elements was supposed to proceed in a slow controlled way; he also proposed a solution to the main problem of confining the extremely hot plasma, heated up to million of degrees, and keep it off the walls of the reactor. He came up with the idea of using a field of force for the plasma-heat insulation, in particular an electrostatic field in the first version. He proposed that two spherical electrostatic grids placed under a negative and positive potentials would accelerate and confine plasma. Lavrent'ev's proposal initiated the Soviet program on controlled nuclear fusion research after that Andrei Sakharov reviewed his letter positively: "the author formulates a very important and not necessarily hopeless problem".

Sakharov mentioned a number of difficulties in realizing the electrostatic confinement and pointed out that the grid must have "wide meshes and a thin current-carrying part which will have to reflect almost all incident nuclei back into the reactor [2]. In all likelihood, this requirement is incompatible with the mechanical strength of the device". Sakharov was deeply impressed by the idea of Lavrent'ev

such that he emphasized that regardless of the results of further discussion "at this point, we must not overlook the creative initiative of the author". Sakharov realized that the two main new features of Lavrent'ev ideas would be the basis of a possible theory of fusion reactor: 'The heat-insulating effect of a field-force' and the low-density of confined particles. However, the main problem was in the long ranges of particles, which would inevitably lead to undesirable interactions of high-energy particles with the construction materials [4]. Here came the Sakharov idea to arrange for the trajectories of freely moving particles not to leave a prescribed volume by using the magnetic field lines of force. Then the theory of the magnetic thermonuclear reactor came into the scene based on the idea of magnetic thermal insulation of the plasma. In fact, a charged particle in a strong magnetic field follows a helix along a magnetic field line of force and therefore, a high-temperature plasma must be created inside a toroidal solenoid. A negligible curvature of the solenoid would allow particles to impact the chamber walls only as a result of interparticle collisions, that is as a result of diffusion across the magnetic field. However, the trajectory of a particle can shift after each collision only by a distance on the order of the Larmor radius (about 1 cm for deuterium ions and less then 1mm for electrons at $B = 50kG$ and plasma temperature $Tp = 50keV$); therefore, the energy transfer to the construction elements of the reactor is greatly reduced [2]. In October 1950, I. E. Tamm and his former postgraduate student A. D. Sakharov, formulated the initial principles of magnetic confinement of high temperature plasma. In the October of the next year, 1951, Sakharov evaluated the parameters of the magnetic thermonuclear reactor (MTR) with magnetic confinement of plasma and by neglecting the curvature of the plasma torus, according to a cylindrical model. The provisional parameters of the MTR thermonuclear D-D reactor were: the major and minor radii of the plasma torus were $R = 12m$ and $a_p = 2m$, $B = 50kG$ $(i.e.5T)$, $n = 10^{14}cm^{-3} = 10^{20}m^{-3}$,$T = 100keV$ and a power $P_{DD} = 880000kW$.

The main problem of the closed toroidal systems was found by Sakharov in the toroidal drift of charged particles. Interestingly, in order to eliminate the vertical drift of charged particles in the toroidal magnetic field relative to the torus plane, Sakharov suggested a suspending coil on the chamber axis, carrying a toroidal current whose magnetic field would convert magnetic field lines of force into helical lines, thus creating a system of nested toroidal magnetic surfaces. In other words, the rotational transformation of the magnetic field, was provided by a superposition of a toroidal magnetic field and a magnetic field of electrical current along a conductor located in the chamber axis (also known as Levitrons). Later he chose to create such a magnetic configuration by driven current directly in the plasma

itself by induction. To sustain the current-carrying plasma ring in equilibrium, he suggested a toroidal copper housing cut in two places: along the torus to allow the introduction of the toroidal magnetic field, and across the torus for the introduction of toroidal emf which would generate and sustain electric current in the plasma. Parameter comparison of that D-D reactor with those of today's projects based on a deuterium-tritium mixture reveals close coincidence of reactor dimensions [7]. The authors had noted that MTR could be used for tritium breeding (100g per day) or 233^U production (8kg per day). Sakharov noted at this point that the energy production value of 233^U which could be burnt in a conventional reactor would greatly exceed the heat liberation in the nuclear fusion reactor itself. These remarks clarify that the decisive factor for enacting the decision on the CNF program at the time was the possibility of manufacturing charges for hydrogen or atomic bombs. In 1957 this system was given the name Tokamak.

The MTR project followed the announcement made by Argentina's president Juan Peron on March 25, 1951: the experiments by a German physicis Ronald Richter succeeded in a 'controlled release of atomic energy at a superhigh temperature of millions of degrees without using uranium fuel'. The announcement had a sort of domino effect: all the scientific communities of Europe, USA and USSR, had an intensification of their classified CNF research programs. In Great Britain, after the first experiments with toroidal discharges in 1949 by P Thonemann [8] they came to the implementation of pinch effect by S W Cousins and A A Ware [9]. In the USA, the CNF research was brilliantly directed by the seminars of Edward Teller. In 1951, L. Spitzer invented the stellarator as a solenoid shaped into a 3D figure of 8. The proposal of Spitzer was approved and signed with a research project contract with Princeton university (i.e. the matterhorn project). The inititative to declassify the CNF research came from the USSR with organizing the All-Union conference in 1955 and then with the first public disclosure of fusion research in April 1956 at the atomic research center of Harwell (GB), where I V Kurchatov gave a public lecture titled "on the feasibility of thermonuclear reaction in a gas discharge". Why there was a necessity of declassifying such an important research? It has to be clear that many innovative proposals were investigated during the 1950s, including different confinement configurations, both magnetic and electrostatic, methods to enhance fusion cross-section (e.g. muon catalysis), but the majority of the efforts focused on magnetic configurations such as linear or toroidal pinches, magnetic mirrors and stellarators. These were the main proposals on what a fusion power plant might look like. A deuterium fuelled tokamak system was considered by Tamm and Sakharov [10] while the DT fuelled stellarator concept was proposed by Spitzer and others [11].

The weakness point of all these studies were that they all assumed MHD plasma stability and plasma energy losses due to only bremsstrahlung radiation and classical diffusion across the magnetic field. Small laboratory experiments were initiated with a minimal understanding of plasma stability, primitive technologies and few diagnostics.

All the first tests of fusion machines, in USSR, US, Europe revealed the first main feature of the phenomena under investigations: plasma is a complex media dominated by collective interactions between particles, waves and fields. These early attempts were marred by plasmas which exhibited strong collective instabilities that prevented plasma parameters from exceeding $T \sim 100eV$, far from the $10keV$ needed for fusion. Anyway two main results were achieved: the exhibition of major plasma instabilities and low confinement properties. In the few cases where confinement could be measured, the plasma diffusion was much larger than classical diffusion, and closely resembled the Bohm diffusion [12] observed in the Calutron ion sources used to separate uranium isotopes. Let's focus on the USSR results before the declassifying procedure, since they represent the main causes of that process. The experiments were basically empty of success since they were just storming direct rapid discharges. Vacuum conditions and changes in the scenario of preparing the discharge were explored to improve the experimental activity on deuterium plasma pinch which finally, on July 4 1952 led Filippov's group to provide a main result, full of profound disappointment, but extremely important for the future of the program: the pinch instability did not allow the temperature to rise with increasing current.

In fact, at the Kurchatov institute the need to inject toroidal current led to a proposal to forgo the toroidal magnetic field completely. The main effort was first concentrated on pinches in which, according to the Bennett relation $J^2 = 4c^2NT$ [13], the plasma temperature must grow in proportion to the square of the current, $T \sim J^2$ [2]. As we have seen, Sakharov highlighted the main problem of the toroidal drift of charged particles and he suggested two methods to close the drift trajectories inside the chamber. The first of them we already mentioned, and it consisted in adding a poloidal magnetic field created by an internal current ring suspended by cables or by a horizontal magnetic field. The second one consisted in inducing a high-frequency current in the plasma itself; this technique was more realistic and led to experiments with a single-pulse discharge sent from capacitor batteries[2]. After the results of Filippov's group, the theory of pinch stabilization by a longitudinal magnetic field again reoriented the studies towards A D Sakharov's suggestion: to use both the toroidal magnetic field and the toroidal current. However, their functions had, in a certain sense, changed: in the new system, the toroidal current

provided equilibrium and plasma confinement, while the magnetic field served to create the discharge stability[2]. Nevertheless, no increased plasma temperature was revealed since both the toroidal and cylindrical experiments had ceramic chambers. It followed that overheating of parts of the chamber wall with low thermal conduction caused strong sputtering, plasma pollution and intense UV radiation leading to low plasma temperatures, approximately at a level of $10 \pm 30eV$. In 1955, the first tokamak-like machine was built: the TMP experiment, which still had a ceramic discharge chamber with a helical metallic insert. Silicon lines in the plasma radiation spectra were evidence of chamber wall evaporation caused by high thermal loads [14]. In conclusion, a temperature not exceeding 30 eV was typical for a long time and there was no progress either in pinches or in toroidal systems. The only short lived innovations were related to RF electromagnetic field confinement techniques of hot plasma but without appreciable results. Theoretical studies of stability on plasma models with a well-defined edge pointed unambiguously to the unavoidability of segments with convex magnetic lines of force, through which plasma could leak out of the confinement volume [2]. The profound pessimism towards the feasibility of solving the CNF problem took over the whole scientific community for more than five years. Interestingly, the worldwide research groups on CNF didn't know that they were all struggling on the same challenges: plasma instabilities and Bohm diffusion.

2.4 After 1958 Geneva conference

The first international conference with a large number of reports related to CNF field was the conference on "ionization phenomena in gases" which was held in Venice in June 1957. The year 1958 was the turning point: in January the British papers announced that the ZETA facility in Harwell had reached a plasma temperature of 300eV. The ZETA results, which proved to be erroneous, were the last intriguing story before the 2nd Conference on Peaceful Uses of Atomic Energy in Geneva. At this meeting, the scientific status of various small scale experiments was characterized by the exhibition of strong instabilities. Several theoretical papers described the requirements for plasma equilibrium and the use of energy conservation principle to predict plasma stability. This energy principle was formally described in a number of papers in the late 1950s [15] and at the 1958 Geneva meeting [16]. The theory of a new science was proposed to be ready for leading the experimental methods on the achievement of the main goal of nuclear fusion on Earth. The theory focused on the two main problems that were found before the 1958: the exhibition of major

plasma instabilities and low confinement properties. In fact, the global MHD instabilities were the most dangerous since, when plasmas experienced a concave line averaged magnetic field curvature, they could push the plasma across the field lines very rapidly at the speed of sound. This was strictly related to the second main problem: the low confinement properties; in fact, early simple mirror machines had such bad curvature and the energy confinement time was orders of magnitude lower than what was expected on the basis of particle collisions [4]. The theory was a star to follow: the energy principle developed a decade before became the standard technique for evaluating the macroscopic stability of an ideal plasma in various magnetic configurations. Ioffe showed that in an MHD unstable mirror plasma the curvature could be changed from bad to good, leading to a stabilization of the large scale instabilities, by changing the magnetic configuration with a superimposition of an hexapole magnetic cusp. This new configuration led, because of the suppression of the macroscopic instability, to an increasing confinement time by a factor of 30 [17, 18]. All the laboratories experienced the disappointment of low confinement results. It can be interesting to analyze it also from the experimental point of view and not only from the theoretical one, provided by MHD theory. This is strictly related also to the problem of plasma equilibrium, which will be the topic of the next sections. Considering the confinement properties, these were initially determined by the presence of plasma contamination due to the use of a glass or even quartz vessel in the experiment. The problem of contamination was resolved by using cleaned metallic walls and by improving the pumping. The first machine with all metal chamber, without insulating inserts was the T-1 device, which could be considered the first tokamak. Its importance is clearly evident from its experimental results by which it was shown that, despite the lacking arcing on dielectrics, the dominant role in the power balance of hot plasma was played by energy losses caused by the vacuum ultraviolet radiation of impurities [7]. It practically led to the next step in the confinement research: finding the ways to mitigate radiating losses in order to allow plasma temperature to increase. At the same time the problem of confinement was strictly related to the problem, already mentioned, of plasma stability and, a step before, of plasma equilibrium. The latter is clearly visible in its whole importance by considering the magnetic configuration which theoretically is based on the idea of plasma equilibrium: the stellarator. The stellarator was deeply explored in Princeton when the vertical drift due to toroidal magnetic curvature was canceled by twisting the magnetic lines of force or using helicoidal windings around a more conventional vessel shape. Anyway the results still were disappointing but the reason only became clear a few years later: error fields would destroy the magnetic

surfaces due to resonant effects. As the level of accuracy and rigorously methodology increased in the CNF research field, all the fusion machine experiments in the world were considered by the scientists as the evidence of thermo-insulation of plasmas in toroidal systems corresponding to the so-called empirical Bohm's formula. It was clear from the produced results that the plasma confinement properties could be characterized by Bohm scaling [19] where the energy confinement time scaled as $\tau_B \sim Ba^2/T_e$, which means that the thermo-insulation worsens with the rise of the plasma temperature. A major theoretical and experimental effort was made to understand the cause of Bohm diffusion. Several new aspects were considered in the following years, Ohkawa and Kerst [20] put forward the idea of minimum average B stability in a torus using a toroidal multipole field created by current-carrying ring(s) within the plasma. Experiments during the mid- to late 1960s confirmed that interchange instabilities could be stabilized by this technique with confinement times increasing to $> 50\tau_B$ in low temperature $5 - 10eV$ plasmas [21]. At the 1965 IAEA meeting in Culham, most experiments continued to be limited by Bohm diffusion, but a quiescent period was discovered while analysing the current ramp down phase of ZETA experiment [22]. The quiescent period coincided with the formation of a reversed current layer that had strong magnetic shear, and provided evidence that magnetic shear could stabilize instabilities in a toroidal plasma. The spontaneous generation of reversed fields in toroidal plasmas was shown by Taylor [23] to be a consequence of relaxation under constraints to a minimum energy state. This result represented a new class of toroidal magnetic confinement systems which will be called Reversed Field Pinch (RFP) configuration.

The breakthrough on toroidal devices came again from the Kurchatov institute: at the 1968 IAEA meeting at Novosibirsk, Lev Artsimovich impressed everyone present when he reported that tokamak T3 reported improved confinement with central electron temperatures reaching $\sim 1keV$, confinement times $> 30\tau_B$ [16] in the order of some milliseconds which far exceeded all values previously obtained. Furthermore these results represent the first major international fusion research collaboration, with transfer of equipments from Culham laboratory to the T-3 installation at Kurchatov laboratory. In fact, questions were raised regarding the validity of the Russian measurements of electron temperature based on diamagnetic loop measurements of the total plasma stored energy and charge exchange analysis of atoms escaping from the plasma (i.e. soft x-ray diagnostics)[7]. The electron temperature was measured by laser scattering method, i.e. by the Thomson scattering system, of the Culham laboratory which confirmed the data obtained by the Kurchatov institute. This confirmed that the long standing Bohm barrier had been

broken with $\tau_E > 30\tau_{Bohm}$ in a hot plasma [16]. The demonstration came with the explanation that limiting the plasma current so that the edge q value (inverse rotational transform) was greater than 3 would eliminate the most damaging MHD instability[4]. The results of this international experiment, the first in nuclear fusion history, established tokamaks as the basic direction for further research on magnetic plasma confinement, worldwide [7].

During the 1970s, it is peculiar to notice the ambition in the world fusion program plan, since overlapping experiments occurred, with the construction of new devices before experimental results from the preceding generation were available. On the other hand, a long range vision and program was going to rise in the scientific conscience in the worldwide CNF research: the plan was to develop fusion energy based on systems studies of fusion power plants [24] in order to define the technical characteristics of a future fusion power plant and then the scientific steps needed to reach it. The construction of four large tokamaks (JET,TFTR,JT-60 and T-15) was initiated with a 10-fold increase in size and plasma current relative to previous tokamaks. In fact, all the tokamak devices in the world had confirmed that the confinement did increase with the size and the field strength as hoped but it was clear that temperature could not exceed 1keV as the ohmic heating power diminished as $T_e^{-3/2}$. Additional heating power revealed to be the next major challenge in order to heat the plasma and reach ignition conditions. Beam sources and RF heating systems were firstly developed and tested on medium size tokamaks. By the end of the decade, several methods were available for plasma heating purposes towards thermonuclear temperatures. Theoretically, the main contribution was the progress in the understanding of transport phenomena driven by collisions in full toroidal geometry, the so called neoclassical transport theory [25]. This led, inter alia, to the prediction of the bootstrap current [26] which was later observed in a toroidal multipole by Zarnstorff et al [4]. Now, it is still impossible to calculate the energy and particle transport in tokamaks from first principles, since because of plasma turbulence many real mechanisms of losses are not clear; energy losses through the electron component channel exceeded by tens times those predicted by a neoclassical theory [7]. Furthermore, the additional power allowed to investigate the energy confinement time dependence on additional heating power, significantly larger than the ohmic one, with the possibility of exceeding the temperature limit of the ohmic heating. This was demonstrated by two main medium size tokamaks, PLT and T-10, which were characterized by higher plasma currents, in the range of $1MA$, and several additional heating systems: ECRH, ICRH and neutral beam injection. PLT achieved ion temperatures of $5.8keV$ using neutral beam injection into low density

plasma, thus exceeding, for the first time in a tokamak, the minimum T_i needed for fusion [27]. T-10, with the high efficiency ECR plasma heating systems, in the order of 70-80%, reached the thermonuclear electron temperature value of 10keV [7]. A comment is needed at this point: the analysis of the tokamak experimental results was beginning to change in the late 70s, with a more pragmatic view of perspective, mainly dictated by the long range vision of nuclear fusion program; this change in the scientific analysis of the collected data is represented by the necessity of finding empirical dependences (also known as scalings) of energy confinement time by deduction from geometrical size, magnetic field value, discharge current and plasma density [28]. It was, and still is, very important to establish scaling laws for the energy confinement time. This we will see, would allow to collect all the worldwide tokamaks results in the ITER database. Another important result, in this vision, was strong ohmic heating reached by the high field tokamak Alcator-A, which achieved the $n\tau_E \sim 3\ 10^{19} m^{-3} s$ [29] with a favourable scaling $\tau_E \sim na^2$. The strong auxialiary heating power, which exceeded the ohmic heating, revealed the true scaling of confinement global time: it was observed that the confinement time decreased as auxialiary heating power was increased [30]. This result was observed in all the tokamaks once the auxiliary heating began to exceed the ohmic heating, and it was labelled as "low mode of confinement". The phenomenon, firstly observed with NBI heating and successively reproduced with the RF heating, led to the creation of the first international database. Then, the result was systematized by Goldston in terms of scaling law as $\tau_E \sim {I_p/P_{aux}}^{0.5}$ [31], which revealed to be a weaker form of Bohm scaling and would prevent the large tokamaks under construction from attaining their goals, and would project to unreasonably large fusion reactors [16].

It was in this slack scientific methodology that the theoretical tradition came back into the scene to bring new water to the mill. In fact, it is important to stress that, despite the empirical knowledge, in the beginning of 1970s, a fundamental scientific research on non-circular plasma equilibria was developed by Artsimovich and Shafranov. Their proposal of a tokamak with elongated plasma cross section to improve its performances (see [32]), had two effects, one in the short range of time and the other, the most important, in the long time involving the whole future of CNF research. In the short time, a series of tokamak with non-circular cross sections (e.g. T-9, T-8, T-12, TBD) showed the possibilities for plasma equilibrium formation on a non-circular form, the growth of efficiency of using a magnetic field volume and the creation of a poloidal divertor configuration. In the long range of time, the indirect effect of the elongated plasma equilibrium led to two important results in CNF history: the discovery of high confinement mode operation (i.e.

H-mode regime) and the subsequent development of the Tokamak optimization of plasma performances. The new shaped plasmas were the main actors of experimental champaigns of 1980s. The ASDEX tokamak, operating in a divertor configuration, reproduced the L-mode scaling results when the ion grad-B drift was away from the divertor X-point. However, when the ion grad-B drift was towards the X-point, the density and hence the confinement doubled relative to the L-mode [33]. This confinement barrier, spontaneously occurring at plasma edge above a certain power threshold, was called high confinement mode of operation, or H-mode, and it was quickly confirmed on the other medium size tokamaks proving the phenomenon to be universal. The discovery helped to start new theoretical studies on the physics of the transition and also to understand the plasma transport in a tokamak. The conditions of H-mode occurrence and the scaling of both H-mode confinement and its power threshold were established during the following decades. The H-mode scaling was the basis for the ITER design and today, the H-mode regime has been chosen as the baseline operating mode for ITER [34]. The effects of the H-mode was clearly visible in the late 1983 in ALCATOR-C results: by using pellets injection it reached values of product between confinement time and density of 6 10^{19} while temperature was about $1.5keV$ [16]. The $n\tau_E$ values were comparable to that needed for breakeven while the temperature values were not.

The second important consequence of shaped plasma was in terms of plasma performances which could be improved by optimizing the plasma cross-section shape and edge plasma wall interaction. This result can be historically found in the 1968 IAEA conference, when Ohkawa proposed to replace the copper current-carrying rings in a strongly stable toroidal multipole with localized plasma currents [35]. The PMC, Plasma Current Multipole, configuration evolved into the doublet series, and Doublet II was among the first experiments to observe the benefits of cross-section shaping on confinement in the mid 1970s [16].The results of these experiments were that even a single localized plasma current in a vertically elongated cross section could support increased plasma currents and hence achieve higher beta and confinement time. Furthermore, the theoretical understanding of plasma beta, and experimental measurements of confinement time, led to create the basis for the prediction of the operating space limits in tokamak configuration: the most importants are the empirical density Greenwald limit [36] and the Tryon's limit on normalized plasma pressure [37]. We do not have to forget that the main goal of CNF research is to produce energy from nuclear fusion, which means building the first suitable nuclear fusion reactor. It was in this view that, besides the medium size tokamaks, a class of large tokamak experiments (i.e. JET, TFTR and JT60) came into operations in

the 1980s. A brief digression about the analogies, not only scientifically speaking, between these three large experiments (JET, TFTR and JT60) is proposed. All of these three machines were built in 6 years; furthermore, after their first plasma, all of these experiments were able to access new plasma regimes, with unpredictable behaviours. This point is of extremely importance since it means more than what it appears. In fact, these large experiments, as also the medium size tokamaks, have shown the ability to push beyond the knowledge they represent, revealing unforeseen phenomena of nature. This consideration is extremely important since it represents the aspiration of knowledge intrinsically present in the CNF research methodology, from the dawn until that years. An experiment goes beyond when the scientific operator acts through him. Sometimes, in the real world, it could also overlap with the idea that, that period of outstanding scientific progress was made possible by the large investments made during the late 1970s and early 1980s. However this consideration is not always true. What is true for sure is that the results of the three large tokamaks were clearly determinant for the following two decades up to now. By 1986, TFTR had achieved reactor temperatures, $T_i \sim 17keV$ [16], identified also the bootstrap current [38] and extended $n\tau_E$ to record values at low T [39]. The Joint European Torus JET had extended the H-Mode to large tokamaks with a provisional divertor thereby doubling $n\tau_E$ to values of the Lawson product $n\tau_E$ 300 times larger than those achieved on T-3 [40]. The JT-60 Phase I goals were achieved by 1988 and an ambitious upgrade to JT-60U was initiated in 1989. For all the 1980s, the three large tokamaks continued to push the operational conditions of plasma in terms of triple product by reaching temperatures beyond the 35 keV, by approaching breakeven values of $n\tau_E$ in high temperature deuterium plasmas and by extending plasma duration up to $60s$ at lower parameters [41]. A second generation of optimized tokamaks were built after the 1980s (e.g. ASDEX Upgrade, JT60U, DIII-D, ...), tipically known as 'upgraded machines', with the main goal of extending the knowledge in terms of optimization of plasma performances. This was strictly related to the creation of an international confinement database which led to non-dimensional scaling laws based on first principles and on a 'wind tunnel' approach; thus, the 'Gyro Bohm' scaling character of H-mode confinement was confirmed.

The step beyond was the experimental campaigns focused on the deuterium-tritium mixture since the pure deuterium one have predicted that a size of megawatt fusion power could be generated by means of a balanced D/T mixture. Many technological challenges were involved, including safety containment for tritium, remote handling, diagnostic compatible with large neutron flux and so on. JET campaigns involved 10 % of tritium added to deuterium plasma for two pulses, each one of them

producing a peak fusion power of $1.7MW$ and a fusion energy of $2MJ$ per pulse. The amount of produced fusion power can be significant only if it is significant in comparison with the power consumed to heat the plasma initially; this is quantified by the fusion gain factor $Q = P_{fusion}/P_{heat}$. The first production of fusion power is characterized by a Q factor of about 0.15, meaning a clear unfeasible condition. TFTR made a 50% DT experimental campaign producing peak fusion power of $10MW$ for $1s$ with a Q factor of about 0.3. The importance of these experiments was mainly in the ability of synthesize all the technological and physical knowledge reached until that point. In the fall of 1997, JET carried out a series of ~ 100 DT pulses reaching fusion power levels of $16MW$ for the $\sim 1s$, and $22MJ$ of fusion energy per pulse using longer-duration lower-power pulses [16]. The maximum fusion gains achieved were $Q \sim 0.65$. JET also extended alpha heating experiments and ICRF heating scenarios in DT. A near ITER scale closed cycle tritium plant was tested successfully during this phase. JET made a major contribution to fusion technology by demonstrating remote handling of components inside the vacuum vessel.

All of these large tokamaks experiments operating in DT, JET and TFTR, are characterized by the fact that the significant amount of produced fusion power was in any case less than the power consumed to heat the plasma initially. The necessity of a new experiment was clear since the goal was to demonstrate that it is possible to achieve a fusion power output significantly greater than the power input. This is in fact the aim of the ITER project whose dimensions were indicated by the scaling laws above mentioned derived from collective data of all tokamaks in the world in order to reach its $Q = 10$ objective. The scientific community cooperation was formalized in the last decade with the so called broader approach to magnetic fusion between Europe and Japan which is closely associated also with other satellite projects related to ITER. The development of fusion materials (IFMIF) facility for the neutron studies on material properties, computing with the new International Fusion Energy Research Centre (IFERC) and steady state tokamak operation with the construction of the new Japanese large superconducting device, JT60-SA. ITER goal is to demonstrate the scientific and technological feasibility of fusion energy for peaceful purposes which is the same goal of the fathers of the fusion. ITER is expected to achieve sustained burning plasma conditions with $Q \sim 10$ at power levels of $\sim 500MW$ for $\sim 400s$ yielding $\sim 200GJ$ per pulse. In longer pulse operation, ITER is expected to achieve $Q \sim 5$ at power levels of $\sim 350MW$ for $\sim 2500s$ yielding $\sim 900GJ$ per pulse.

2.5 Same horizon, different paths

Curiously enough, scientists in each of the first three countries starting their CNF research based on a closed toroidal system discovered their own approaches to magnetic plasma confinement. Thus, the three magnetic confinement configurations for a toroidal plasma known as Tokamak, Stellarator and RFP, are the result of three different scientific communities in the same field of research, respectively located in USSR, USA and Europe. It is quite difficult to find a similar behavior in the progress of a scientific field in modern history; it looks more close to what happened in the 17th century when individual scientists followed independently their own approach to the same field of research. In CNF case this behaviour involved entire communities of scientists. Nevertheless, this phenomenon is represented by several experiments with toroidal gas discharge, each one representative of the three main scientific communities involved in the CNF research. In the UK, these experiments were based on a field of "toroidal pinches with reversed toroidal magnetic field", abbreviated to RFP (Reversed Field Pinches). Currently, the largest machine of this type exists in Padova, Italy, called RFX-mod experiment. In USSR, as we have seen, the proposal made by A D Sakharov and I E Tamm for a "magnetic thermonuclear reactor" led to "tokamak" systems, which grew to dominate the world program of CNF research. On the other hand, in the USA, L. Spitzer invented the closed system of magnetic confinement with nested magnetic plasma surfaces in which each magnetic line of force extends along the system (the topological torus) while rotating by a certain angle ('rotational transform') and covers the whole closed toroidal surface; this approach generated the fundamental research field of steady-state "stellarators" or "helical" systems of magnetic plasma confinement.

These three magnetically confinement configurations have all the same purpose which is to maintain a hot plasma by confining it and keeping it away from the vacuum container wall by using appropriate strong magnetic fields. Furthermore, these configurations belong to a group of methods of thermoinsulation and heating of plasma which includes all the methods of obtaining equilibrium plasma configurations in which the pressure of the plasma is balanced by magnetic pressure. This is the fundamental topic known as 'plasma equilibrium'.

2.6 Nuclear fusion reactions

Nuclear energy is described by Einstein's formula $E = mc^2$ describing that in nuclear reactions, $A + B \rightarrow C + D$, the net energy is released if there is a mass defect:

$$(m_A + m_B)c^2 \rightarrow (m_C + m_D)c^2 \tag{2.1}$$

In laboratory fusion energy, reactions involving hydrogen isotopes are considered, where the deuterium-tritium reaction, represented in Fig. 2.3 is the most promising one.

The product of the D-T reaction are of two types: the α-particles or He^4 which are electrically charged products that can be captured by a confining magnetic field, and the neutrons which are electrically neutral so that they can escape from the magnetic configuration. The former are responsible for the heating of the plasma while the latter are extremely important in the tritium breeding which is a very expensive nuclear fuel. In each elementary D-T reaction event, a nucleus of tritium disappears and a fast $14.1MeV$ neutron is produced that subsequently leaves the plasma. By surrounding the fusion reactor chamber with a neutron multiplier, i.e. beryllium, able to use the fast neutron to induce $(n, 2n)$ reactions, the initial neturon flux may be increased and utilized for tritium breeding by disintegration of the Li^6/Li^7 breeding blanket and recovering the fusion energy. The other fusion fuel, the deuterium, abounds in the oceans: out of 6500 molecules of water one molecule is D_2O. Thus, in principle, one litre of sea water contains $10^{10}J$ of deuterium fusion energy [42]. This is a factor of about 300 more than the combustion energy of one litre of gasoline, which yields 3 10^7J.

A number of other fusion reactions also exist, as reported in Fig. 2.4, but they are less probable to be initiated in terms of fusion cross-section. However, complete burn of all available D_2 would involve these reactions. An important aspect to highlight is that the nuclear fusion that we are taking into account is not the nuclear fusion that power the stars. In fact, the fusion nuclear reactions that take place, for example in the sun, are not of the D-T type and they do not produce neutrons but neutrinos. The fusion process of the sun burns up the hydrogen, and the energy is radiated away. This difference is extremely important because a future fusion reactor will be subjcted to an extremely high neutron flux that leads to several challenging factors on technological aspects.

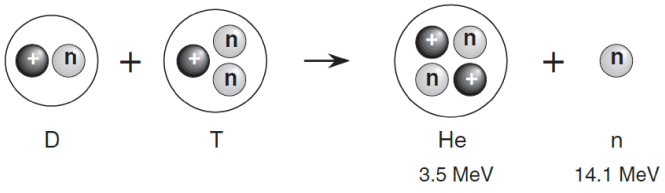

Figure 2.3: Deuterium-tritium reaction.

$$
\begin{aligned}
\mathrm{D}^2 + \mathrm{D}^2 &\rightarrow \mathrm{He}^3\ (0.8\,\mathrm{MeV}) + \mathrm{n}\ (2.5\,\mathrm{MeV})\,, \\
\mathrm{D}^2 + \mathrm{D}^2 &\rightarrow \mathrm{T}^3\ (1.0\,\mathrm{MeV}) + \mathrm{p}\ (3.0\,\mathrm{MeV})\,, \\
\mathrm{D}^2 + \mathrm{T}^3 &\rightarrow \mathrm{He}^4\ (3.5\,\mathrm{MeV}) + \mathrm{n}\ (14.1\,\mathrm{MeV})\,, \\
\mathrm{D}^2 + \mathrm{He}^3 &\rightarrow \mathrm{He}^4\ (3.7\,\mathrm{MeV}) + \mathrm{p}\ (14.6\,\mathrm{MeV})\,,
\end{aligned}
$$

Figure 2.4: Other nuclear fusion reactions.

Typical numbers associated with thermonuclear fusion reactors, as presently envisaged, are: temperature $T \sim 10^8 K = 10\ keV$, power density $P \sim 10\ MW\ m^{-3}$, particle density $n \sim 10^{21}\ m^{-3}$, time scale $\tau \sim 100s$ [42]. On the other hand, typical numbers associated with thermonuclear reactions in the stars, in particular the core of the Sun, are extremely different for a prospective fusion reactor on Earth: temperature $T \sim 1.5\ 10^7 K$, power density $P \sim 3.5\ W\ m^{-3}$, particle density $n \sim 10^{32}\ m^{-3}$, time scale $\tau \sim 10^7 years$ [42].

2.7 Magnetic confinement of fusion plasmas

On earth, two approaches are possible in order to reach thermonuclear fusion. One aims to confine the plasma for a very short time τ but at a very high density n: this is fusion by inertial confinement, where laser beams (or beams of electrons or ions) converge on a target (plasma) in order to bring it to the thermonuclear state. The second approach, is that of magnetic confinement where the plasma ionised particles are confined within a magnetic field configuration. As we have seen in Sect. 2.3, the density in the magnetic confinement approach is much lower than in inertial case, that is the reason why the confinement time, which represent the relaxation time of the plasma energy due to heat conduction, must then be more significant, of the order of a second. ITER for example should reach $\tau_E = 3.7s$.

More practically, no material containers can hold plasmas with densities of $10^{20}\ m^{-3}$ and temperatures of $100 - 300\ 10^6\ K$ during times in the order of minutes, or at least seconds, without immediately extinguishing the 'fire' [42]. One way to solve this problem is to make use of the confining properties of magnetic fields, in particular closed magnetic geometry facilitating stable, static plasma equilibrium with roughly bell-shaped pressure and density profiles and nested magnetic surfaces [42].

In the beginning of magnetic confinement fusion, the thermoinsulation of plasmas by means of magnetic fields could be divided into two basic groups: the methods of accelerating plasma by electrodynamic forces and the methods of obtaining equi-

librium plasma configurations. It is known that the latter revealed to be the most promising one, and they represent all the configurations in which the plasma pressure is balanced by the magnetic pressure. The two alternatives are explicitly distinct if we express the problem of magnetic confinement in terms of magnetohydrodynamics, which deals with the general laws of behavior of a conducting fluid in a magnetic field. In doing this we will follow the Artsimovich article of 1958 [43] since it clearly highlights an important physical assumption that will be applied also in the plasma modelling for electromagnetic control: the possibility of neglecting the plasma inertia term. This assumption is considered fulfilled because inertia term is small compared to the pressure gradient. As we will see in Chap. 3, the electromagnetic control is based on the same physical assumption of neglecting plasma inertial term because the time-scale of interest is much longer than the Alfven time and therefore the plasma can be assumed to evolve through a sequence of MHD equilibria [44], i.e. mass density is considered very small [45]. We will see in the next section that this corresponds to consider slow discharge phenomena.

Assuming fulfilled the conditions of macroscopic behaviour of the plasma as a conducting single fluid, the equation describing the behaviour of a plasma under the action of electrodynamical forces is stated in Eq. 2.2.

$$\rho \frac{d\mathbf{v}}{dt} = \mathbf{J} \times \mathbf{B} - \nabla p \tag{2.2}$$

Now, $\mathbf{v}$ and ρ are respectively the velocity and density of an elementary volume of plasma moving under the action of electrodynamic forces and a pressure difference. The electrodynamic force acting on a unit volume of plasma is represented by the first term on the right-hand side of the equation. It is due to the interaction between the magnetic field and the currents flowing in the plasma ($\mathbf{B}$ is the magnetic field and $\mathbf{J}$ is the current density).

The equations highlight the two extreme cases, each characterizing a large group of confinement methods. The two cases are determined by applying or not the negligible plasma inertia term assumption. The first category, is determined by assuming a small gas kinetic pressure, leading to the balance of electrodynamical forces by "inertial forces":

$$\rho \frac{d\mathbf{v}}{dt} = \mathbf{J} \times \mathbf{B} \tag{2.3}$$

Under these conditions, the plasma as a whole will acquire under the action of electrodynamic forces a directed velocity which may considerably exceed the random thermal velocity of the ions [43]. The kinetic energy of directed motion due to

acceleration of the plasma in the magnetic field may then be utilized for subsequent heating of the substance (in processes of the implosive compression type, during impact of accelerated plasmoids on a target, etc.). Characteristic of this type of plasma-magnetic field interaction is the short duration of the process. In order of magnitude, it is equal to a/v, where a is the distance traversed by the plasma under the action of the accelerating forces, and v is the velocity attained. In cases of practical interest, the duration of this acceleration process should be of the order of $\sim 10^{-6}-10^{-5}s$. Obviously, such momentary pulsed processes will be of considerable interest only if it is possible to utilize them as the first phase in heating the plasma. This phase should result in the transformation of kinetic energy into heat and in the transition to some quasi-stationary state in which the rapid inertial motions remaining after the first phase should damp out within a very short time [43].

The second category occurs if acceleration of the plasma is small and if the "inertial term" on the left-hand side of the equation may be disregarded compared with the pressure gradient. In this case the gas-kinetic and magnetic pressure balance each other for all times, determining a plasma equilibrium state:

$$\nabla p = \mathbf{J} \times \mathbf{B} \tag{2.4}$$

In order to understand the range of applicability of this assumption, it is useful to introduce a simple quantitative criterion which may be used to differentiate between "slow" and "fast" phenomena, which led to neglect or not the plasma inertial term. In particular, following [43], the distinction can be made without going deeply inside the MHD wave analysis of plasma and just by considering fundamentally different the discharge conditions for the cases where current builds up at a slow rate and cases where the current rises at a fast rate. A quantitative criterion which may be used to differentiate between "slow" and "fast" discharges is the ratio of the current rise-time to the period of inertial radial oscillations of the plasma column [43].

In the slow phenomena, or in this view in the slow discharge, hundreds of inertial oscillations may occur in rarefied gas discharges with peak currents of the order of $10^5-10^6 amp$ and durations of the first half-period of the order of $10^{-3}s$. On the other hand, "fast" discharges are characterized by the occurrence of only two or three radial oscillations before the current reaches its peak value . An investigation of pulsed discharges with a very high rate of current build-up (from 10^{10} to $10^{11} amp/sec$) has shown that irrespective of whether such discharges occur in linear tubes or in toroidal chambers, the main role is played by acceleration of the plasma by electrodynamic forces [43]. This class of experiments were based on the idea of obtaining a high density in a compressed plasma column over a short period of time. In the initial

phase of the pulsed discharge the plasma is pinched to the axis of the discharge tube. This compression is the first stage of rapid oscillation of the plasma column. Maximum temperature and density is reached when the column radius is a minimum [43]. In slow discharges the gas-kinetic pressure of the plasma may be expected to balance the electrodynamical forces and the column temperature will be raised at the expense of Joule heat. The fundamental relation between plasma equilibrium and plasma stability is brilliantly highlighted again by Artsimovich [43], with simple considerations that can be now used to introduce the main field of electromagnetic control of plasma. An equilibrium state of this type will be suitable for heating of the plasma to very high temperatures only if the following two conditions are satisfied: the plasma column should not be in contact with the walls and the state under consideration should not only be in equilibrium but be stable as well. One may imagine a multiplicity of ways for attaining such equilibrium plasma configurations characterizing a quasi-stationary state of plasma in a magnetic field. As already pointed out previously, the history of fusion science lead to the adoption of methods for confinement and heating of plasma in systems with toroidal geometry; the three main families are: Tokamak, Reversed Field Pinch(RFP) and Stellarator.

2.8 Magnetic confinement configurations

The main problem of toroidal configuration is that, in general, any force with component perpendicular to the magnetic field, results in a drift velocity $v_d = \dfrac{\mathbf{F} \times \mathbf{B}}{qB^2}$. Two charge dependent drift velocities can occur because of toroidicity. The first is due to the fact that toroidal bending produces an inhomogeneous magnetic field with a gradient in the inward direction. In this case, the effective force is expressed via the magnetic moment of the particle and leads to the so-called "grad-B drift" whose direction depends on the particle charge. The second contribution is due to the curvature of the magnetic field lines which produces a centrifugal force drift which is also charge-dependent. Both drifts lead to charge separation, which produces a vertical electric field with a resultant electric force that produces a charge independent $\mathbf{E} \times \mathbf{B}$ drift which carries ions and electrons radially outward and destroys the confinement.

As already pointed out in Sect. 2.3 by Sakharov, the problem of toroidal drift of charged particles can be solved by the introduction of an additional poloidal magnetic field component. In this case, the field lines results in helices lying on toroidally nested surfaces as shown in Fig. 2.5b [46]. The additional component of the magnetic field in the poloidal direction, θ, causes the $\mathbf{E} \times \mathbf{B}$ drift to cancel,

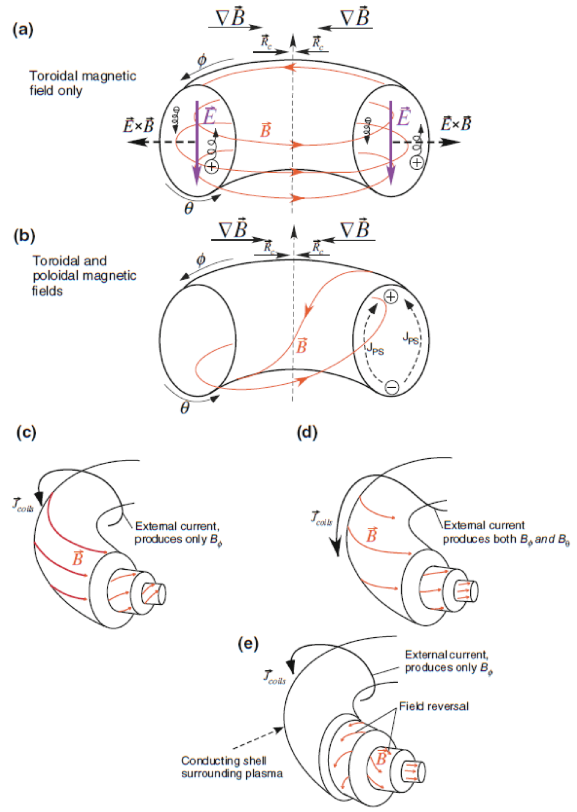

Figure 2.5: **a** A simple toroidal magnetic field produces particle drifts, charge separation and ultimately confinement loss due to the $E \times B$ drift. **b** A helical magnetic field removes charge separation. **c** Tokamak. **d** Stellarator. **e** Reversed Field Pinch (RFP).

on average going in the toroidal direction, ϕ [46]. The poloidal projection of the Pfirsch-Schluter currents, which provide charge cancellation, is shown in Fig. 2.5 [46]. Actually, the three most advanced magnetic confinement configurations make use of this concept: tokamaks, stellarators and reversed field pinches. The difference between these configurations is determined by the magnitude of the poloidal field and by its source. In all cases, magnetic field lines describe helices around nested toroidal surfaces, which form sequence around a single closed curve (i.e. magnetic axis). The helical winding of a field line is a topological quantity which can be characterized by the relation between the toroidal winding of the field line $\delta\phi$ during one poloidal turn around the torus, the so-called safety factor q:

$$q(r) = \frac{\delta\phi}{2\pi} \tag{2.5}$$

The safety factor plays an important role in plasma stability since it can be defined as the inverse of the rotational transform with a normalization chosen such that $q = 1$ corresponds to a topology where the field lines close upon themselves after

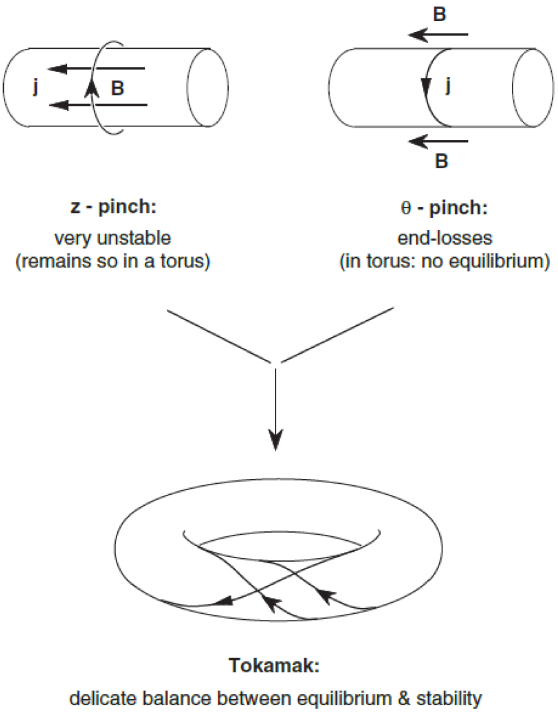

Figure 2.6: Interaction of currents and magnetic fields: a schematic history of plasma confinement experiments.

one revolution the short way and one revolution the long way around the torus. The safety factor is the quantity that is typically used to describe 2-D axisymmetric configurations such as the tokamak and reversed field pinch. As its name implies the "safety factor" is a qualitative indicator of stability. High q is "good" for stability while low q is "bad" [47].

In tokamaks, the poloidal magnetic field is produced by the plasma current and is much smaller compared to the primary toroidal magnetic field. The plasma current is induced by a transformer action where the plasma acts as the secondary transformer winding. The toroidal magnetic field in the tokamak is produced by external currents in the toroidal field coils which encircle vacuum chamber. The main limitation on the stability of tokamak plasma is the Kruskal-Shafranov limit [48] [49], which imposes a limit on the maximum total plasma current. Therefore, keeping the current below the limit results in a "poloidal" magnetic field much smaller than the dominant toroidal magnetic field. Crudely speaking, the tokamak configuration cures the main problems of the z-pinch (its instability due to the curvature of the poloidal magnetic field) and of the θ-pinch (its end losses) by combining them into a single configuration as shown in Fig. 2.6 [42]. In the stellarators, the poloidal magnetic field is produced by currents in external conductors. Thus, plasma current is not necessary for confinement. In the reversed field pinch (RFP) configuration, the

amplitude of the poloidal magnetic field produced by the plasma current is comparable with the toroidal magnetic field. The toroidal magnetic field is produced by external currents as in tokamaks but also by the plasma (dynamo), and it decreases with distance from the plasma center and reverses direction near the plasma edge. The physical relaxation process of MHD instabilities play a key role in the RFP configuration, resulting in a magnetic field weaker compared to the Tokamak and stellarators; furthermore the plasma does not satisfy the Kruskal-Shafranov stability criterion. A conducting shell around the plasma is a way to stabilize the plasma against MHD perturbations. In order to manage these control tasks, RFPs are equipped with a large set of control coils to act on the plasma. In that sense, the RFP is a nice testbed for different control approaches which then can be transferred to the tokamak case. In terms of triple product required for the reactor, the concept is behind modern tokamaks and stellarators [46]. Before focusing on the electromagnetic control of fusion plasmas, which involves the control of a plasma in an equilibrium state, it is necessary to briefly define the plasma equilibrium problem.

2.9 Plasma equilibrium in a magnetic field

The aim of the theory of plasma equilibrium in any configuration is to determine the global magnetic confinement topology and the physical characteristics of the underlying basic equilibrium state for a plasma in a magnetic field. The main assumption that holds for most fusion applications is that this state is assumed to be static, i.e. the background plasma velocity and the time derivative of the other variables vanish. In the tokamak configuration this assumption of static equilibrium is satisfied to a rather high degree of precision [50]. The MHD equations for static equilibrium are about the best satisfied plasma equations we know [50], and a plasma at rest must satisfy them at all:

$$\mathbf{J} \times \mathbf{B} = \nabla p \tag{2.6}$$

$$\nabla \times \mathbf{B} = \mu_0 \mathbf{J} \tag{2.7}$$

$$\nabla \cdot \mathbf{B} = 0 \tag{2.8}$$

As already said in Sect. 2.7, if the pressure balance equation defined in Eq. 2.9, is not satisfied, the plasma would immediately accelerate to huge velocities and there is no way to prevent it from smashing into the vacuum chamber wall. We already know that the configuration adopted to avoid the particle losses along the magnetic field is the toroiodal geometry. The complete equilibrium problem in a toroidal

geometry requires the solution of two qualitatively different problems: the internal pressure balance inside the plasma (i.e. radial pressure balance) and the position control of the plasma column as a whole by means of magnetic fields produced by currents in external coils (i.e toroidal force balance [51] [47]).

The internal pressure balance involves the radial plasma pressure balance which is needed since the hot core of plasma tends to expand radially outward along the minor radius r; the radial equilibrium is achieved by balancing the magnetic force, i.e. Lorentz force $\mathbf{F}_{Lorentz} = \mathbf{J} \times \mathbf{B}$, with the kinetic pressure gradient force, i.e. $\mathbf{F}_{pressure} = -\nabla p$. The final pressure balance is perpendicular to the magnetic field, since parallel component provides tension only along the magnetic field and is not able to counteract the plasma pressure expansion:

$$\nabla_{\perp}(\frac{B^2}{2\mu_0} + p) - \frac{B^2}{\mu_0 R_c} = 0 \tag{2.9}$$

Two general properties of the magnetic field lines, magnetic pressure and magnetic field line tension, play an important role in this balance. The combination of the magnetic field pressure gradient, $-\nabla_{\perp}(\frac{B^2}{2\mu_0})$, and the magnetic field tension, $\frac{B^2}{\mu_0 R_c}$, gives a resultant force, which counteracts plasma pressure force and provides radial force balance Eq. 2.9.

The second problem is the toroidal force balance. It involves multiple contributions that lead to a net outward force along the major radius, R. The first contribution is due to the $1/R$ dependence of the toroidal magnetic field which implies that the plasma column cannot be in equilibrium with it alone; in fact, it produces a toroidal magnetic field pressure that is much larger on the inside, the high field side, than on the outside, the low field side. The effect is partially compensated by the slightly smaller area on the inside but the quadratic dependence of the magnetic pressure dominates. The result is an outward force in the major radius direction, which is larger than the inward force due to magnetic tension [50]. To ensure equilibrium, countermeasures are needed. The first contermeasure is, as already seen in Sect. 2.8, the introduction of an additional magnetic field component by driving a toroidal current in the plasma. The induction of the toroidal plasma current is possible because of the coupling, due to the change in time of the poloidal magnetic flux through the central hole of the torus, to the toroidal current in a set of (primary) windings surrounding the toroidal chamber. The net toroidal current produces a rotational transform that allows toroidal equilibrium by averaging out the vertical "grad-B" drift and the curvature drift. Unfortunately, the presence of a toroidal plasma current has an adverse effect on the equilibrium: the production of an addi-

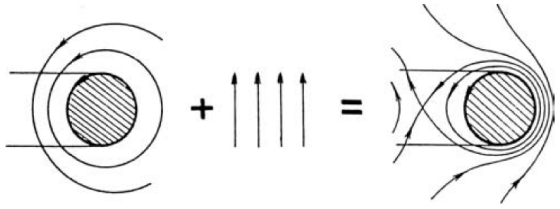

Figure 2.7: The external vertical field effect on plasma equilibrium.

tional outward force, called the *hoop force*, occurs. This force follows from the basic fact of electrodynamics that a current-carrying ring tends to increase its size in order to reduce the magnetic field strength for given magnetic flux trapped inside the ring [50]. The poloidal field also has a $1/r$ dependence and since the tension force on the inner surface is just the product of the magnetic pressure with the surface area it follows that there is a net outward force along the major radius due to the toroidal current. The second countermeasure is the creation of a homogeneous vertical magnetic field, i.e. in the Z-direction, by means of a toroidal current in a set of external poloidal field coils as shown in Fig. 2.7 [52]. Obviously, this counter measure is to be taken together with the first one, since a homogeneous vertical magnetic field has no effect on the toroidal θ-pinch (non-)equilibrium part of the tokamak, but it does have an effect on the toroidal z-pinch part by interacting with the toroidal plasma current [50]. In fact, as highlighted by Fig. 2.7, the external vertical field increases the magnitude of the poloidal field on the outside, but decreases it on the inside. Therefore, the final resulting magnetic pressure will be inward and then able to counteract the *hoop force*.It is clear now where the tokamak configuration flexibility originates: the configurations has three external current parameters, the one controlling the toroidal magnetic field, the one controlling the poloidal magnetic field (indirectly via plasma current) and the one controlling the external vertical field. The last contribution to the outward force is the volume averaged effects of the gradients of the plasma pressure, also known as *tire tube force*. The name refers to the analogous situation in which the internal air pressure stretches the outside surface area of an inflated rubber tire tube more tightly than the inner surface area. It is possible to express the total toroidal outward force in terms of plasma pressure and poloidal field, see [50], by introducing two fundamental plasma global parameters in nuclear fusion: the poloidal beta β_p and the plasma internal inductance, l_i, defined respectevely in Eq. 2.10 and Eq. 2.11. The poloidal beta represents the average plasma pressure compared to the magnetic pressure of the poloidal field at the plasma boundary, i.e. measured in terms of the square of the total toroidal current flowing in the plasma. The internal inductance is a dimensionless quantity

and it is linked to the magnetic energy in the plasma region.

$$\beta_p = \frac{2\mu_0 < p >}{B_p^2(a)} = \frac{8\pi^2 a^2}{\mu_0 I_p^2} < p > \tag{2.10}$$

$$l_i = \frac{< B_p^2 >}{B_p(a)^2} \tag{2.11}$$

The expressions of each outward force contribution added together provides valuable information about the design requirements for the vertical field circuit, in particular how large the vertical field must be to center the plasma as a function of toroidal current and geometry, see [50]:

$$B_V = \frac{\mu_0 I_p}{4\pi R_0}[\beta_p + ln(8R_0/a) + \frac{1}{2}l_i - \frac{3}{2}] \tag{2.12}$$

In terms of equilibrium of a fusion reactor it would seem at this point that as one increases the pressure, one simply has to simultaneously increase the applied vertical field to keep the equilibrium. This turns out to be an incorrect conclusion since the issue is subtle and is related to additional equilibrium constraints imposed by stability considerations (see [42] [50] for details). The global equilibrium description proposed here wants to highlight the fundamental necessity of maintaining a plasma in equilibrium with external controllable actions provided by active coils. The topic is extremely important since only once the forces are balanced, the pressure surfaces and flux surfaces form closed contours, allowing the averaging out of the vertical drifts by the rotational transform. The equilibrium set of equations consisting of Eq. 2.6 - Eq. 2.8, can be also represented conveniently in terms of flux functions, which leads to so-called Grad-Shafranov equation for the poloidal flux [50]. This equation is fundamental in terms of plasma modelling for electromagnetic control purposes as we will see in the next chapter.

2.10 Final considerations on CNF

The research on CNF can be summarized with few numbers: since the 1958 Geneva conference, the plasma temperatures have been increased by a factor of 3000, the plasma confinement $n\tau$ by a factor of 3000 and the figure of merit, i.e. the triple product $nT\tau_E$, being increased by a factor of 10 million. An additional factor of 10 is needed for large scale fusion power production, as shown by the Lawson diagram in Fig. 2.2. The Lawson confinement parameter $n\tau_E$ has been increased to values near that required for breakeven $Q = 1$ in a DT plasma, and within a factor of 10

of that required for a fusion power plant [16]. I would like to report the words of Edward Teller about the future of thermonuclear power at 1958 Geneva conference:

"I believe that thermonuclear energy generation is possible. The problem is not quite easy. I will also say that on the path there may be some little flowers to be picked. Plasma physics has importance in the cosmic arrangement of things, as we heard in Professor Alfven's paper during this session. It may have important technical applications other than energy production. If we want to shoot for the jackpot, for energy production, I think that it can be done, but do not believe that in this century it will be a thing of practical importance. It is likely that we shall be dealing with an intricate machine which is inaccessible to human hands because of radiation and on which all control and maintenance must proceed by remote control. The irradiation of materials by neutrons and gamma rays will cause the properties of these materials to change. Surfaces bombarded by the bremsstrahlung radiation will get heated more fiercely than is the case in any portion of our present nuclear reactors. You can operate the machine to the extent that this one surface can be cooled, the rest of the machine being at a relatively low temperature. These and other difficulties are likely to make the released energy so costly that an economic exploitation of controlled thermonuclear reactions may not turn out to be possible before the end of the 20th century. Nevertheless, the ultimate goals toward which we are working are apt to be highly rewarding. When economic thermonuclear energy production becomes feasible we shall reap a number of important benefits. The fuel of the thermonuclear reactor is cheap and practically inexhaustible so that, if I may put it this way, we have deuterium to burn. Thermonuclear reactors produce less dangerous radioactive materials and, when once brought under control, are not likely to be subjected to dangerous excursions. Therefore, they can be operated more safely than fission reactors. Finally, the interaction of a hot plasma with magnetic fields opens up the way to the direct production of electrical energy. This may be of great practical advantage since high-temperature heat exchangers and many moving parts could be eliminated. Now I have a question: Can all this be done? I think we are at a stage similar to the stage at which flying was about one hundred years ago. There are some wise people now, as there were at that time, who have proved that it cannot be done. I should like to say that those people were perhaps better off because at least they saw the birds. All we can see are the sun and the stars. The sun produces thermonuclear energy by brute force or, what is worse, by sheer inertia. Other people will say that the sun does it with the help of infinite patience. I do not think any physicist wants to go along either of those directions."

Now we don't need to believe that thermonuclear fusion energy generation is

possible, we know it is. This science picked up many flowers on the path, solving problems which 50 years ago appeared to be unsolvable. But Teller's feeling is more truthful today than that day. That is the reason why a moral justification for fusion science is not necessary since each scientist could find the ethic purposes in its efforts of contributing to one of the most difficult goal of human being: the generation of energy out of water.

Chapter 3

Background and literature review: plasma modelling and control

The chapter gives a description of the main topic in which the thesis is inscribed: the electromagnetic modelling and control of magnetically confined fusion plasmas. An introduction to the electromagnetic control is given including a description of the system under investigation (i.e. the tokamak). The importance of the plasma modelling in relation with the control of the system is highlighted and then formulated in terms of a mathematical description of the problem. Finally, an overview of the mathematical models adopted for plasma modelling and control is given, with an emphasis on the perturbed equilibrium approach, which is the one adopted in this thesis.

3.1 Introduction

Control means, in everyday life, producing a desired result. It can be stated that, since 1958, humans are trying to control plasmas in order to get the result they want: nuclear fusion. That could be the first meaning of controlled nuclear fusion. But what we are really trying to control? A system of course, which is a set of self-contained processes under study. In our case the study is focused on plasma by means of all the human products surrounding it and able to confine it. In general, it is possible to consider as a system any plasma in equilibrium and, since a plasma cannot confine itself, this statement implies the existence of a field force structure acting to confine it. In our case this field structure is the result of a device called tokamak. The final goals involved in producing energy from nuclear fusion reactions, are basically two: understanding and controlling the tokamak system.

One of the most important results in modern science, and particularly relevant

in controlled nuclear fusion, is the shift of paradigm from empirical design approach, which dominated the early stage of tokamak experiments, to the formalism called model-based design approach. Even after that, the problem was, and still is, non-trivial mainly because of the nature of the system under investigation: the tokamak. In fact, the twin goals of understanding and controlling are complementary because effective systems control requires that the systems be understood and modeled. The tokamak system is a high order, strongly nonlinear dynamic system, which involves a wide class of physical phenomena. The double goals cannot be satisfied in a whole; the best way to handle them is to separate the tokamak control problem into two major classes: the electromagnetic control, under which this thesis is inscribed, and the plasma kinetic control.

Plasma kinetic control refers to controlling particle feed rates and heating to modify the plasma density, temperature, pressure, and current density. Due to the distributed parameter nature of tokamaks, it is important to control not only spatially averaged values of these physical variables but also their spatial profiles. Energy confinement, stability properties, and the fraction of noninductive current, which is fundamental for steady-state operation, can be improved through control of internal pressure and current profiles [45]. On the other hand, the electromagnetic control refers to controlling the electromagnetic field structure related to the plasma equilibrium properties needed for the experimenters. It can be viewed as the first primordial control mechanism, since it is performed by means of the first agent by which the plasma is sensitive: the magnetic field. The control is performed by many actuators around the plasma itself, whose are the whole set of active coils distributed around the vessel that contains the plasma itself. These coils currents generate the magnetic fields necessary to control the plasma system with feedback control regulation. In practice the control can involve the plasma vertical or horizontal position of the plasma column, the shape of the plasma cross section or the value of the total plasma current. Both the electromagnetic and kinetic control are extremely important for avoiding or stabilizing the MHD instabilities and also for the optimization of tokamak performances.

3.2 The tokamak system

From an electromagnetic point of view, the tokamak system can be modelled by a set of nonlinear partial differential equations describing the interaction between the plasma and the circuits. This will be described in details in Sect. 3.4. On the other hand, the controller design techniques are based upon the availability

of ordinary differential equation (ODE) models, usually linear, time invariant, and of low order. For what concern the modelling of the tokamak system, the main problem is related to the modelling of the physical complex plasma system; for this purpose, it is necessary to introduce physical simplifying assumptions and of using approximate numerical methods to obtain a model detailed enough to catch the principal phenomena involved in the electromagnetic control. Furthermore, the model should be simple enough to make it useful for controller design. Some of these assumptions are related to physical aspects of the system while others concern the level of accuracy of the description of the system that we want to achieve. This is strictly related to the level of complexity of the model itself, e.g. linearized vs nonlinear models or 2D vs 3D models. Nevertheless, all the models assume the same physical assumptions, which has been already introduced in Sect. 2.7, and that are summarized in the following:

1. plasma mass may be neglected, as already discussed in Sect. 2.7, so that the inertial term becomes negligible. This assumption is certainly satisfied on the typical time scale considered in the shape and position control design problem, which is much longer than Alfven time and determined by the electromagnetic times of conductors surrounding the plasma. Physically this assumption means that the plasma equilibrium state exists at each time instant and the plasma moves instantaneously, i.e. with no inertia, through these equilibrium states. Thus, as the system slowly evolves in time, the plasma passes through a continuing sequence of quasi-static MHD equilibria, each satisfying $\mathbf{J} \times \mathbf{B} = \nabla p$. The only dynamic behaviour is in the time evolution of the currents flowing in the conducting structures [45]. It is important to stress that, we use the time-independent form of the momentum equation in static condition ($\mathbf{v} = 0$), see Eq. 2.6. In fact, stationary MHD equilibria ($\mathbf{v} \neq 0$) are not taken into account in the electromagnetic modelling of fusion plasmas, even if substantial equilibrium flows are observed in many current fusion experiments [47]. Even so, the modelling of such stationary equilibrium flows is characterized by a high level of mathematical complexity.

2. plasma behaviour is supposed to be axisymmetric, namely, independent of the toroidal angle. As a consequence of this assumption, our problem is reduced to a two-dimensional one, fully described by the Grad-Shafranov equation and the evolution of plasma equilibrium is determined only by the magnetic field averaged along the toroidal angle.

3. plasma behaviour can be described by means of a finite number of global

parameters, which means a small number of degrees of freedom associated to them. It is assumed that the total plasma current I_p, the poloidal beta β_p and the internal inductance l_i provide a sufficient basis for representing plasma equilibria [53]. Practically it means that the three degrees of freedom are able to characterize the source term of the problem, i.e. the plasma toroidal current density.

These three assumptions define the basis for the so-called perturbed equilibrium models, firstly introduced in [54] and improved later in [44]. The modelling activity is based on this approach by using the computational tools that belongs to this class of models. Turning back to the level of complexity of these models, the main differences are determined by the level of description adopted for representing the region inside the plasma and the region outside of it. Focusing on the plasma description, remembering that all the previous physical assumptions still hold, which means for example that the plasma is intrinsically 2D, the linearized plasma response model obtained through the CREATE-L code [44] will be used. This class of model describes the plasma behaviour, in a neighbourhood of an equilibrium configuration, from an electromagnetic point of view. It is widely used for the plasma shape and position control system design since it can be reformulated in state-space form. Furthermore, the nonlinear axisymmetric time evolution of the plasma equilibrium can be described again inside the previous physical assumptions by means of the CarMa0NL model [55].

Considering the region outside the plasma, the linearized plasma response models can represent the conductors around the plasma, both active and passive, with a 2D description, as in the CREATE-L model, or with a 3D volumetric description, as for the CarMa[56], CarMa0 models [57]. The same considerations holds for the non-linear model which can take into account 3D or 2D conducting structures. Obviously, the increasing level of complexity led to an increasing level of computational time and computational power needed for the simulations.

3.3 The role of electromagnetic control

The electromagnetic control of fusion devices involves several plasma properties that revealed to be fundamental to reach ignition conditions. These properties are basically related to the shape of plasma cross section and can be summarized, in first approximation, in the importance of the elongated cross section in fusion plasmas. As we have seen in Sect. 2.4, the adoption of vertically elongated plasmas led to an improvement of plasma performances in terms of confinement, MHD stability,

optimization of the occupation of the available vacuum chamber volume (this is true only for a "D" shaped vacuum chamber) and so on. Unfortunately, vertically elongated plasmas are vertically unstable; these instabilities grow with Alfven time scale (i.e. μs) and can theoretically be stabilized by surrounding the plasma with a sufficiently close perfectly conductive wall. In real world, the surrounding conducting structures can passively slow the motion of plasma to a timescale related to their resistive magnetic field diffusion time (i.e. ms), making feedback control possible. The vertical position control is the basic system for a fusion device with elongated plasmas. It is not trivial to say that this was not the first type of control system in the past since circular plasmas were performed in the first decades of CNF research. Furthermore, the control of the plasma involves also the shaping of the plasma cross section which plays an important role in several aspects of magnetic confinement physics. In the first experiments on tokamaks with elongated plasmas, feedback control was used only to stabilize the unstable mode. Successively, other geometrical parameters were controlled by feedback; usually the controlled shape geometrical descriptors are the distances between the plasma boundary and the vessel at some specific points. These plasma-wall distances are called 'gaps'. In the first studies on magnetic confinement of fusion plasmas, research efforts concentrated on the radial position control of circular, vertically stable tokamak plasmas. In this case, the plasma cross-section is not elongated and therefore the vertical stabilization is not needed. In traditional tokamak design, a decoupling procedure is applied to the overall magnet system with double purposes: the first aims to obtain a functional definition of the magnet sub-systems by properly selecting the different dynamics of windings related to different control aspects. As example, the ohmic heating winding (i.e. the central solenoid) controls the ohmic magnetic flux and thus the plasma current, while a vertical field circuit controls the plasma major radius. The second aims to impose the same dynamics to different coils of the same sub-system, which means that, for example, different poloidal field coils can be treated as independent SISO channel. In this way, the coil current references can be tracked compensating for electromagnetic interactions between coils of the same system. In general, the control of plasma current, position and shape is fundamental for both circular and elongated plasmas.

3.4 Mathematical modelling of axisymmetric plasma equilibrium

The system under investigation, i.e. the tokamak or any other magnetic fusion device, is a complex system which needs a detailed model describing its complex features. The most obvious of them is the presence of different space regions, each of them characterized by different physical phenomena and being a part of the computational domain. Four main regions can be recognized as shown in Fig. 3.1: the plasma region Ω_p, which is the region occupied by the plasma; the vacuum region Ω_v includes non-conductive and non-magnetic materials, which means that neither plasma nor currents are present in this region; the active coils region Ω_a, which is the region occupied by the conductors that drive the currents of the magnet system, and finally the passive conducting structures region Ω_c, which is the region occupied by all the conductors that are not fed by applied voltages. The electromagnetic modelling of the tokamak system concerns the description of the relevant fields in all the three regions as we will see in a while.

The assumption of axial symmetry along the toroidal angle consists, in the cylindrical coordinate system (R, ϕ, Z) shown in Fig. 3.2, that the magnetic field is independent of the toroidal angle. This assumption led to formulate the vector fields of the tokamak system, i.e. the magnetic field $\mathbf{B}$ and the current density $\mathbf{J}$, as functions of scalar fields, respectively the poloidal flux function $\psi(R, Z)$ and the poloidal current function $F(R, Z)$ (or toroidal magnetic field function), by simply imposing

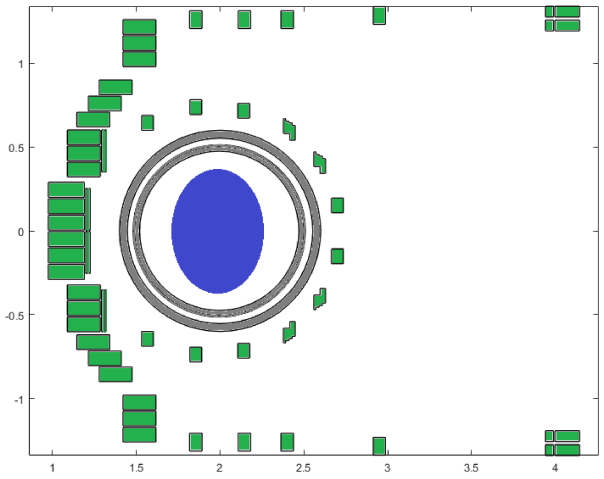

Figure 3.1: The main regions of a tokamak machine described with different colors; in blue the plasma region Ω_p, in grey the passive conducting structure region Ω_c, in green the active coils region Ω_a and in white the vacuum region Ω_v

the divergence free condition on **B** and **J** and the axisymmetry of the system:

$$\mathbf{B}_p = \frac{1}{R}\nabla\psi \times \mathbf{e}_\phi = -\frac{1}{R}\frac{\partial\psi}{\partial z}\mathbf{e}_R + \frac{1}{R}\frac{\partial\psi}{\partial R}\mathbf{e}_z \tag{3.1}$$

$$\mathbf{J}_p = \frac{1}{\mu_0 R}\nabla F \times \mathbf{e}_\phi = -\frac{1}{\mu_0 R}\frac{\partial F}{\partial z}\mathbf{e}_R + \frac{1}{\mu_0 R}\frac{\partial F}{\partial R}\mathbf{e}_z \tag{3.2}$$

Both of these functions are defined apart from an additive constant which can be chosen such that ψ represent the poloidal magnetic flux per radian and F the poloidal current function both within a circular contour defined by $R = const$ and $Z = const$. The poloidal flux $\psi(R, Z)$ per radian is the magnetic flux with the circumference obtained by revolving the point (R, Z) around the $Z-$axis and normalized to 2π:

$$\psi = \frac{1}{2\pi}\int_0^R \int_0^{2\pi} B_z(\rho, Z)d\phi d\rho = \int_0^R B_z(\rho, Z)d\rho \tag{3.3}$$

This flux can be viewed as the flux of the central solenoid which serves to maintain the toroidal current in the plasma and does not affect the plasma equilibrium. The poloidal current function $F(R, Z)$, is the poloidal current linked with the circumference obtained by revolving the point (R, Z) around the $z-$axis and normalized to 2π:

$$F = \frac{1}{2\pi}\oint B d\mathbf{l}_\phi = RB_\phi \tag{3.4}$$

The poloidal current function can be viewed as the total current in the windings which produce the toroidal magnetic field. Therefore, the magnetic field can be written as:

$$\mathbf{B} = \frac{1}{R}\nabla\psi \times \mathbf{e}_\phi + B_\phi \mathbf{e}_\phi \tag{3.5}$$

in which the first term on the right-hand side of Eq. 3.5 gives the projection of the

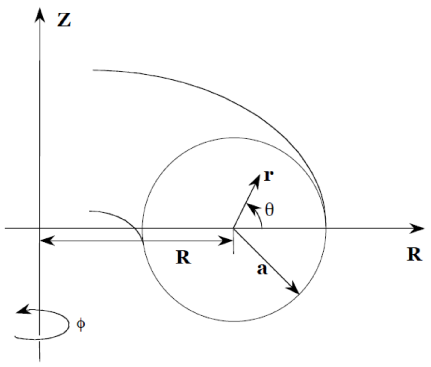

Figure 3.2: The system of toroidal (r, θ, ϕ) and cylindrical coordinates (R, ϕ, Z)

magnetic field on the poloidal plane (poloidal magnetic field), while the second term gives the toroidal component (toroidal magnetic inductance field).

This formulation is fundamental since it permits to model all the space regions of the tokamak system with the same mathematical structure of equations; the only variations from each region would affect only the source term. The equation is easily obtained from Ampere's law by substituting Eq. 3.5 in it, and by introducing the differential elliptic operator $\triangle^*$, one finds:

$$\mathbf{J} = -\mu_0^{-1}\nabla \times (\frac{1}{R}\nabla\psi \times \mathbf{e}_\phi + B_\phi \mathbf{e}_\phi) = -\mu_0^{-1}\frac{1}{R}\triangle^*\psi\ \mathbf{e}_\phi + \frac{1}{R}\nabla F \times \mathbf{e}_\phi \tag{3.6}$$

where:

$$\triangle^*\psi = R^2\nabla\cdot(\frac{1}{R^2}\nabla\psi) = R\frac{\partial}{\partial R}(\frac{1}{R}\frac{\partial}{\partial R}\psi) + \frac{\partial^2}{\partial z^2}\psi \tag{3.7}$$

By projecting Eq. 3.6 along the toroidal direction we obtain the final equation of interest:

$$\triangle^*\psi = -\mu_0 R J_\phi \tag{3.8}$$

Eq. 3.8 is a partial differential equation for the poloidal flux function. This equations is able to model all the space regions involved in the system, the active coils with their currents, the passive conductors driving the eddy currents, the vacuum field and the plasma region. What varies is only the source term. The already mentioned Grad-Shafranov equation is a special case of Eq. 3.8 where the source term , i.e. the toroidal plasma current density, is defined as follow:

$$J_\phi = -R\frac{dp}{d\psi} - \frac{1}{\mu_0 R}F\frac{dF}{d\psi} \tag{3.9}$$

This can be obtained by simple considerations on the force equilibrium equation Eq. 2.6; the field lines of the magnetic field and of the current density lie on isobaric surfaces (surfaces where the pressure is constant). This is easily highlighted by taking the scalar product between $\mathbf{B}$ and ∇p. As a consequence of the fact that the magnetic field lines lie on the isobaric surfaces, these surfaces are also called magnetic surfaces. The limiting magnetic surface, which approaches a single magnetic line where the pressure is maximum, is called the magnetic axis. Furthermore these surfaces are also constant poloidal flux surfaces as stated by $\mathbf{B}\cdot\nabla\psi = 0$. Therefore, on the poloidal plane the current density, the magnetic field and the pressure are constant on each flux surface and they can be expressed, again, as a function of the

scalar function poloidal flux. The detailed derivation of the Grad-shafranov equation can be found in [50].

The modelling of plasma equilibrium is completely defined by the following set of nonlinear partial differential equations:

$$\triangle^* \psi = \begin{cases} 0, & R \in \Omega_v \\ \mu_0 R J_\phi, & R \in \Omega_a \cup \Omega_c \\ -\mu_0 R^2 \dfrac{dp}{d\psi} - F\dfrac{dF}{d\psi}, & R \in \Omega_p \end{cases} \tag{3.10}$$

The problem can be directly solved by properly assign the source term for each region of solution, i.e. the current density; see [45] for details on the formulation. Furthermore, in order to find a unique solution, a set of boundary conditions must be provided. The boundary conditions are a consequence of the poloidal flux definition, including a regularity assumption of the magnetic field. It is important to point out that the model describing the electromagnetic behaviour of a tokamak machine in the absence of the plasma is linear; it is clearly shown in Eq. 3.10, that the presence of the plasma makes the model nonlinear. The source of nonlinearities are basically two: the plasma current density, which is a function of the unknown ψ, and the free boundary of the plasma which is a nonlinearity itself. In fact, the boundary of the plasma region is usually unknown and therefore also the plasma region which is one of the solution domains. In other words this is a free boundary problem, the boundary $\partial\Omega_p$ of Ω_p being one of the unknowns to be determined.

Two class of problems can be described by the same set of equations Eq. 3.10: the static MHD equilibrium problem and the evolutionary MHD equilibrium problem. The solution of the static MHD equilibrium problem requires the prescription of the plasma current, the active coil currents, the plasma current density profile parameters and the proper boundary conditions, all referred to a single time instant (i.e. the equilibrium time instant). On the other hand, the evolutionary MHD equilibrium problem relates to a time evolution of the plasma equilibrium in the quasi-static approximation; the solution in time of Eq. 3.10 requires the definition, at each time instant, of the plasma current and the external currents, which are given by circuit equation, as well as boundary and initial conditions. The initial condition provides the magnetic flux distribution at the starting time.

These two class of equilibrium problems are fundamental in the plasma modelling for control purposes; in particular the evolutionary MHD equilibrium problem is the usual starting point for the derivation of a linearized plasma response model, as we will see in the next sections. Furthermore, the set of equations describes also a wide

class of plasma equilibrium problem solvers which can be direct or inverse solvers, free or fixed boundary and so on. Details on plasma equilibrium problems can be found in [58] [59].

The difficulties in finding an analytical solution to this problem for the real device geometry and the intrinsic nonlinear nature of the problem requires the use of numerical approaches for the determination of a solution. Various numerical algorithms can be used to treat the nonlinearities (Picard, Newton, ...). Furthermore, the original partial differential equation problem can be turned into a discrete problem by discretizing the domain of the solution in cells (or elements) in order to obtain an algebraic formulation ready to be solved by computational numerical methods; for example, a "weak" formulation of the problem can be given (e.g. in the finite element method), as well as working out the linearized problem which is useful in the numerical solution (e.g. Newton's method), in the control problem and in the study of stability of displacements of the plasma [60]. Alternatively, global algebraic formulation or integral fromulations can be given. The reader can find more details about computational methods for plasma equilibrium problem in [50] and [61].

3.5 Plasma current density parametrization

For what concerns the plasma region, the toroidal current density is completely determined by the assignment of the functions $p(\psi)$ and $F(\psi)$, as stated by Eq. 3.9. Although the problem of determining this current density could be, in principle, included in the main problem defined by Eq. 3.10, by adding a certain number of equations related to the diffusion and to the transport of the plasma particles, it is simpler, in terms of modelling and computational cost, to adopt an approach based on experimental evidence and assign J_ϕ inside the plasma as a parameterized function [60]. It has been shown, see [53], that the toroidal current density for circular plasmas can be expressed as a function of r/a where a is the minor radius of the plasma and r is the minor radius of the magnetic surface under consideration. Furthermore it can be extended to arbitrary cross-sections by using the following parameterization [60]:

$$J_\phi = \lambda \left[\beta_0 \frac{R}{R_0} + (1-\beta_0)\frac{R_0}{R} \right] (1-\bar{\psi}^{\alpha_M})^{\alpha_N} \tag{3.11}$$

where

$$\bar{\psi} = \frac{\psi - \psi_a}{\psi_b - \psi_a} \tag{3.12}$$

is the normalized poloidal flux, ψ_b and ψ_a being the poloidal flux at the plasma boundary and at the magnetic axis respectevely, R_0 is the characteristic radius of the device (typically the centre of the vacuum chamber). The four parameters used to characterize the toroidal current density are λ, β_0, α_M, α_N and they can be respectively associated with the physical quantities I_p, β_p, l_i and q_0 (i.e. the safety factor at magnetic axis). The total plasma current is the current flowing through the poloidal plane in the plasma region; the parameter λ is a normalization factor specified in terms of the total current I_p, i.e. $Ip = \int J(\psi)dA$. The poloidal beta, previously defined in Eq. 2.10, is a measure of the efficiency of the plasma confinement since it represent the ratio between the pressure energy and the magnetic energy in the plasma. The internal inductance, already defined in Eq. 2.11, is a dimensionless quantity (i.e. internal inductance of the plasma per unit length) and it is linked to the magnetic energy in the plasma region. It also characterizes the "peakedness" nature of the current density profile: for a flat current density profile $l_i = 0.5$, while in the case of parabolic current $l_i = 11/12$. In general, much higher is the value assumed by l_i, the more the current profile is spiked.

The problem that we wish to solve, which is strictly related to plasma modelling for electromagnetic control purposes, is the direct equilibrium problem; given the parameters β_0, α_M, α_N, the currents I_i in the active coils and the total plasma current I_p , finding the solution of Eq. 3.10 means finding the triplet $(\psi(R,Z), \partial\Omega_p, \lambda)$ meaning the poloidal flux $\psi(R,Z)$ in all the computational domain, the plasma boundary $\partial\Omega_p$ and the λ parameter, satisfying the equations Eq. 3.10 with the associated boundary conditions. This allows to characterize the plasma equilibrium. It is evident how much the determination of the degrees of freedom (β_0, α_M, α_N) is fundamental for the correct equilibrium reconstruction. This topic, again with the current density parametrization, will be discussed deeply in Chap. 6.

3.6 Literature review

The derivation of linearized mathematical model describing the interaction between the plasma and the surrounding conducting circuits was of fundamental importance in the development of the plasma electromagnetic modelling and control field of research. Before the model based approach, the modelling and control of plasma was based on empirical observations made through the development of new experiments based on the previous one already existing. On the other hand, the model based approach is characterized by the linearization of the problem, for example the one defined in Eq. 3.10; it is very useful as much for the numerical solution of the prob-

lem as for the study of the linear stability of displacements of the plasma or for the solution of control problems such as position control. The linearization procedure provides the two main approaches in plasma response models for electromagnetic control purposes: the rigid displacement model and the perturbed equilibrium approach.

The modelling activity related to the plasma equilibrium problem shown before, has only recently been considered in its entirety in relation of electromagnetic control. In fact, the first plasma control models did not consider the plasma region as described by Grad-Shafranov equation, since these models were preferred to simplify the problem by approximating the plasma to a rigid current carrying ring, i.e. the rigid displacement model. The rigid displacement model is based on plasma circuital model or simply circuit model, used for modelling the plasma-vessel-coils system, in which the plasma is modelled as a rigid wire loop, or multifilament wired loops, free to move vertically. Neglecting the plasma mass the plasma vertical motions are described by a lumped parameter model. A circuit model is used in [62] to analyse a feedback system consisting of a single passive coil and an active feedback coil. It is proved that proportional feedback of the plasma vertical position can stabilize the system, provided that the shielding effect of the passive coil, measured by the mutual inductance, is sufficiently small [45]. However, this result is not quantitatively extendable to a massive structure of passive conductors[45]. The main limitation of the rigid displacement model is that the plasma is considered as rigid body with a single degree of freedom: this approach does not account for plasma shape deformations, which involve modified force equilibria. Also the multifilament model does not eliminate the main problem of the circuit approach, namely, that the plasma is modelled as a rigid body with a single degree of freedom since it can only impose one global constraint, namely total vertical force balance, and does not guarantee local equilibrium of the forces [45]. Furthermore, the inconsistency of the rigid displacement with local MHD equilibrium yields to an incorrect estimation of the growth rate especially for triangular plasmas. In addition, the rigid displacement models are based on a knowledge of the vertical plasma position, whereas, in practice, only flux measurements are available [54]

The second approach to model plasma behaviour, i.e. the non-rigid displacement model, simple but reliable for description of plasma response and fundamental for the electromagnetic control task is the so-called perturbed equilibrium approach.

3.7 The linearized perturbed equilibrium plasma response model

The linearized perturbed equilibrium plasma response model is a linearized non-rigid model of the vertical plasma displacement firstly introduced in [54] and then improved in [44]. The model describes the plasma behaviour, in a neighbourhood of an equilibrium configuration, from an electromagnetic point of view, and permits to obtain a linearized model in the state space form able to reproduce the features of the plasma that are relevant to the control of current, position and shape. The main assumptions of the perturbed equilibrium approach were already introduced, for what concerns the physical aspects, in Sect. 3.2; now we list the assumptions involving the circuits and surrounding structures:

1. The mathematical model for the conducting structures is the standard eddy current model, i.e., the quasi-stationary Maxwell equations $\partial D/\partial t \to 0$.

2. The time evolution of the coil currents is described by the standard circuit equations (with zero applied voltages for passive circuits).

3. The use of integral formulations allows for a unified treatment of circuits and eddy currents (even in the 3D case).

The model is usually derived from the evolutionary MHD equilibrium which consists of the usual circuit equations coupled with the Grad-Shafranov equation for the plasma which can be viewed as a constraint as we will see in a while. In fact, the circuit equations consist in the time derivative of the flux linked with the circuits plus the resistive contribution for each circuit, both active and passive; this set of circuit equations can be written in matrix form as stated by Eq. 3.13:

$$L\dot{x} + Rx = u \tag{3.13}$$

where L is the inductance matrix, R is the resistance matrix, x is the vector of the circuit currents, u is the vector of circuit voltages and $\dot{x}$ represent the derivative of the variable x with respect of time t. The inductance matrix L has the self-inductance coefficients for each circuit on its diagonal and the mutual inductances between different circuits off diagonal. The resistance matrix R is diagonal, representing the resistance of each circuit. A detailed description of the computation and construction of matrices L and R can be found in [44]. Finally, a voltage source is present only on the active circuits, while the passive conductors have zero value. Furthermore, Eq. 3.13 represent a system of circuits with inductors, resistors, and

voltage sources that can be used to control the active circuits currents; the time variations of these currents are opposed by the eddy currents induced in the conducting structures. Note that once the vector x is assigned, it is possible to evaluate the poloidal flux function at each point of the poloidal plane without considering the plasma contribution, i.e. vacuum solution. In fact, thanks to the numerical formulation adopted to solve the problem, assigning x is equivalent to assign the toroidal current density on the conductors, see [45] for a detailed description.

Now, it is fundamental to take into account the effect of the plasma on all the conductors: an additional electromotive force could appear on each circuit as a consequence of the time variations of the current density inside the plasma. These time variations of the plasma state are due to changes in the plasma current internal profile or also to the movements of the plasma ring. This led to consider the plasma as a circuit coupled to the circuits of active and passive conductors. Therefore, an additional source term defining the dynamic behaviour of the currents flowing in the conducting structures in the presence of the plasma must be added, which is the variation of the flux produced by the plasma on these structures ψ_p. This quantity, ψ_p, can be calculated by solving an equilibrium problem when the vectors x, $W = [\alpha_M, \alpha_N, \beta_0]$, and the total plasma current I_p have been assigned. The new matrix equation for the dynamic behaviour of the currents flowing in the circuits is:

$$L\dot{x} + Rx + \dot{\psi}_p(x, W, I_p) = u \tag{3.14}$$

In other words, these circuits equations must be linked to the MHD Grad-Shafranov equilibrium equation by imposing it as a constraint that has to be treated numerically (since it has an analytical solution only for small special cases). This is the main difference between the rigid-displacement models and the perturbed equilibrium approach. The MHD Grad-Shafranov equilibrium is defined by the currents in the external circuits, the total plasma current and the toroidal current density, which by assumption is defined by means of three global parameters $\alpha_M, \alpha_N, \beta_0$. This means that providing these information, it is possible to compute every information of the plasma equilibrium problem and therefore also the plasma flux linked with the circuits ψ_p.

Assuming to have a plasma equilibrium point, defined with pedix 0, it is possible to linearize Eq. 3.14 in the neighbourhood of the equilibrium point (x_0, W_0, I_{p0}); a detailed analysis of the linearization procedure can be found in [45] [60] [44]. The final linearized model is:

$$L^*\delta\dot{x} + R\delta x + E\delta\dot{W} = B\delta u \tag{3.15}$$

where the L^* matrix is called the modified inductance matrix, meaning modified by the presence of the plasma. This model gives the evolution of the currents in the conducting structures and of the total plasma current, where x are the variables playing the role of state variables of the plant to be controlled. The state space form of the plasma linearized model is:

$$\delta\dot{x} = A\delta x + B\delta u + E\delta\dot{W} \tag{3.16}$$

Eq. 3.16 has to be completed with the static equation relating the inputs (the u vector) and the state variables x to the output variables to be controlled y, see [44]:

$$\delta y = C\delta x + D\delta u + F\delta W \tag{3.17}$$

The matrices in Eq. 3.15 are calculated by using numerical codes; the dimension of the state space vector x depends on the number of finite elements used to discretize the tokamak structure. Here can be viewed the role played by the computational tools with different level of complexity (e.g. 2D and 3D models). Another important point, in which it is possible to see the plasma modelling impact, is that the state space matrices strongly depend on the plasma configuration; the state space matrices are time varying in the various phases of the plasma discharge scenario and they may also be discontinuous in time for example when nonlinear phenomena, such as transition from limiter to divertor configuration, occurs.

Chapter 4

The RFX-mod tokamak

In this chapter, a brief description of the RFX-mod device is given, with particular emphasis on its operations as low-current tokamak. Firstly, we introduce the RFX-mod as RFP experiment. Secondly, we introduce RFX-mod as a magnetic confinement device by showing its main technical aspects which allows it to operate also as a tokamak. Thirdly, the RFX-mod circular tokamak activity and its results are briefly described. Finally, the RFX-mod shaped tokamak is described including results and perspectives.

4.1 The RFX-mod experiment

RFX-mod is the largest Reversed Field Pinch (RFP) device in the world (Fig. 4.1), able to confine a 9 m^3 plasma, with temperature of about 1.4 keV, within a toroidal vessel with 2 m and 0.459 m major and minor radii respectively. Similarly to a tokamak, the RFP carries a toroidal plasma current confined by an equilibrium magnetic field whose main components are toroidal and poloidal. Contrarily to a tokamak, the RFP confines the same plasma current with an average toroidal field which is a factor of ten smaller than that in a tokamak. Thus, poloidal and toroidal magnetic fields are comparable in amplitude. Furthermore, the toroidal magnetic field produced by the external coils is extremely small compared with the one in a tokamak, of the order of some mT during the flat-top reversal phase in a typical MA RFP plasma discharge, since the field is mainly produced through a self-organization process by currents flowing in the plasma itself. In fact, when the plasma current is raised above $1MA$, the plasma self-organizes spontaneously into a helical equilibrium configuration (i.e. QSH, quasi-single-helicity). Moreover, the self-organization can proceed up to the point where the magnetic axis becomes helical and the plasma enters in a state where the core of the equilibrium is helical, while the edge is almost

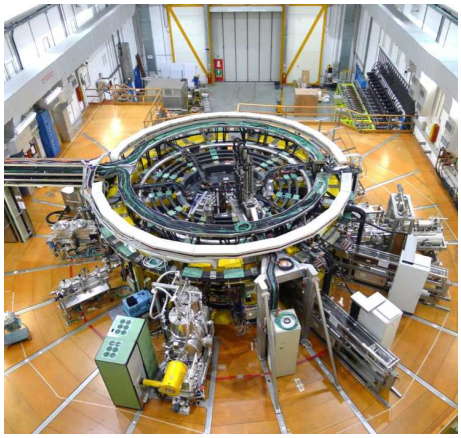

Figure 4.1: The RFX-mod experiment

axisymmetric (i.e. SHAx state) [63]. It is important to highlight these results because they had, and still have, a multiple impact on the RFX-mod scientific programme and, more important, on the fusion scientific community. The first point to stress is strictly related to the nature of the RFX-mod device: the Reversed Field Pinch configuration; because of its purely ohmic heated nature, and its confinement increases with plasma current [63], the assessment of fusion perspectives of the RFP configuration requires a careful exploration of the multi-MA regime. In this effort, the control of plasma quantities is a key requirement for successful operation at high performance. In this field, the active control of plasma equilibrium and stability is a key topic for every fusion magnetic configuration, thus the RFP knowledge of this field can be easily translated to tokamak and stellarator communities. In addition, as we have seen, the advanced confinement helical states reached by RFX-mod have three-dimensional features that are relevant for stellarator configurations. The second point of view, which is the most important since it involves directly this thesis, is that RFX-mod is, in engineering speaking, an extremely flexible device. It means, for example, that the toroidal field circuit can provide toroidal magnetic field far in excess of that needed for RFP operation. In other words, RFX-mod can be operated also as medium size low current tokamak. Many similarities exist between RFP and tokamak, and they are all exhibited in the RFX-mod device which is the only experiment in the world able to confine plasmas in both the magnetic configurations. It is in this framework that this thesis takes place.

4.2 The RFX-mod device

A RFP plasma requires both toroidal and poloidal components of magnetic field, provided respectively by the toroidal field winding (TFW) and by the poloidal field

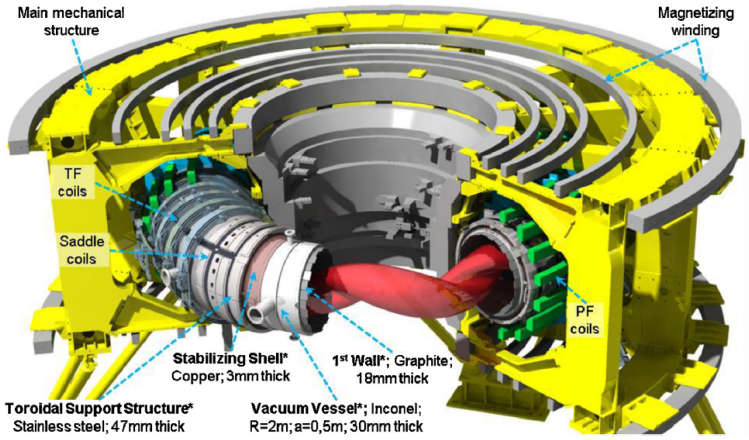

Figure 4.2: Overview of the RFX-mod device

winding (PFW) plus the plasma current itself. RFX-mod is provided with two poloidal field windings: the field shaping winding (FSW), devoted to controlling the equilibrium field, and the ohmic heating winding (OHW) devoted to generating the flux swing. A large flux swing must be provided by the OHW, since the toroidal loop voltage must be high during the plasma current rise and relatively high also during the flat top phase. A maximum current of 50 kA can be driven by the OHW able to produce a maximum flux swing of 15 Wb. An air core design was adopted, mainly for the better stray field control that it enables [64]. The TFW system consists of 48 coils uniformly distributed along the toroidal direction and subdivided into twelve sectors, each consisting of four coils permanently connected in series; each group is connected to an independently controlled power supply unit. The FSW system, the most important for equilibrium and control, is made of equal coils symmetrically placed with respect to the equatorial plane and connected in series to form eight FS sectors. The two coils of each couple are connected in series and their current is controlled independently, by means of a thyristor power supply, so that a wide range of field configurations can be achieved while the total magnetomotive force of the winding is kept equal to the plasma current [65], thus providing the required high operational flexibility. Each coil has 24 turns. This number gives the electromagnetic parameters L and M which provide a built-in balance of the voltage induced in the FS coils and in the OH sectors, which are connected in parallel. In this way the FS currents naturally approach the required values, minimizing the voltage and power demand from the thyristor power supplies [64]. The maximum operating current in coil $FS8$ is 6.25 kA, while the inner coils have lower currents: the peak current averaged among all coils is 5.2 kA. The saddle coil system is constituted by a set of 192 saddle coils, subdivided into 4 toroidal arrays each of them consisting of 48 coils, mounted inside grooves machined in the outer surface

of the toroidal support structure to carry out active control experiments of MHD modes. Each coil is fed by its own power supply, which can perform an independent control of the current in the coil. RFX-mod is also characterized by three passive conducting structures surrounding the plasma. A thin ($3mm$) passive stabilizing shell made of copper, characterized by a resistive penetration time for the vertical magnetic field (m= 1,n= 0) of about 50 ms, that is much shorter than the discharge duration. The shell surrounds the vacuum vessel to assure the passive stabilization of MHD modes. The vacuum vessel chamber is composed by 72 elements made of INCONEL625, welded together equipped with a total number of 96 ports for gas input, vacuum pumping and diagnostic systems. Finally, the stainless steel Toroidal Support Structure (TSS) surrounds the vessel and the shell, providing the support for the saddle coil system, the toroidal field windings and the rings supporting the field shaping coils. The TSS structure is 47 mm thick and consists of 4 parts with two insulated butt joint poloidal gaps and one insulated equatorial gap (the inner one). A complete schematic overview of the RFX-mod passive conducting system is represented in Fig. 4.2 [66].

4.3 The RFX-mod circular tokamak

The tokamak configuration is characterized by a large toroidal field and a small poloidal field with an aspect ratio (R_0/a) typically of ~ 3. The combination of field ratio and aspect ratio leads to a safety factor satisfying the Kruskal-Shafranov limit $q \geq 1$, which represent an MHD limit to the maximum toroidal current that can flow in the plasma; violation of the current limit leads to violent MHD unstable behavior that rapidly terminates the plasma and can in fact cause physical damage to the surrounding vacuum chamber [47]. On the other hand, no stability limitations exist for the safety factor in the RFP configuration, therefore no constraints on the aspect ratio of the machine exist. Thus, the RFP is in general considered as a large aspect ratio circular cross section configuration. RFX-mod is characterized by a relatively small aspect ratio of $R_0/a = 2.0/0.459 \sim 4.4$ which had been chosen in order to limit many engineering parameters [64]. Curiously, this value of aspect ratio is exactly in the middle of 3 and 5 which are the typical values for the aspect ratio of an ohmic tokamak and an RFP respectively. As introduced in the previous section, the RFX-mod toroidal field winding are very flexible, able to drive a maximum current of 18 kA at which correspond a maximum toroidal bias field of 0.7 T which is far in excess of that needed for RFP operation. While operating as RFP, the RFX-mod plasma has a circular cross section but, thanks to the significant flexibility of power

supplies and of the magnet system, the device can drive also circular and shaped tokamak plasmas. In fact RFX-mod is equipped with a close fitting Field Shaping Winding (FSW), made up of 8 couples of Field Shaping Coils (FSC) symmetrically arranged with respect to the equatorial plane and whose connection with power supplies can be modified. The overall passive conducting structures (i.e. shell, vacuum vessel and TSS) are characterized by a total time constant of 65 ms, which allowed to design the plasma horizontal position control system based on FSW currents [67]. The plasma position control system has been used also to start the circular tokamak operations. The operational space was defined by the aspect ratio of the machine (i.e. 4.3) and the toroidal field values allowed by the TF windings (i.e. up to $0.7T$): it was possible to operate the device as low current circular tokamak with plasma current up to 150 kA, safety factor up to 3 and discharge duration up to $1s$. The main scientific goal was to apply the knowledge acquired on active control of MHD modes in the RFP configuration in order to exploit the active control system directly in the tokamak configuration. This led to the possibility of reaching stable operation at edge safety factor below 2, opening the possibility of low-q scenarios for tokamaks device which were always refused because of the stability issues posed by the m= 2, n= 1 unstable kink mode. Active feedback stabilization of m= 2, n= 1 mode was obtained in circular discharges at $1.3 \leq q(a) \leq 2$ [68]; it was shown that in the absence of active control, the $(2, 1)$ current driven RWM led to a disruption with $q_{edge} > 2$ while when the feedback control is applied the mode is suppressed for the whole pulse duration at $q_{edge} = 1.8$. An additional important result in terms of feedback control was that the mode control is successful only if the aliasing of the sideband harmonic generated by the feedback coils is subtracted from the radial field measurements (clean mode control, CMC technique [69]). In any event, from the perspective of MHD equilibrium and stability it is worth noting that the regime of operation of RFX-mod as a tokamak corresponds to the so-called ohmic tokamak, in which the plasma is heated entirely by the induced ohmic plasma current. Here, the plasma acts as the secondary of a transformer. In this regime the plasma β is low and the toroidal field is slightly paramagnetic $B_\phi(0) \sim B_\phi(a)$ [47] while in RFPs the toroidal field is highly paramagnetic. Since the plasma resistivity decreases with increasing electron temperature (i.e., $\eta \sim T^{-3/2}$) there is a practical upper limit to how high the temperature can be raised solely by ohmic heating: $T_{max} \sim 3 - 5\ keV$ [47].

The typical operations of a low$-\beta$ tokamak are quantitative similar to an RFP, but qualitatively not. Assuming t_0 as the time instant in which the plasma current exist, initially, at time $t < t_0$, the premagnetisation phase exists: the toroidal field

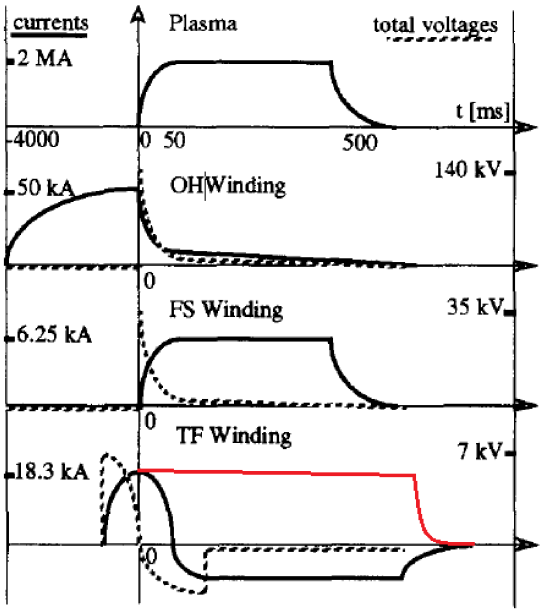

Figure 4.3: Typical RFP plasma discharge operations; the toroidal field behaviour of Tokamak operation is represented in red

winding are charged up leading to a large steady state B_ϕ field as it can be seen from Fig. 4.3. Also the ohmic heating winding, the coils responsible for the flux swing, are charged up. At time t_0, the flux swing occurs by decreasing the ohmic heating current through the transfer resistor producing a flux swing and a loop voltage: the plasma breakdown occurs and the plasma current rises. After a short time, on the order of milliseconds, the plasma becomes fully ionized and achieves a steady state power balance between ohmic heating and thermal conduction losses. The plasma is maintained in quasi-steady state as long as the flux continues to swing at a constant rate in the primary of the transformer. This is the requirement to induce a constant (in time) toroidal electric field in the plasma which drives the quasi-steady state toroidal current. Once the transformer runs out of volt-seconds the toroidal current can no longer be maintained and the plasma decays away. The time period of quasi-steady state current is known as the "flat-top period" and it is here that most of the interesting physics takes place [47]. In the RFP, during the whole plasma current rise phase, the toroidal field current decreases to zero and then reverses; the FS currents rise together with I_p, providing equilibrium field and magnetomotive force (MMF) compensation. At $t \sim t_1$ the plasma current reaches its flat-top value and the power supplies are turned on in order to sustain the plasma current and, to sustain the reversed toroidal field and to provide equilibrium fields: this arrangement is maintained until the plasma current starts to decay. On the other hand, the tokamak toroidal field is kept constant during the whole discharge

as it can be noticed by the red behaviour in Fig. 4.3. Note that, for both the configurations, while the current is ramping up and during flat top operation the current in the vertical field coils must be carefully programmed to hold the plasma in toroidal force balance. The shaping coils are also carefully programmed to generate the desired cross sectional shape of the plasma which was chosen as circular in the early days of fusion research, but now usually corresponds to an elongated, outward pointing "D" [47].

In current high β tokamak experiments the plasma always passes through an ohmic phase before the auxiliary heating is applied. Ohmic heating is a simple way to produce a relatively high-temperature, high-density, high-quality target plasma into which auxiliary power can be efficiently injected and absorbed [47]. Because of its many advantages in terms of plasma performance, the shaped plasma cross section is the main feature of high β tokamak operations. This moved to the study of non-circular magnetic configurations for the RFX-mod tokamak operations.

4.4 The RFX-mod shaped tokamak

The achievement of H-mode regime in RFX-mod and the possibility of exploiting the highly flexible MHD active control system to perform tokamak plasma control experiments (e.g. ELMs mitigation, edge transport control by means of resonant magnetic perturbation RMP, ...) is a goal of RFX-mod tokamak experimental activity. In order to increase the studies addressed in the circular tokamak operation, the achievement of non-circular magnetic configurations was necessarily envisaged. In fact, the main requirement to obtain an H-mode regime is to achieve magnetic configurations with internal X-points, i.e. divertor-like. Thus, the RFX-mod operated as shaped tokamak, with non-circular cross section plasmas including double null (DN) configurations and single null one, both upper (USN) and lower (LSN). Firstly, by properly re-connecting the FSW but keeping the up-down symmetry of the magnetic field system, elliptical shape plasma and double null magnetic configurations were initially accomplished [1]. Based on these results, the design and implementation of a feedback shape control for Single Null (SN) discharges, requiring a deeper modification of the FSW series connections and in particular to break the up-down symmetry, was performed. In the case of lower Single Null (LSN) configurations, the plasma equilibirum was commited only to the field shaping winding (FSW) and magnetizing winding (MW) currents with the central upper field shaping coils, i.e. FS4U and FS5U in Fig. 4.4 [1], disconnected. In addition to the disconnection of these coils, the currents in FS3, FS4L and FS8 are reversed with

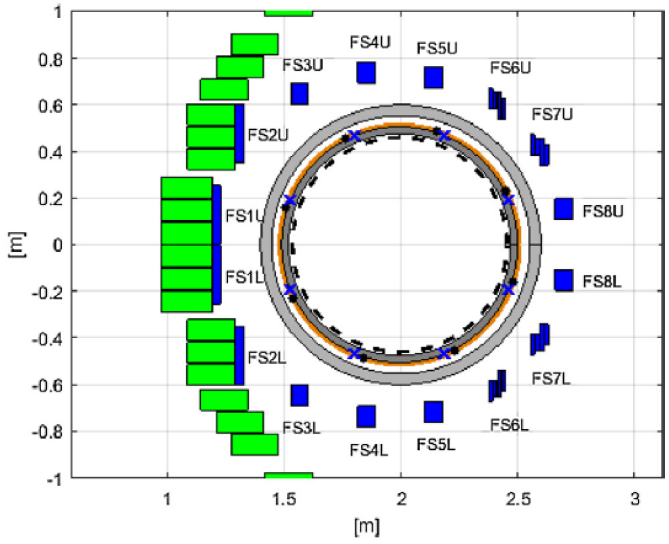

Figure 4.4: RFX-mod partial poloidal cross section: MW (green), FSW (blue), vacuum vessel (dark grey), copper shell (orange), toroidal support structure (light grey), first wall (blackdashed line), poloidal flux loops (blue crosses), pickup coils (black dots). Saddle coils,saddle probes and Toroidal Field Winding are not represented.

respect to the standard configuration. On the other hand, upper Singlle Null (USN) configurations required the disconnection of the same field shaping coils but in the lower part of the machine, named FS4L and FS5L in Fig. 4.4. Details on shaped operations of RFX-mod can be found in [1]. The vertical displacement control was possible thanks to the integration of the equilibrium control system with the MHD control system whose active saddle coils can generate the required horizontal field in real-time. In fact, the $m = 1$, $n = 0$ vertical stabilization was left to the outer and inner arrays of MHD control saddle coils, assumed as working in anti-series.

According to the previous experience, a fully model-based approach was followed, which included the design of a Single Null equilibrium configuration by means of a MHD non linear equilibrium solver, the derivation and validation of a linearized plasma response model, the design of an inner, faster feedback control loop for plasma vertical stabilization, the order reduction of the stabilized model, the preparation and testing of a reliable realtime algorithm for plasma boundary reconstruction, the design, implementation and operation of the shape control system. A detailed description of the design and operation of the RFX-mod plasma shape control system can be found in [1]. In particular, the derivation and validation of the linearized plasma response models adopted for the design of the control system is the first topic covered by this thesis and it will be discussed in the next chapters. Now it is important to highlight that the achievement of a H-mode regime was the aim

of executing shaped tokamak discharges in RFX-mod: recent experiments showed evidences of the onset of this regime [70], giving the opportunity to further develop the electromagnetic modelling and control of RFX-mod shaped plasmas.

4.5 The RFX-mod magnetic measurement system

In all fusion machines, including RFX-mod, the plasma shape is characterized by a certain number of geometrical descriptors, called plasma-wall gaps. These are a typical example of the importance of magnetic diagnostics in electromagnetic control of fusion machines. The RFX-mod magnetic measurements system is constituted by 192 biaxial pick-up probes and an equal number of radial saddle coils regularly distributed in poloidal and toroidal angles. The magnetic pickup coils adopted in the control activity are placed close to the shell inner surface and they have been designed for a circular cross section discharge. They provide measurements of both toroidal B_t and poloidal B_θ magnetic field components. The pickup coil magnetic sysyem of measurement is then constituted by 4 arrays of 8 poloidally equally spaced bi-axial pick-up probes located in 4 toroidal sections at $r = 0.5085m$. For the equilibrium reconstruction, the toroidal averages of the 8 probes located at the same poloidal angle are taken. In addition, there are 8 uniformly distributed poloidal flux loops located at $r = 0.5065m$. The sensor geometry is depicted in Fig. 4.4. Two additional informations are used in the electromagnetic modelling adopted in this thesis: the estimation of the β_p and the the plasma boundary reconstruction which both can be generally derived from magnetic measurements. The plasma boundary reconstruction is based on the extrapolation of the poloidal magnetic flux and magnetic field in the vacuum region inside the sensors. This is based on a hybrid toroidal-cilindrical formalism that is described in details in [71]. The β_p estimation has been carried out from the global quantity $\beta_p + l_i/2$ which is derived from magnetic measurements by exploiting the reconstructed flux surfaces as described in details in [71].

Chapter 5

Problem formulation

The present thesis aims at the development of an overall model of the plasma-conductors-controller system of RFX-mod shaped tokamak configuration for electromagnetic control purposes, with particular focus on vertical stability. Thus, the RFX-mod device is described by models of increasing complexity and involving both theoretical and experimental data. The CREATE-L code is used to develop 2D linearized plasma response models, with simplifying assumptions on the conducting structures (axisymmetric approximations). Such models, thanks to their simplicity, have been used for feedback controller design. The CarMa0 code is used to develop linearized plasma response models, but considering a detailed 3D description of the conducting structures. These models provide useful hints on the accuracy of the simplified models and on the importance of 3D structures in the plasma dynamics. The CarMa0NL code is used to model the time evolution of plasma equilibria, by taking into account also nonlinear effects which can come into play during specific phases (e.g. disruptions, limiter-to-divertor transitions, L-H transition etc.).

The overall activity can be divided in two main parts: the first one involves the modelling of numerically generated low-β plasmas, which are used as a reference for the design and implementation of the plasma shape and position control system; the second, is strictly related to the results of the experimental campaigns on shaped plasmas from low-β to H-mode regime. The two parts, and the related experimental campaigns involved in the activity, will be deeply described in the following sections. Several challenges and peculiarities characterize the project in both the modelling and control frameworks. Strong plasma shape and different plasma regimes (i.e. low-β to H-mode plasmas), deeply affect the modelling activity and require the development of several numerical tools and methods of analysis. From the control system point of view, non-totally observable dynamic and model order reduction requirements allowed a full application of the model based approach in order to

successfully design the plasma shape and vertical stability control system.

5.1 Modelling of low-β shaped tokamak plasmas

The first part concerns the production of linearized plasma response models for the design of plasma shape and vertical position control system. The activity is based on theoretical data generated by the MAXFEA equilibrium code and then used to derive the linearized model through the CREATE-L code [44]. Two reference models have been produced for the magnetic configurations interested in shaped operations: the lower single null (LSN) and the upper single null (USN). The CREATE-L models are the most simple in terms of modelling complexity, because the conducting structures are described within the axisymmetric approximation. On the other hand, the simple but reliable properties of the CREATE-L model led to the successful design of the RFX-mod plasma shape and control system [1], which has been successfully tested and used to increase plasma performances involved in the second part of the thesis. Then, an investigation on the possible 3D effects of the conducting structures on these numerically generated plasma configurations has been carried out by producing linearized models with an increased level of complexity. A detailed 3D volumetric description of the conducting structures of RFX-mod has been carried out and included in the plasma linearized models through the CarMa0 code [57]. A comparison between the accuracy of this model and the previous 2D one has been performed. The different assumptions and approximations of the various models allow a clear identification of the key phenomena ruling the evolution of the n=0 vertical instability in RFX-mod tokamak discharges, and hence, provide fundamental information in the planning and the execution of related experiments and in refining the control system design. Finally, the nonlinear evolutionary equilibrium model including 3D volumetric structures CarMa0NL [55] has been used to model nonlinear effects by simulating a "fictitious" linear current quench.

5.2 Experimental campaigns of RFX-mod shaped tokamak

A first experimental session has been carried out in order to assess the performance of the multivariable LQG (Linear Quadratic Gaussian) shape controller designed by means of the CREATE-L model. Small variations of the gap references have been applied to test the system response; the control system robustness has been evaluated by perturbing the equilibrium conditions with a small variation of macroscopic

parameters such as β_p and l_i. After this preliminary assessment of plasma shape and position controller, the operations were focused to increase the plasma performance towards the H-mode regime. Thus experimental campaigns spanning different plasma regimes, from the naturally low-β to the edge biased induced H-mode plasma [70], were performed. The L-H transition can be induced by a polarized inserted electrode able to modify the plasma edge properties, and therefore, to access the H-mode [72]. The aim was to investigate the wide space of experimental parameters relevant in the L-H transition for the RFX-mod plasmas with the polarized inserted electrode.

The H-mode is achieved when a certain threshold power is surpassed. This threshold power, like the energy confinement, depends on plasma parameters in both gross as well as subtle ways: controlled experiments have been conducted to study regimes in which the H-mode is accessible, and these device-specific studies have been coupled to a statistical approach in order to understand what variables are the key to obtaining the H-mode [73]. The power threshold for L-H transition is a function of several parameters such as plasma electron density, toroidal magnetic field, plasma and machine geometry as stated by the simple scaling law: $P = n_e B_\phi R^{2.5}$ [74]. A full description of L-H power threshold scaling laws can be found in [73] and references therein. Besides these parameters described by scaling laws, additional hidden variables can play a role in modifying the power threshold such as first wall conditioning, plasma shaping, X-point number and positioning, plasma dynamics, and so on. Therefore, a careful control of the magnetic configuration is necessary for the achievement of the H-mode regime.

The RFX-mod shaped tokamak experimental campaign involved mainly Upper Single Null (USN) plasmas simply because of the presence of an edge polarized electrode on the bottom part of the vacuum chamber. First of all, low-β plasmas have been produced and controlled in vertical position and shape without the presence of the electrode. Then, by inserting the electrode but keeping it turned off, plasmas with increased plasma density have been produced before trying to access the H-mode. These plasmas will be called intermediate-β plasmas and they are characterized by an increased value of poloidal beta, a strong shaping both in horizontal and vertical directions aimed to explore its role in the L-H transition, and a peculiar experimental evidence: the oscillations of the eight distances (gaps) of the plasma boundary from the first wall starting at the time instant of activation of the shape controller and persisting through the whole discharge. This evidence led to disabling the shape control system in the following experimental shots, including the one with the edge biased induced H-mode plasma. The most important feature of

these plasmas in RFX-mod is the uncommon magnetic configuration characterized by a strong shaping on both the horizontal and vertical directions.

5.3 Modelling of RFX-mod shaped experimental plasmas: from low-β towards H-mode regime

The second part of the thesis involves a modelling activity strictly related to the results of the experimental campaigns. In particular, new linearized models for the experimental plasmas in USN configuration have been carried out for all the plasma regimes involved in the experimental campaign, i.e. from low-β to H-mode. An iterative procedure for the production of accurate linearized plasma response models has been realized in order to handle the experimental data. The new plasma linearized models allowed further investigations on vertical stability, including 3D wall effects, in the three different plasma regimes (i.e. low-β, intermediate-β, H-mode). Furthermore, the axisymmetric plasma linearized models (CREATE-L) have been analyzed in the framework of the control theory revealing peculiar features in terms of associated SISO transfer function for vertical stability control, and in terms of full MIMO model for shaping control. The last, was also useful to speculate about the oscillations on the eight gaps seen in some experimental intermediate-β plasma shots. Furthermore, a non-linear time evolution of the plasma discharge for a low-β plasma, has been carried out by using the evolutionary equilibrium code CarMa0NL.

Chapter 6

Methodology

This chapter describes the methodology developed to produce, analyze and optimize the electromagnetic plasma modelling of RFX-mod shaped tokamak plasma equilibria. The computational tools involved in the study are briefly described, concerning both the production of plasma linearized models and the nonlinear time evolution analysis of plasma equilibria. A description of the method adopted for the production of accurate linearized plasma response models is presented; it can be distinguished in two classes: the first one involves linearized models of numerically generated low-β equilibria, which were used for the design of the controllers; the second one is related to the experimental plasmas produced by the control system previously designed. These plasmas span a wide class of regimes, from the low-β to the H-mode. The iterative procedure developed for the production of accurate linearized plasma response models from experimental data is described. These new models have been used to test the plasma shape control system with simulations act to investigate experimental oscillations of the plasma-wall gaps. The methods for the investigation of shaped plasma vertical stability in RFX-mod are described. The aim is to find a possible relation between plasma parameters and vertical instability. This phase consists of two different parts. The first one, concerns the solution of the inverse plasma equilibrium problem for the production of numerically generated plasma equilibria with variations on the experimental plasma parameters. The second part, describes the statistical method adopted to compare the mean values of the plasma parameters showing different behaviours in terms of vertical stability.

6.1 Computational tools

The modelling activity, concerning the electromagnetic control of plasma equilibrium, has been deeply described in Chap. 3. It has been seen that linearized

plasma response models in the framework of perturbed equilibrium approach are widely used for the design of the plasma control system. These models are derived from the evolutionary MHD equilibrium problem presented in Sect. 3.4. The computational tools adopted in this thesis, cover both the production of linearized perturbed equilibrium plasma response models and the solution of the evolutionary MHD equilibrium problem. For what concerns the first, two computational tools have been used: the CREATE-L and the CarMa0 codes. Regarding the second, the CarMa0NL code [55] has been adopted. In the framework of the linearized plasma response models, the mathematical formulation of the two codes is basically the one described in Chap. 3; in any case, the next section provides a brief description of the methods behind these computational tools without going into the mathematical details. For the reader interested in a full mathematical description of the tools, it is suggested to see in [44] and [57] for the CREATE-L and CarMa0 respectevely. Both of the tools provide a state space model for the plasma equilibrium under investigation, with an axisymmetric description of the plasma, but with a different description of the surrounding conducting structures; the CREATE-L is a fully 2D model while the CarMa0 allows to a 3D volumetric description of the passive surrounding structures. This distinction is fundamental since it allows to highlight the 3D effects of the passive conductors on the growth rate of the vertical instability. Furthermore, the higher level of complexity requires a higher level of computational power and also a higher level of computational time. Another point to highlight is that, as already seen in Chap. 3, the number of states of the state space model is determined by the number of discretization made to represent the passive surrounding structures in terms of computational domains. In fact, both the computational tools need to discretize the domain of the solution into finite elements. The same considerations on computational cost, level of complexity and discretization of the computational domain still hold for the CarMa0NL code, which solves a much more complex problem because of the time dependent analysis. A brief description of the methods behind the CarMa0NL code is given in the next section. A detailed mathematical analysis can be found in [55].

6.1.1 The CREATE-L and CarMa0 linearized plasma response models

The computational methods adopted by CREATE-L and CarMa0 are slightly different. The CREATE-L is a 2D finite element method in which the unknown is approximated by means of piecewise second order polynomial functions. Then, following Chap. 3, the overall plasma response model can be recast in a circuit equation in

terms of modified inductance and resistance matrices or equivalently in a state space form. On the other hand, the CarMa0 computational tool self-consistently couples the linearized plasma response model, computed as in CREATE-L, with a 3D time-domain eddy currents integral formulation, which requires only the discretization of the conducting structures [75]. A surface S is chosen in between the plasma region and the conducting structures, through which the interaction can be decoupled as follows. The instantaneous plasma response to a given set of magnetic flux density perturbation on S is computed as a plasma response matrix. The effects of 3D structures on plasma is evaluated by computing the magnetic flux density on S due to 3D eddy currents. The currents induced in the 3D structures by plasma are computed by using an equivalent surface current density on S which produces the same magnetic field as plasma outside the coupling surface. The overall plasma response model can again be recast in a state space-form. Outside the coupling surface some 3D conductors are located. Their treatment is analogous to what already reported in [76], where an integral formulation for eddy-current problems in nonmagnetic structures is presented and implemented in the CARIDDI code [75], which is a finite element code. This integral formulation assumes as a primary unknown the current density in the surrounding structures to which an integral operator is applied; thus, the regularity conditions at infinity are automatically taken into account and only the conducting domain is discretized with a finite element mesh. Furthermore, the solenodaility condition on the current density is imposed by introducing the electric vector potential with two component gauge. Giving a finite elements discretization of the conducting structures, the electric vector potential is expanded in terms of edge elements. The gauge is imposed by computing a tree-cotree decomposition of the mesh and retaining only the degrees of freedom related to the edges belonging to the cotree. Details on the formulation of CARIDDI and CarMa0 can be found respectively in [75, 76] and [57].

6.1.2 The CarMa0NL model

The CarMa0NL code is a nonlinear evolutionary equilibrium model including 3D volumetric structures in the quasi-static limit. The basic idea of the CarMa0NL is to describe the plasma by solving the non-linear axisymmetric perturbed equilibrium problem instead of the linearized 3D MHD equations as in CarMa or the linearized perturbed equilibrium problem as in CarMa0. In this way it is possible to treat self-consistently the non-linear evolution of an axisymmetric plasma surrounded by 3D volumetric conducting structures providing the means to study situations in which plasma non-linear effects and 3D volumetric effects instantaneously appears, e.g.

disruptions, ELMs, limiter-diverted transitions, current quenches, etc. The same coupling procedure of CarMa0 holds. The new main assumption is that plasma evolution is considered as being axisymmetric even in presence of 3D structures: this means that we consider only the $n = 0$ component of the plasma evolution modal expansion. As a consequence, any axisymmetric plasma perturbation induces 3D eddy currents in the surrounding structures which produces 3D magnetic "error" fields. These will cause plasma perturbations which are in principle 3D but that are considered 'averaged' along the toroidal direction in such a way that the plasma reaction to a 3D magnetic error field is treated as being axisymmetric along the torus. The CarMa0NL code solves the non-linear set of equations obtained combining the plasma equation with the free boundary equilibrium problem via Newton-Raphson method. Furthermore, the time evolution of the profile parameters is known and prescribed as inputs.

6.2 Discretizing the RFX-mod device for computational purposes

The three computational tools require two different discretizing technique of the computational domain; the CREATE-L is a 2D FEM differential code, which requires the discretization of all the computational domain, including vacuum space region as soon as the conducting regions, into a number of finite elements. It is over the finite elements that the unknown is approximated by means of piecewise polynomial basis functions. The RFX-mod mesh so needed is two dimensional, with triangular elements each one characterized by three nodes defining the element and three midpoints for each edge; these are needed since the piecewise basis functions are polynomials of the second order. The 2D mesh representation of RFX-mod device is represented in Fig. 6.1, where the coupling surface and the two different space domain regions are highlighted with different colors. On the other hand, the 3D computational tools named CarMa0 and CarMa0NL, belong to the class of integral formulations in which, differently from the FEM based on a differential formulation, only active regions need to be discretized, i.e. no vacuum representation is needed. Therefore, the domain has been discretized in 3D taking into account the details of the geometry of RFX-mod.

The passive stabilizing shell is characterized by an inner equatorial gap and a poloidal cut which have been taken into account in the 3D mesh as it can be seen form Fig. 6.2; the Toroidal Support Structure (TSS) is also characterized by an external equatorial gap, properly taken into account in the discretization process,

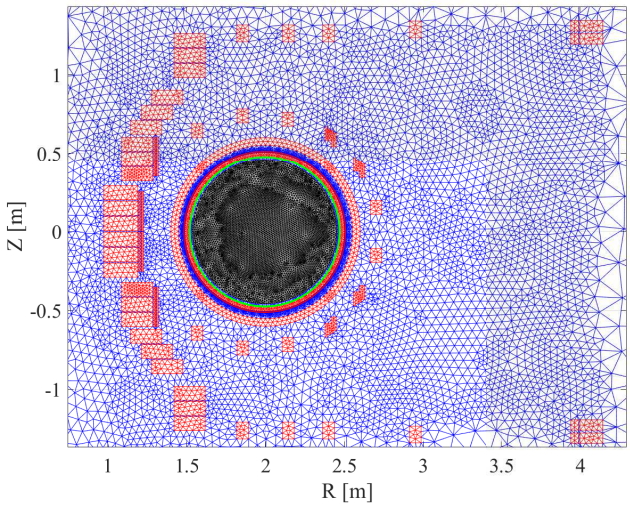

Figure 6.1: 2D mesh of RFX-mod with different space regions highlighted in different colors: conductors in red, coupling surface in green, vacuum region in blue and plasma region in black.

see Fig. 6.3. The vacuum vessel chamber is the only component purely axisymmetric as shown in Fig. 6.4. The 3D computational domain of the CarMa0 code is defined by these three passive conductors, considered all together or just few of them in relation of the analysis performed.

On the other hand, the CarMa0NL code requires also the representation of the active conductors while the CarMa0 none. Thus, the 3D meshes used for both the tools differ only for the presence or none of the active conductors; the active coils 3D mesh is represented in Fig. 6.5. An additional 3D mesh obtained from the revolution around the z-axis of the 2D mesh has been used in order to verify the

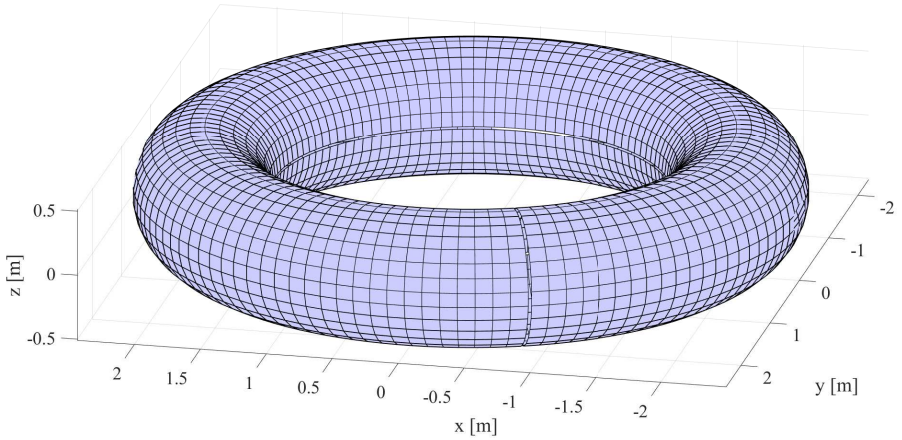

Figure 6.2: 3D mesh of RFX-mod of passive stabilizing shell including the inner equatorial an poloidal cut.

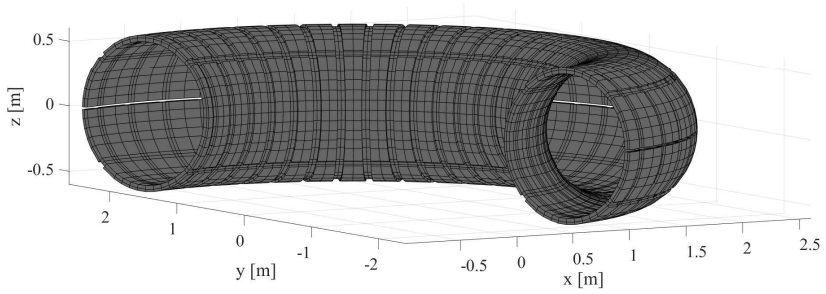

Figure 6.3: 3D mesh of the RFX-mod toroidal support structure including the equatorial cut.

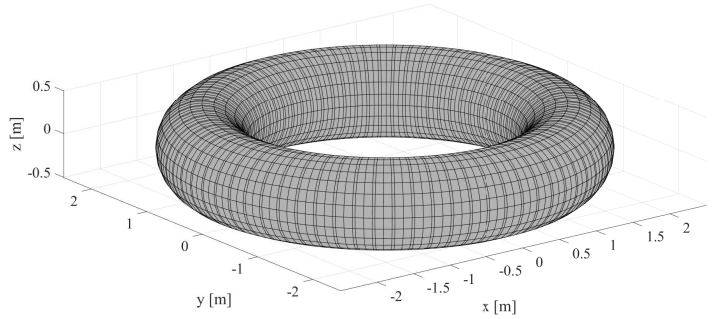

Figure 6.4: 3D mesh of the RFX-mod vacuum vessel chamber.

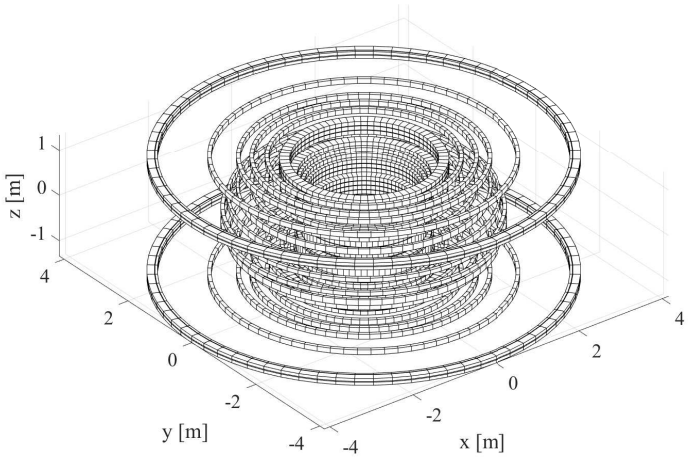

Figure 6.5: 3D mesh of RFX-mod active conductors.

correct implementation of the 3D models to RFX-mod device geometry. Each 3D analysis has been firstly tested with this 3D axisymmetric mesh and the results have been compared with the one produced by the CREATE-L.

It is important to recall that the dimension of the state space vector x depends on the number of finite elements used to discretize the tokamak structure. Thus it is clear that a 2D representation gives a state space model characterized with a less number of state with respect to a 3D one which on the other hand gives a detailed description of the system. Nevertheless, model order reduction analysis can highlight how many states are relevant to the system dynamics; this point will be briefly described in Sect. 6.5.2, where the design of the control system is presented.

6.3 Low-β reference plasma methodology

The shape and position control system used in all the experimental campaigns was based on a linearized MIMO plasma response model which had been derived from USN low-β equilibrium data through CREATE-L code [44]. The 2D MHD equilibrium non linear solver MAXFEA [77] and the CORSICA program [78], have been used to evaluate coil current values and to study proper connections [1] in order to obtain Lower Single Null (LSN) and Upper Single Null (USN) configurations. Typical plasma parameters for RFX-mod shaped plasmas and the reference coil currents for both the LSN and USN configurations are summarized in Tab. 6.1 and Tab. 6.2 respectively. It is important to notice that the data in Tab. 6.1 are purely theoretical, which means that are not directly related to real experimental low-β plasmas but only to numerically generated plasma equilibrium by means of the MAXFEA equilibrium code. These data are taken as a reference for the control system design and for RFX-mod shaped tokamak standard operations. The methodology adopted is the following: the equilibrium data is produced by the MAXFEA equilibrium code and used to derive the linearized plasma response model by means of the CREATE-L code; this has been used as the starting point for the design and implementation of the plasma shape and vertical position control system. Despite the fact that this method is simple and gives good results, it faces a certain number of uncertainties. In fact, like any equilibrium code, MAXFEA needs to define the free parameters of

$I_p[kA]$	β_p	l_i	q_0	$< B_t > [T]$
50	~ 0.11	~ 1.06	~ 1.03	0.55

Table 6.1: Typical parameters of RFX-mod LSN and USN low-β plasmas.

Coil	LSN [A]	USN [A]
IM1	1827	1860
IM2	87	73
IM3	-1931	-223
IM4	-758	-780
IFS1	-284	-272
IFS2	-1565	-1567
IFS3	1145	1160
IFS4U	0	1930
IFS4D	1931	0
IFS5U	0	-1707
IFS5D	-1702	0
IFS6	-387	-381
IFS7	-262	-293
IFS8	197	199

Table 6.2: Typical coil currents values of RFX-mod LSN and USN low-β plasmas.

the problem, which are the one that define the plasma current density profile. In the case of MAXFEA, the parametrization of the plasma current density is similar to the one defined in Sect. 3.5 but without the second exponent α_N. The values assigned to the shape parameter (α_M) have always been chosen by assuming that the current density profile of RFX-mod has a peaked profile as stated by the value of l_i in Tab. 6.1. In fact, remembering that $l_i = 11/12$ is related to a parabolic profile, and higher values characterize more peaked profiles, the parametrization adopted in MAXFEA gives, once the safety factor on axis parameter is fixed to ~ 1, more peaked profiles with lower values of α_M. On the other hand, the parameter related to the poloidal beta, β_0, is strictly constrained by fact that only low-β plasmas were involved in this phase of the experiments. These considerations lead to the use of the following values for the free parameters of the MAXFEA code for both the USN and LSN magnetic configurations: $\alpha_M = 0.7$ and $\beta_0 = 0.1$.

The CREATE-L code uses the same input as the MAXFEA equilibrium code, but with the additional parameter α_N, related to the safety factor on axis. It is important to recall that the safety factor on axis is not a controllable parameter since it is determined by the plasma, and in particular by the value of its current density on axis. Accordingly to the standard inductive tokamak scenario, the safety factor profile is monotonic from the magnetic axis radius to the plasma edge, with a value on axis of ~ 1; thus, we assume $\alpha_N = 1.001$. The resulting plasma current density profile is represented in Fig. 6.6 and it has been used for the production of the low-β reference linearized plasma response model of both USN and LSN

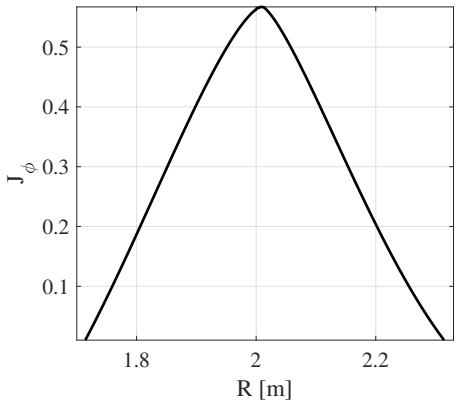

Figure 6.6: Plasma current density profile of numerically generated low-β reference plasma equilibrium with $\alpha_M = 0.7$, $\alpha_N = 1.001$, $\beta_0 = 0.1$.

magnetic configurations.

The CREATE-L model is the lowest in terms of level of complexity since it works in the axisymmetric approximation for both plasma and conductors; on the other hand, its simple but reliable properties led to the successful design of the RFX-mod plasma shape and control system [1]. An investigation on the possible 3D effects of the conducting structures on these numerically generated reference plasma configurations has been carried out by increasing the level of complexity; the CarMa0 code [57] has been used to develop also linearized plasma response models but considering a detailed 3D description of the conducting structures. Comparison between the accuracy of this model and the previous 2D one has been performed by means of the fictitious 3D axisymmetric mesh described in Sect. 6.2. The different assumptions and approximations of the various models allow a clear identification of the key phenomena ruling the evolution of the n=0 vertical instability in RFX-mod tokamak discharges and hence provide fundamental information in the planning and the execution of related experiments and in refining the control system design. The results of this phase will be described in details in the next chapter.

6.4 An iterative procedure for the production of accurate linearized plasma response models

The method adopted in Sect. 6.3 for the production of plasma linearized models has always been used with theoretical values for both the plasma current density parameters and the input equilibrium currents (i.e. active coil and plasma total current); once applied to experimental data, it did not lead to accurate results. This is due to the fact that, since no dedicated diagnostics are present in RFX-mod,

Shot no.	β_p	$t_{eq}[s]$	Plasma regime
36922	~ 0.1	0.6	low-β
39036	~ 0.5	0.5	intermediate-β
39039	~ 0.5	0.5	intermediate-β
39040	~ 0.5	0.5	intermediate-β
39068	~ 0.5	0.4	intermediate-β
39084	~ 0.75	0.71	increased-β/H-mode
39122	~ 0.8	0.85	H-mode
39123	~ 1	0.85	H-mode
39130	~ 1	0.7	H-mode
39135	~ 0.7	0.5	increased-β/H-mode
39136	~ 0.65	0.5	increased-β/H-mode

Table 6.3: Number of shots under analysis, equilibrium time instant and plasma regime

the plasma current density parameters have been kept fixed to the theoretical values previously assumed, while the equilibrium currents have been set from experimental measurements.

In order to provide a connection between computational tool and experiments, the aim was to develop a general procedure, based on an iterative scheme, for the production of linearized plasma response models through the CREATE-L code, in any kind of plasma regime with high level of accuracy with respect to the experimental data. The necessity of such a procedure was clearly highlighted in all the experimental plasmas involved in the H-mode campaign which are characterized by increasing values of β_p and a strong shaping focused to explore the L-H transition. The new methodology is based on an iterative procedure for the estimation of the CREATE-L free parameters by solving a constrained non-linear minimization problem. The shots considered in this study are related to the USN tokamak operations spanning all the poloidal beta achieved in the RFX-mod tokamak (i.e. low-β, intermediate-β, biased induced H-mode regime). Eleven experimental shots have been identified and considered in the analysis as summarized in Tab. 6.3.

6.4.1 The iterative procedure

The iterative procedure proposed is in principle valid for any kind of equilibrium code, since it is related to the estimation of the best values of the free parameters of the code to describe the reference experimental data as accurately as possible. Once a plasma current density profile is established by a mathematical parametrization of it, the problem is to determine the best values of the profile parameters. In our case, by following the parameterization of the CREATE-L code, the three parameters are

(α_M,α_N,β_0) related to (l_i,q_0,β_p) respectively. This leads to searching the solution of a constrained non-linear minimization problem, in which we want to minimize a parameter that relates the values of the experimental poloidal field measured by the 8 magnetic pick-up coils with the computed values given by the model. It has been chosen to minimize the difference between the measured and the computed values of the poloidal field, i.e. the tangential component B_θ, normalized with respect to the experimental values, in the known form of normalized chi-square defined as

$$\bar{\chi}^2 = \sum_{i=1}^{N_{sensors}} \frac{(B_{\theta_i}^{experimental} - B_{\theta_i}^{simulated})^2}{|B_{\theta_i}^{experimental}|} \tag{6.1}$$

where $N_{sensors} = 8$ is the number of magnetic pick-up coils able to measure the poloidal component B_θ of the magnetic field, i.e. the tangential component. The quantity $\bar{\chi}^2$ is defined for each set of computed and experimental values of poloidal magnetic field related to a given set of degrees of freedom $W = [\alpha_M,\alpha_N,\beta_0]$. Therefore the problem can be stated as a non-linear constrained minimization problem of finding a vector W that is a local minimum to the scalar function $\bar{\chi}^2(W)$ subject to constraints on the allowable W:

$$\begin{cases} \min_W \ \bar{\chi}^2(W) \\ L \leq W \leq U \end{cases} \tag{6.2}$$

where L and U are respectevely the lower and upper boundary values of W.

The research of the solution is carried out using the $fmincon$ function of MATLAB with the default interior point algorithm. The algorithm satisfies bounds at all iterations and solves a sequence of approximate minimization problems. The approximate problem is a sequence of equality constrained problems which are easier to solve than the original one; the method is then based on the method of Lagrange multipliers and the Karush-Kuhn-Tucker KKT conditions. By default, the algorithm first attempts to take a direct step, i.e. Newton step, for the solution of the KKT equations via a linear approximation. If it cannot, it attempts a conjugate gradient CG step. Since the Hessian is unknown, the algorithm computes a quasi-Newton approximation to the Hessian of the Lagrangian at each iteration. Details about the interior point algorithm can be found in the MATLAB optimization toolbox user's guide. Before starting the iterative scheme two main steps are needed: the preliminary phase and the initialization phase.

The preliminary phase is needed in order to get a basic case model that will be used as a reference for the one produced by the minimization procedure. This basic linearized model is obtained by using the experimental data for the active

Run	Number of initial points	Approximated computational time [s]
1	10	< 30000
2	20	30000
3	40	40000 - 60000
4	80	90000 - 150000

Table 6.4: List of runs for the procedure

coil currents including the internal-external saddle coil circuit, which provides the vertical stability of the elongated plasmas. The dof for this basic model assume reasonable values: $\alpha_M = 0.7$,$\alpha_N = 1.001$, $\beta_0 = \beta_p$, $I_p = I_{rogowski}$. This preliminary phase is important because the poloidal magnetic flux values of the equilibrium configuration produced by the basic case will be used as initial guess for launching the CREATE-L code at each iteration of the procedure. The initialization phase simply defines the number of initial points of each degree of freedom for the minimization procedure. The number of points is obviously the factor that mainly determines the computation time of the procedure. For this reason different runs, with increasing number of initial points, will be performed for each plasma configuration under analysis as reported in Tab. 6.4.

6.4.2 Choosing the degrees of freedom

A preliminary modelling activity of experimental plasma in the RFX-mod tokamak device, both in circular and shaped configuration, based on the methods adopted in Sect. 6.3 revealed several challenges in the way to get accurate results in terms of plasma linearized models (CREATE-L) and non-linear time evolution analysis (CarMa0NL). In particular a non-negligible sensitivity of static equilibria on variations of the total plasma current has been detected in the production of the linearized models for the H-mode experimental campaign [79]. At first this was interpreted as a lack in the computational tools due to the effect of the edge polarized electrode used in the campaign not being included in the model; nevertheless a further analysis on shots without electrode shown the same sensitivity, as we will see in Sect. 7.2. Therefore the total plasma current has been set as an additional degree of freedom in the standard set related to plasma current density profile. This leads to have 4 dof with 4 different constraints on their possible values, reported in Tab. 6.5. The total plasma current and the parameter related to the poloidal beta have been allowed to assume variations up to 10 % of their experimental values. The boundaries on the other two degrees of freedom have been chosen with the physically reasonable values for the RFX-mod plasmas.

Boundary	α_M	α_N	β_0	I_p
L	0.5	0.9	$\beta_p - 0.1\beta_p$	I_p
U	2	1.1	$\beta_p + 0.1\beta_p$	$I_p + 0.1I_p$

Table 6.5: Lower and upper boundaries for the degrees of freedom

6.4.3 An important clarification

The iterative procedure described previously has to be considered as a mean to get a good linearized plasma response model or in other words to get a model with accurate matching in terms of external magnetic measurements useful for control purposes. Despite the fact that this kind of iterative procedures have been widely adopted in the past as a method for plasma current profile determination [80, 81, 82, 83, 84], this would not be the case. We can't forget the restrictions on magnetic diagnostics already accurately discussed in [85]. It cannot be forget that the self-field of the plasma outside itself is completely determined by the plasma-vacuum surface and the magnetic field on it [86, 87]. Therefore the plasma magnetic field measured outside the plasma only gives information related to its boundary! And this will be our only purpose in the estimation of the plasma current density parametrization, which means find the best parametrization that gives us the best match between the computed and the experimental poloidal magnetic field. Furthermore, since these externally measured magnetic signals can correctly be used to estimate the plasma boundary [1], finding the best poloidal field match will naturally leads us to the best plasma boundary match. We will see that the models obtained by the procedure are better in terms of $\bar{\chi}^2$ and magnetic poloidal flux topology with respect to the models obtained in the preliminary phase, including a more accurate agreement with the plasma boundary estimated by poloidal magnetic field measurements.

6.5 RFX-mod shaped tokamak control system

The aim of designing a control system is to modify the behaviour of a plant to suit our objectives. In particular, design refers to the process of changing the control system's parameters to reach specified objectives. These parameters can be the unknown constants in a controller's transfer function, or in its state-space representation; this choice led to distinguish between the classical design and the modern design of control systems. The RFX-mod plasma shape and position control system is a great example of the applications of both the approaches of designing a control system. The vertical position control system can be stated as a classical design while the

plasma shape control system belong to a modern approach. Let's see the main differences of these approaches in control system design theory.

In general, the classical design consists of varying the controller transfer function until a desired closed-loop performance is achieved. The classical indicators of the closed-loop performance are the closed-loop frequency response, or the locations of the closed-loop poles. For a large order system, by varying a limited number of constants in the controller transfer function, we can vary in a pre-specified manner the locations of only a few of the closed-loop poles, but not all of them [88]. This is a major limitation of the classical design approach; in other words, situations in which the locations of multiple poles cannot be chosen independently from each other may occur. This puts serious limitations since all the poles could contribute to the closed-loop performance and then the the classical design approach may fail to achieve the desired performance objectives when only a few poles are being directly affected in the design process. Further problems could arise in situations in systems where this design approach led to the mathematical cancellation of an unstable pole with a proper zero at the same location; this approach is practically unreliable since the cancellation is not perfect and then the system still remains unstable. Additional problems could arise in the case of systems with positive zeros where again it cannot be canceled by a proper unstable pole of the controller since such a cancellation leads to internal instability [89]. The design technique of placing the closed-loop poles at desired locations is called pole-placement approach. This is the design approach adopted in the plasma position control system design as we will see in Sect. 6.5.2.

On the other hand, the modern design is based on the the state-space approach using full-state feedback that provides sufficient number of controller design parameters to move all the closed-loop poles independently of each other. Full-state feedback refers to a controller which generates the input vector able to achieve the reference state-vector in the steady state, while counteracting the affect of the noise, according to a control-law. The desired state vector, and the noise state vector, are generated by external processes, and act as inputs to the control system. Designing a control system using full-state feedback requires that the plant must be controllable, otherwise the control input generated by the controller will not affect all the state variables of the plant. Furthermore, all the state variables of the system must be measurable, and capable of being fed back to the controller. The controller thus consists of physical sensors, which measure the state variables, and electrical or mechanical devices, called actuators, which provide inputs to the plant based on the desired outputs and the control-law. Modern controllers invariably use digital electronic circuits to implement the control-law in a hardware. The controller gain

matrices, relating the inputs produced by the controller to the desired state vector and noise, are the design parameters of the control system. However, it is rarely possible to measure all the state variables since state variables could not be even physical quantities. Furthermore, an overabundance of design parameters for multi-input multi-output MIMO systems occurs since only a limited number of design parameters can be found from the closed-loop locations. Thus, the Optimal control provides an alternative design strategy by which all the control design parameters can be determined for MIMO systems. It allows us to directly formulate the performance objectives of a control system, producing the best possible control system for a given set of performance objectives. The word optimal means that there are many ways of doing a particular thing, but only one way which requires the least effort. Such a control system which minimizes the cost associated with generating control inputs is called an optimal control system and it allows to directly address the desired performance objectives, while minimizing the control energy. This is done by formulating an objective function which must be minimized in the design process. However, one must know how the performance objectives can be precisely translated into the objective function, which usually requires some experience with a given system. This is the design approach adopted in the plasma shape control system design as we will briefly see in Sect. 6.5.3.

The RFX-mod shaped tokamak control system can be viewed as the interconnection of two sub-systems acting on different time scales: the vertical position control system and the plasma shape control system. In fact, the vertical stability control is characterized by a much shorter time scale than the plasma shape control. Thus the overall control system is characterized by two loops representing two sub-system: the inner is the vertical stability control system while the outer loop, is the shape control system which acts in a time scale much larger than the previous. The plasma shape control system has been designed around a linearized Multiple Input-Multiple Output (MIMO) plasma response model where the vertical instability of the elongated plasma is previously stabilized. In fact, the inner loop control system has been designed by selecting the properly single input and single output from the whole MIMO plasma response model in order to derive a SISO system that can be analysed in terms of stability and then stabilized. A brief description of the two control system is given below, but the reader that wants a detailed analysis of the design procedure is suggested to see [1].

Firstly we describe the CREATE-L state space model, then the vertical control system is described with particular focus on the derivation of the associated SISO system; then, the reformulation of the state space model in terms of circuital

transformation matrix, and successively with model order reduction techniques, is described. Finally, once the plasma is vertically stabilized, the full MIMO plasma response model can be used to shape control purposes. The plasma shape control system is briefly described. Then, the reformulation of the MIMO state space model is carried out in order to perform time response simulations to specified inputs, in particular the perturbations on noise and poloidal beta. This is extremely important for simulating the oscillating gaps observed in experimental plasmas.

6.5.1 The state space CREATE-L model

The linearized Multiple Input-Multiple Output (MIMO) plasma response model derived from a generic set of equilibrium data through the CREATE-L code is a dynamical model in state-space representation that can be analysed in the framework of control theory. Now, the state-space representation of a system is not unique, and all legitimate state-space representations should give the same system characteristics. Despite the fact that the state variables can be chosen with freedom, it is strictly needed to ensure that the state variables so chosen are the minimum number of state variables that are required to describe the system. In other words, we should not have too many or too few state variables. In our case, the CREATE-L dynamical model is characterized by 195 states corresponding to the currents of the active circuits (10 FSW, 4 magnetizing winding (MW) sectors, 2 MHD saddle coil null currents), the passive structures (60 Inconel vessel, 59 copper shell, 59 toroidal support structure) and the plasma. This is the case for the voltage driven model, which means the model obtained by using the voltage of the circuits as inputs; if we use the currents as inputs, the state variables are magnetic fluxes linked with the passive conductors. This physical meaning is independent on the analysis that we propose for the state-space plasma model, thus we refer to states not caring if the model is current driven or voltage driven.

Thus, the Field Shaping Windings are characterized by 10 states, instead of 8, one per circuit, because the possibility of disconnection of the upper or lower FS4-5 coils is taken into account by doubling their states. The two currents of the SC arrays must be understood as the n = 0 components of the currents of the two arrays resulting from the anti-series connection of the 48 outer (up) saddle coils with the 48 inner (down) saddle coils [1]. The presence of poloidal cuts on both the shell and the toroidal support structure has been taken into account by imposing the constraint of null total current ; this is reflected by lowering the number of degrees of freedom in their representation which is one unit less than for the vessel.

In the reality, the inputs of the plant are the voltages on the active winding,

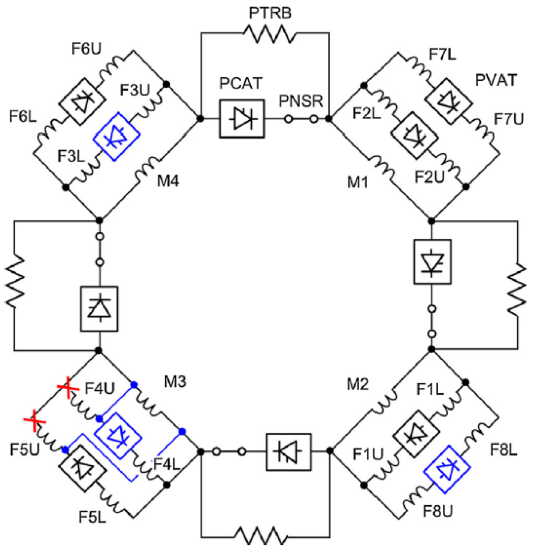

Figure 6.7: Poloidal field system electrical network for lower SN configuration (network-modifications in blue and red).

controlled by the power supplies. Thus, if a current driven state space model is used, it is necessary, as first step, to generate a linear model with the voltages as inputs. This can be done by properly taking into account the real circuit topology and properties of each active winding system as described in next section.

6.5.2 The vertical stability and position control system

The state-space representation of a system is not unique, we can always find another state-space representation for the same system. Now, as mentioned before, the degrees of freedom of the CREATE-L model can be reduced by taking into account the connections of the poloidal field system electric network, as shown in Fig. 6.7. This would inevitably remove some states of the starting model. Firstly the states related to circuit disconnection of the shaped tokamak operations have been removed; in particular, since the control system is related to USN plasmas, the FS4D and FS5D corresponding states have been eliminated. Furthermore, the state corresponding to the current of the up-down saddle coil array was also removed since this SC current component is controlled independently of the equilibrium configuration. Then, a proper reconnection matrix was integrated into the model to express each MW sector current as a function of the currents of the parallel connected FS Coils [1]. The transformation led to 9 voltage reference inputs: 8 of them are the voltages applied to the FS Coils and the last one is the voltage applied to the external-internal saddle coils circuit that acts to stabilize the vertical instability. Thus a final model with a new set of 188 states was obtained, whose outputs include the estimates of the

magnetic field components (8) and the poloidal fluxes (8) at the sensor locations and the estimate of 8 distances (gaps) of the plasma boundary from the first wall at the flux loop poloidal angle. All the model quantities must be considered as variations with respect to the equilibrium values.

In view of the control needs, the output array was then extended by adding the 8 currents of the FS Coils, the current of the outer-inner array of saddle coils, the plasma current and the plasma vertical shift, calculated as the first $sin\theta$ harmonic of the gap signals [1]. As we will see in Chap. 7, RFX-mod is characterized by a slow growth rate of the vertical instability, i.e. $< 10\ s^{-1}$, mainly because of the presence of the highly conducting copper shell and the stainless steel support structure. This slow dynamic allows to use the plasma position instead of the plasma velocity; in addition, the plasma velocity would require a derivative signal which is subjected to more noise. In order to do not to have a conflict between the references on gaps and the position of the plasma, the gaps references are always in terms of harmonics since it can be proved that the first harmonic is related to the position of the plasma, i.e. horizontal and vertical position, while the higher harmonics are related to the shape. These higher harmonics are then transformed into gaps references.

The relatively low requirement in terms of field magnitude can be met by the MHD control saddle coils. In fact, the pairs of outer-inner saddle coils can provide the horizontal component of the magnetic field needed for the vertical stabilization. Moreover, for even safer operation, the saddle coils (SC) power supplies exhibit a much faster time response than the FS coil power supplies. Consequently, a convenient choice was to commit the task of the vertical stabilization to these pairs of saddle coils. Indeed a third further inner loop has been considered in RFX-mod to maintain the vertical stabilization control inside the existing structure of the active control system of MHD modes. This consists of a Mode Controller which produces a set of 192 saddle coil current references, tracked by an equal number of inner current feedback control loops, each of them including a simple proportional gain to optimize the dynamic response. In our case the Mode controller is replaced by the Vertical stability controller which produces the n = 0 current reference for the pairs of outer-inner saddle coils. Thus, to start the design, first the saddle coils (SC) current was singled out from the model output signal array and fed back into the SC voltage input after multiplying by the current controller proportional gain, which in turn was properly scaled to take into account the representation of the outer-inner pairs of 96 independent saddle coils as a single circuit. Then, a Single Input-Single Output (SISO) open loop transfer function was worked out from the MIMO model, where the input signal is the SC current reference and the output

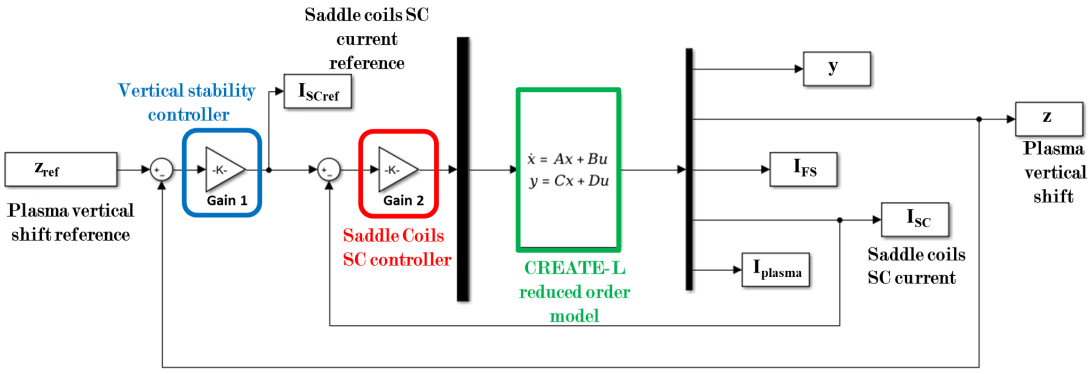

Figure 6.8: Vertical control scheme block diagram.

signal is the plasma vertical shift. Being easily obtainable from the gap signals, this less noisy variable was chosen as the feedback variable.

A simple design approach involved an order reduction of the system by using available MATLAB functions (*balreal* and *modred*) which can deal also with systems including an unstable part. By a similarity transformation a balanced state space realization of the stable part is first obtained and then added again to the unstable part. Note that the new states have no physical meaning now. The Hankel singular values allow estimation of the contribution of each state to the input-output behaviour of the stable subsystem and, consequently, their inspection suggests the number of states which can be discarded to reduce the model order [1]. After comparing different reduction methods and removing different numbers of states, a truncated model was considered for the design of the controller retaining only the unstable dynamics. Details can be found in [1], where it turns out that the higher order dynamics are negligible for the design of the stability control system. Thus, a simple proportional controller was sufficient to stabilize the system. The vertical position output was then fed-back and a new system where the vertical position reference replaced the previous saddle coil array current reference was obtained. The vertical stability and position control scheme is represented in block diagrams in Fig. 6.8. The closed loop plasma vertical shift response was characterized by a time constant about 15 ms. It is important to highlight that this vertical position control design approach involved exclusively low-β reference plasma response models obtained from theoretical data as already described in Sect. 6.3. The same control approach has been used to investigate the vertical stability of the new linearized plasma response models, obtained from experimental data following the procedure in Sect. 6.4. Thus, a validation of the control system has been performed by using a low-β plasma model obtained from experimental data. Then, the same procedure

has been applied to the new models related to plasmas with increased values of poloidal beta.

6.5.3 The shape control system

The multivariable shape feedback control system is constituted by a LQG (linear Quadratic Gaussian) regulator and a Kalman state estimator. These two control operators belong to the class of optimal control theory for designing a control system. Before describing the principle of it, we want to recall the fact that the state variables adopted in the MIMO plasma response model are not accessible, or in other words are not measurable with sensors. Also, some state variable that could be measured can be so noisy that a control system based on such measurements would be unsuccessful. Hence, it is invariably required to estimate rather than measure the state vector of a system. The fundamental question is: how to perform an estimation of the state vector if it cannot be measured? The answer lies in observing the output of the system for a known input and for a finite time interval, and then reconstructing the state-vector from the record of the output. The mathematical model of the process by which a state-vector is estimated from the measured output and the known input is called an observer (or state estimator). An observer that estimates the state-vector based upon statistical (rather than deterministic) description of the vector output and plant state is the Kalman Filter, which is an optimal observer for multi-output plants in the presence of process and measurement noise, modeled as white noises.

The Kalman filter allows to obtain an accessible feedback variable, or in other words an estimation of the dynamic of the system by which the controller acts with signals in order to modify the dynamic of the real system. The filter has as inputs the vertical position and the voltages directly applied, without perturbations. It is important to use the full voltages since the filter has to be able to compensate and react to possible perturbations. The only variables on which the controller could act in order to affect the dynamic of the system are the estimated states produced by the Kalman filter. Then, the optimal regulator is combined with the optimal observer, i.e. the Kalman filter, in order to reach an optimal compensator for the MIMO system. Since the optimal compensator is based upon a linear plant, a quadratic objective function, and an assumption of white noise that has a normal, or Gaussian, probability distribution, the optimal compensator is popularly called the Linear, Quadratic, Gaussian (or LQG) compensator. The LQG controller consists of a Kalman state estimator and a LQ optimal gain matrix calculated by minimizing a quadratic cost function [1]. In view of real time implementation of the control

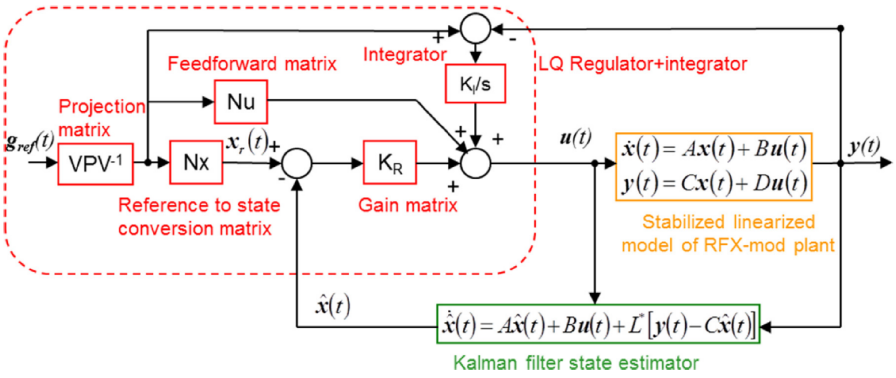

Figure 6.9: Full control scheme with plant model, Kalman state estimator, LQ regulator and integrator.

system, it is necessary to limit its order so as to meet the process speed requirements compatibly with the h/w characteristics[1]. Thus, the design of the Kalman filter and the controller are deduced from a reduced order plant. A satisfactory agreement was found with 38 states (with no physical meaning) out of the original 188 [1]. A detailed description of the designing procedure for the plasma shape control system can be found in [1]. The overall shape control system scheme is represented in block diagrams in Fig. 6.9.

6.6 Testing the control system

The need of testing the plasma shape control system rises with the peculiar experimental evidence of the intermediate-β experimental plasmas: the oscillations of the eight distances (gaps) of the plasma boundary from the first wall starting at the times instant of activation of the shape controller ($t_i = 0.51s$) and persisting through the whole discharge. The oscillating gaps were an unexpected behaviour of the plasma since the linearized plasma response model adopted for the plasma shape control design, i.e. the low-β reference one, did not show evidences of that. The new linearized plasma response models related to experimental data give the possibility to investigate the nature of these plasma oscillating gaps; in fact, a model of these plasmas at a time instant before the one at which the shape control system is activated gives the opportunity to perform a time response simulation of the plasma shape control system subjected to specified inputs. The purpose is then to obtain the plasma oscillating gaps from the model under the action of the shape control system reproducing the same conditions adopted in the experiments. Assuming the plasma vertically stable, which means that the plasma vertical position has been stabilized, the time response analysis can be carried out by means of SIMULINK, with a proper

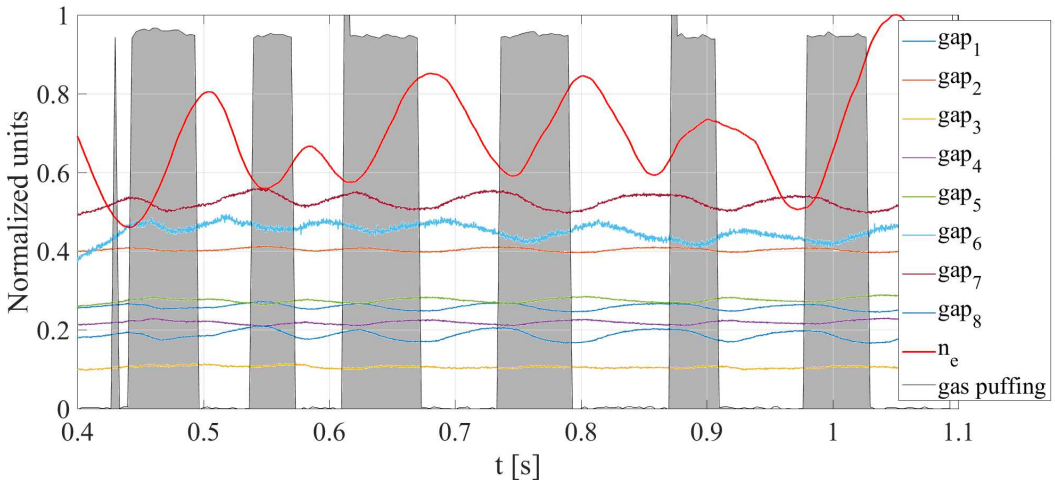

Figure 6.10: Shot no. 39068, experimental oscillations of the eight gaps and the measured plasma density related to the activation of the gas puffing (grey area).

block diagram description of the plasma shape control system. The inference that we can get from this analysis relies on the assumptions of the CREATE-L model: since the CREATE-L is an electromagnetic model, if the oscillating gaps are reproducible, then these oscillations should have an electromagnetic nature captured in some way by the model. The closed loop shape control is started by providing the gap reference used in the experiment, with all the controller parameters used in the experiment. Furthermore, an additional input signal should be used to investigate the possible oscillations in the model. This signal can be defined in two different way, leading to two different analysis.

The first approach, involves the definition of a noise perturbative set of signal on the gaps, directly derived from the experimental oscillating gap signal with the same periodicity. This set of noise signal are directly applied to the 8 plasma-wall gap, leading to the limitation of a possibility to confuse the cause with the effect. Anyway it is important to see if the model amplifies these noise signals as a preliminary investigation. The set of noise signals is derived from experimental data by means of an estimation of the variance values of the magnetic pickup coils measurements. In addition, the noise signals of the eight gaps has been modified by adding to each of them a periodic *sin* signal characterized by an amplitude and a frequency derived through the experimental behaviour of the gaps seen in some discharges. The analysis is focused on the plasma discharge no 39068, in which the oscillating gaps are clearly evident. The frequency of the noise signal is derived by assuming a period of oscillation similar to the time scale of the experimental oscillation of the eight plasma gaps which is in the order of $100ms$. This time scale is comparable with the one of the experimental plasma density, i.e. the density

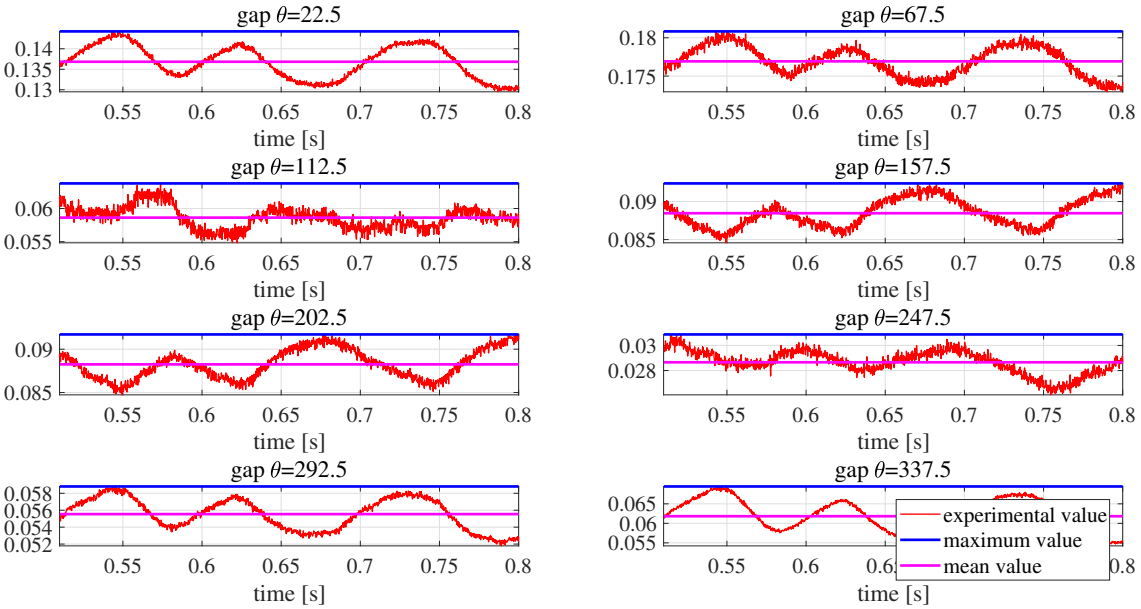

Figure 6.11: Shot no. 39068, experimental oscillations of the eight gaps.

measured by the central line interferometer. The behaviour of the eight gaps and of the plasma density is shown in Fig. 6.10.

The amplitude of the noise periodic signal applied to the gaps is comparable with the amplitude of the variation on the gaps seen in the experimental plasma discharge no. 39068; in particular the amplitude is defined for each gap as the difference between the maximum value and the mean value of the plasma-wall gap as represented in Fig. 6.11. Thus, the set of signals applied as noise on the outputs of the model, including the eight gaps, are represented in Fig. 6.12, Fig. 6.13 and Fig. 6.14.

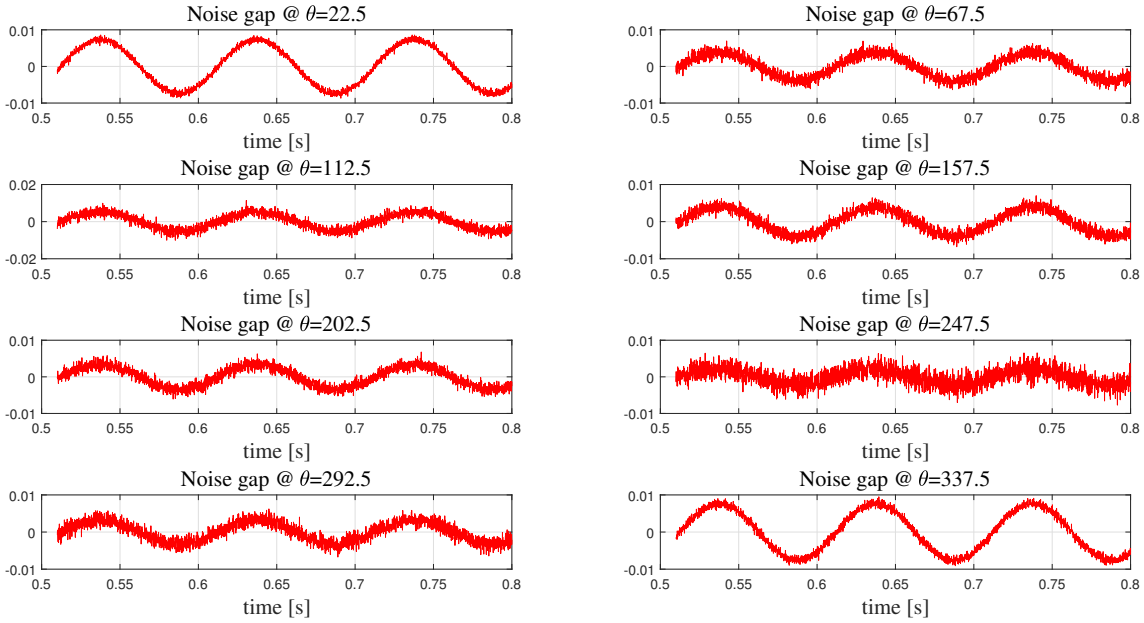

Figure 6.12: Shot no. 39068, noise signals on the eight gaps.

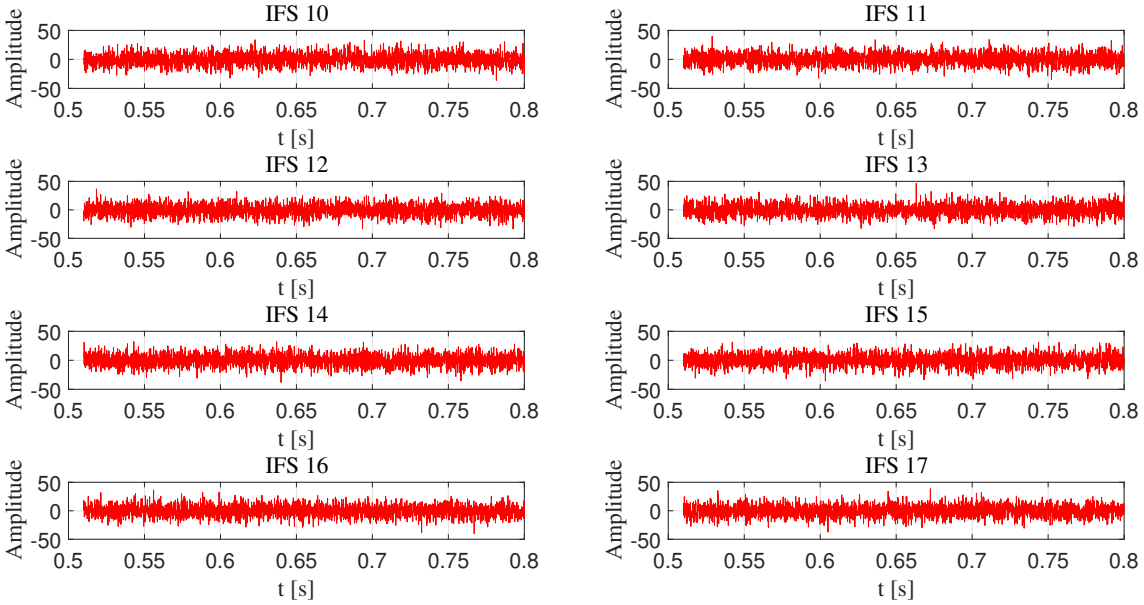

Figure 6.13: Shot no. 39068, noise signals on the outputs of the model.

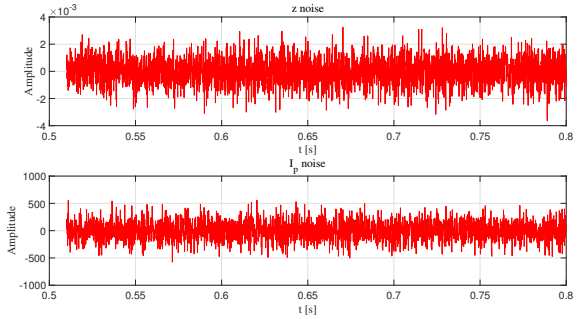

Figure 6.14: Shot no. 39068, noise signals on the outputs of the model.

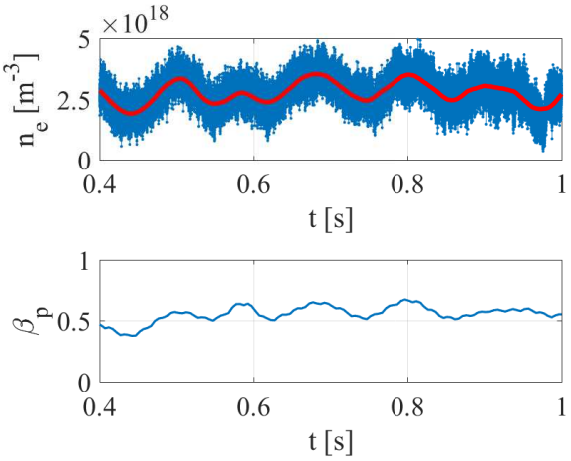

Figure 6.15: Shot no. 39068, experimental oscillations of the measured plasma density and the computed β_p.

The second approach requires the definition of an additional input on the model, representing a perturbation on the plasma β_p. This is the more realistic condition since it has been observed that the oscillations on the gaps occurs only in the plasma discharges with a pulsed gas puffing control. In fact, the gas puffing control is controlled by a periodic signal of activation with a time scale comparable with the one of the plasma density which is in turn comparable with the one of the gap oscillations, as shown in Fig. 6.10. This suggested the hypothesis that the oscillations on the gaps are a sort of *reflection* of the pulsed gas puffing control with a time delay related to the time needed to the new particles to get ionized and become part of the confined plasma. The *reflection* occurs via oscillations on β_p, which is the only plasma parameter directly linked with the plasma density and taken into account by the CREATE-L model. Thus, since the analysis is purely electromagnetic, the only way to take into account the effect of plasma density oscillations is to model the related β_p oscillations. In fact, experiments have shown that the pulsed gas puffing induce, after a short time delay, an oscillating plasma density that is highlighted in terms of oscillating β_p. The behaviour of β_p is shown in Fig. 6.15. In terms of plasma shape control, the β_p can be seen as a disturbance input on the model, directly associated to the gas puffing control density in the real world, and assumed equal to the β_0 parameter in our CREATE-L model; this interpretation requires a reformulation of the state space original equations. In fact, the CREATE-L model relates the β_0 parameter, which is associated to the β_p, to the outputs and the state variables through the matrix F, C, D, as stated by Eq. 6.5. The necessity of reformulation of the state space model in Eq. 3.16 - Eq. 3.17, is due to the presence of the derivative of W; this would require the derivative of the

β_p signal, which is not preferable to use because of noise impact on the simulation. Thus, a substitution of the state space variable δx is performed by defining:

$$\delta z = \delta x - E\delta W \tag{6.3}$$

Thus, the reformulated versions of both the state space model and the static equation relating the inputs and the new state variables z to the output variables, can be found by substitution of Eq. 6.3 in Eq. 3.16 and Eq. 3.17:

$$\delta \dot{z} = A\delta z + B\delta u + AE\delta W \tag{6.4}$$

$$\delta y = C\delta z + D\delta u + (CE + F)\delta W \tag{6.5}$$

It can be noticed from Eq. 6.4 and Eq. 6.5 that the matrices A and C are invariant while the other two additive terms related to inputs u and perturbations W can be viewed as an extended input to the model. The reformulation of the state space model is also reflected in a new block diagram configuration for the plasma shape control system in which the extended inputs, meaning the same input plus the three contained in the vector W, must be provided as sources to the CREATE-L block. For both the approaches, the plasma shape controller has been tuned with the values adopted during the experimental session. The SIMULINK simulation involves all the reference values adopted during the experiment, including the real plasma shape controller parameters, but applied to the new linearized plasma response model which is assumed to be vertically stable. This assumption is fundamental since it involves a result achieved in the vertical stability analysis of the CREATE-L models obtained from experimental plasma and that will be discussed in Chap. 7.

6.7 Methodology for vertical stability analysis

The starting point of the vertical stability analysis is again the linearized plasma response model. The stability criteria of a SISO system is determined by analysing the roots of the denominator polynomial of the associated transfer function, i.e. poles. The system is unstable if either the real part of any one pole is positive, or any one repeated pole has zero real part. Otherwise, it is stable. A stable linear system having all poles with negative real parts is asymptotically stable. In terms of state space representation, the system's stability information are contained in the state-dynamic matrix A, which in fact reflects the previously stated stability criterion. It can be proved that a linear time invariant system in a state-space representation,

is unstable if the state-dynamic matrix A has at least one eigenvalue with strictly positive real part. This eigenvalue represent the growth rate of the instability as time goes by. A detailed description of the stability analysis for system represented by state-space models or by the classical Laplace/transfer function representation can be found in [88].

The point of our interest is that, the vertical stability analysis adopted here is based on the eigenvalue analysis of the state-dynamic matrix derived through the CREATE-L model. In particular, two analysis have been performed; first, the open-loop stability analysis in which the vertical instability is characterized by a growth rate value determined by the surrounding passive conducting structure. It is important to say that in this case the matrix used for computing the growth rate is not the state-dynamic matrix of the CREATE-L model but it is the matrix A_c defined in Eq. 6.6, which can be considered like a state-dynamic matrix for only the passive conductors. Then, a closed loop stability analysis has been performed to the associated SISO system including the action of the proportional controller that stabilizes the unstable mode; in this case, the growth rate is determined by using the state-dynamic matrix of the new state space system obtained by applying the circuit reconnection matrix previously described.

The matrix A_c is then computed as follows:

$$A_c = -L_{cc}^{-1} R_{cc} \tag{6.6}$$

where the pedix c represent the elements of matrices L and R related to the passive conductors in the system. In fact, since the CREATE-L model is obtained by using the active coil currents as inputs, the active coil circuits cannot drive additional currents, therefore they do not provide passive stabilization and must not be considered in the calculation of the unstable mode growth rate, i.e. eigenvalue. Another point to stress is that, the eigenvalue analysis provides a double class of information on the instability. In fact, an instability is determined by an eigenvalue and an associated eigenvector; these two quantities provides informations of different nature. In fact, the eigenvalue gives an information of the time evolution of the instability since it represent the growth rate of the unstable mode. On the other hand, the eigenvector represent a spatial information, in particular it provides information on the structure of the unstable mode; it is important to highlight that by computing the matrix A_c as in Eq. 6.6, the eigenvector representing the structure of the unstable mode can be viewed, in term of physical picture, as a pattern of currents on the passive conductors. Other computations of the A_c matrix are associated to a different physical interpretation of the eigenvector; for example by defining that the

eigenvector would represent a magnetic flux linked with the passive conductors, and not a current, then $A_c = -R_c L_{cc}^{-1}$. In any case, what is important to stress is the double information on instability provided by the eigenvalue analysis: one in space associated to the eigenvector and the other in time associated to the eigenvalue.

It is important, now, to anticipate a result. The proportional controller previously described, see [1], was able to stabilize all the plasmas of the RFX-mod experimental campaign under analysis. On the other hand, a few CREATE-L models representing some experimental plasma discharge of the same campaign were not able to be stabilized by the same proportional controller used in the experiments. These plasmas has shown a saturation of the vertical instability growth rates to very low values, which we will see that were not observable in the experiments. In this cases, the growth rate is associated to the state-dynamic matrix related to the closed loop system, which in other words includes the effect of the proportional gain of the vertical position controller. Despite the simple geometry of RFX-mod and its relatively low performances in terms of plasma current for shaped tokamak operations, the vertical stability of these plasmas revealed to be interesting in its uncertainty. In fact, as we will see in the results, it is in the framework of vertical stability that the necessity of producing plasma linearized models characterized by different values of plasma parameters occurs.

The behaviour difficult to explain was the saturation of the growth rate associated to the unstable $n = 0$ vertical instability under the action of the proportional gain controller in terms of dynamic and also as phenomenon to be controlled by the actuators. One of the possible necessary conditions for this phenomenon to occur is to be researched in the wide window of plasma parameters that these experimental plasmas explore; in fact, these plasmas are particularly far in terms of plasma parameters from the standard tokamak operations in RFX-mod. In other words, several plasma parameters are pushed to high values with respect to the standard tokamak operations as for example the poloidal beta, the plasma shaping and so on. The necessity of exploring the wide range of plasma parameters possibly involved in triggering and sustaining the saturation of the unstable mode under the action of the controller led to the development of a new computational tool able to solve the inverse plasma equilibrium problem. Thus, a new set of plasma equilibria have been used to produce new plasma linearized models spanning several plasma parameters values; these linearized models together with the one obtained from experimental data, have been used to investigate the peculiar behaviour of RFX-mod shaped plasmas in terms of vertical stability from two different perspectives: the one related to the aim of controlling and stabilizing the mode, and the other in terms of searching

the conditions for this phenomenon to occur. The first is related to the control theory approach, including the eigenvalue analysis, of all the available plasma linearized models revealing the saturation phenomenon; the second, has been investigated and addressed by means of a statistical analysis of all the results obtained from both the experimental plasma equilibria and the one produced by the inverse equilibrium code, trying to relate the occurrence of the saturation with a particular difference between the mean values of the plasma parameters of the two possible situations: the presence or not of the saturation.

6.7.1 Inverse plasma equilibrium problem

The inverse fixed boundary plasma equilibrium problem requires the identification of the optimal values for the active coils currents in order to keep in equilibrium a plasma with a prescribed magnetic configuration (i.e. plasma shape and global parameters, namely I_p,l_i,β_p). The solution of the fixed boundary direct equilibrium problem gives the magnetic flux values due to both contributions of the plasma current density and the external conductors currents. At the boundary this relation can be obtained:

$$\psi_b = \psi_b^{coils} + \psi_b^{plasma} \tag{6.7}$$

Since the plasma is shaped by the external fields produced by the external conductors currents, it is of considerable interest for the purpose of this study to compute the singular contribution of these currents to the magnetic flux values at the boundary. The plasma boundary flux contribution ψ_b^{plasma} has been computed by using a filamentary approximation. Then, the coefficients that link the filamentary currents to the plasma boundary flux are calculated and stored in a dense matrix, often referred to as Green matrix. The coils contribution to the flux at the boundary is straightforwardly obtained by subtracting the total flux at the boundary and the plasma current contribution already computed. The fixed boundary problem is obviously characterized by a constant value of the flux at the boundary so the two contributions must be such that by adding them the flux value at the boundary does not change; it is clear that by adding them together, a constant boundary flux value is obtained. After these considerations, the inverse equilibrium problem can be expressed as:

$$R = \|Gx - \psi_b^{coils}\| \tag{6.8}$$

where G is the Green matrix connecting each coil contribution to each boundary point, x is the vector of the unknown currents, ψ_b^{coils} is the coils contribution to the flux due to the unknown currents and R is the objective function which is to be

minimized.

It follows that the solution of the inverse equilibrium problems provides the possibility to reproduce plasma equilibria with predetermined shape and global plasma parameter values (i.e. l_i, q_0 and β_p). Then, by following the procedure in Sect. 6.3, but instead of using the MAXFEA equilibrium code we use the direct equilibrium solver proposed below, several linearized plasma response models of new plasma equilibria has been produced and analysed in terms of vertical stability. It is important to put emphasis on the fact that these new linearized models refer to plasma equilibria which are only numerically generated, not experimentally validated; furthermore, they are important since they represent variations on real experimental plasma equilibria, in the sense that they are derived from real experimental plasma by combining different plasma parameters from different plasma regimes. This will be discussed in detail in Sect. 7.7 but as example, in order to investigate only the effect of the increased value of poloidal beta in the vertical stability, it was necessary to isolate this effect by removing the possible plasma shaping effects on vertical stability. Therefore, a low-beta plasma boundary has been used to select the standard plasma shape for RFX-mod and then the other plasma parameters, such as poloidal flux at boundary, total plasma current, current density parameters (including the one representative of the poloidal beta), have been selected from another experimental plasma with higher β_p values. Other variations on the parameters of experimental plasma equilibria have been performed in order to investigate their effects on plasma stability.

The computational algorithm implemented for the solution of the inverse equilibrium problem is constituted by three main modules: the plasma boundary definition and meshing tool, the direct equilibrium solver tool and finally the inverse equilibrium solver tool. The whole computational tools have been developed under the MATLAB environment, partially by following the previous work in [90].

6.7.2 Plasma domain representation

The first module involves the definition of the computational domain for the fixed boundary equilibrium problem. The plasma boundary has been defined by means of two different tools: the real-time plasma boundary reconstruction algorithm [1] and the extended analytical functional model proposed in [90] by following [91].

The plasma boundary reconstruction algorithm is based on a vacuum expansion of the poloidal flux and magnetic field in a hybrid cylindrical-toroidal formulation. A radial dependence of the magnetic field poloidal harmonics as in cylindrical geometry is assumed, while the relationship between flux and field holds in an axisymmetric

toroidal geometry. Input data are the measurements of the poloidal flux and the magnetic field components at fixed radii and distributed along the poloidal angular coordinate.Fourier harmonic coefficients of both B_θ and B_r can then be derived from the measures of the same magnetic field poloidal component and the poloidal flux, respectively. Thus the algorithm can provide a map of the magnetic field and flux in the vacuum region and the plasma boundary reconstructed in both limiter and diverted configurations (Double Null and Single Null). Details on the algorithm can be found in [1] and [71].

An unstructured mesh is obtained by means of DistMesh, an open source MATLAB code based on a simple algorithm that combines a physical principle of force equilibrium in a truss structure with a mathematical representation of the geometry using signed distance function, which is negative inside the region, zero at the boundary and positive outside the region. Aside from being simple, the *DistMesh* code generates uniform or refined meshes of high quality. Then, the magnetic poloidal flux at the plasma boundary needs to be specified by choosing a proper value from the pre-existing equilibrium reconstructions of experimental plasmas as already discussed in Sect. 6.3 and Sect. 6.4. The direct equilibrium solver needs in fact to specify the computational domain, in terms of plasma region defined by the specification of the plasma boundary, and the boundary condition on that boundary, meaning the poloidal magnetic flux at the plasma boundary, due to the contributions of both the plasma current and the unknown active coils currents. Thus, by solving the direct equilibrium problem, the plasma contribution on the poloidal flux at plasma boundary can be found.

6.7.3 Direct equilibrium solver

The Grad-Shafranov equation has been solved for the fixed boundary equilibrium problem by using a direct global- algebraic formulation, i.e. cell method, in an iterative Picard scheme. Details on this scheme can be found in [90] ; detailed informations on global formulation of physical theories can be found in [92].

The spatial location of the plasma boundary and the mesh of the plasma region is assumed to be given by the previously described computational step. Therefore, the direct equilibrum problem consists of solving the Grad-Shafranov equation only in the plasma region, by using a physical boundary condition of constant plasma boundary flux value along the desired plasma boundary. Thus the self-consistent determination of the plasma-vacuum interface, i.e. plasma boundary, is not a part of the solution procedure and therefore its important non-linearity is not applied to the Grad-Shafranov equation. The problem has a singular mild non-linearity due only

to the dependence of the toroidal plasma current with the magnetic poloidal flux. The implementation of such a boundary condition has been handled directly using the cell method. The solution procedure is obtained with the same plasma current density parametrization adopted by the CREATE-L code, leading the possibility to model the effect of increasing values of β_p on the plasma equilibrium.

The iterative procedure employed to solve the problem is basically a single loop Picard scheme which iterates over the non linear source term, i.e. the toroidal plasma current, and hence converge to a solution with fixed boundary values on the plasma boundary.

6.7.4 Inverse equilibrium solver

The aim is to determine the necessary external currents that gives the prescribed plasma equilibrium conditions; this is equivalent to solve the overdetermined system defined by:

$$Gx = \psi_b^{coils} \tag{6.9}$$

in which the Green matrix G relates the external coils currents x with the magnetic flux contribution of the same external coil currents ψ_{coils}. It is clear that a system is overdetermined if the number of equations is more than the number of unknowns.

In general, considering a system of linear equations $Ax = b$, where A is a $m \times n$ matrix and b is the vector of known terms of dimension m, the system of equations has no solution, that is b is not in the range of A. Nevertheless, a more general problem can be considered: the determination of the vector x such that the residual $R = Ax - b$ has a minimal Euclidean norm. The least squares solution to an overdetermined system of linear equations is the point such that the sum of the squares of the distances from the point to each of the subsets defined by the linear equations is a minimum. Thus the least squares solution to an overdetermined system is not a solution in the sense that it necessarily satisfies every equation of the system. It is a solution in the sense that it is the value of x that comes closest to satisfying all the equations in the above geometrical way [93]. The existence and uniqueness of such solution is defined by the following theorem. *Theorem 1.* Let X be the set of vectors of C^n such that $\hat{x} \in X$ if and only if:

$$min_{x \in C^n} \|b - Ax\|_2 = \|b - A\hat{x}\|_2 \tag{6.10}$$

Supposing that $A \in C^{m \times n}$ with $m \geq n$ and $b \in C^m$; the following properties are valid:

1. $x \in X$ if and only if $A^T Ax = A^T b$, meaning that x is a solution of the system of normal equations.

2. X is a non empty set, closed and convex.

3. the set of X is reduced to a single element x^* if and only if the matrix A has maximum rank.

4. exists $x^* \in X$ such that $\|x^*\|_2 = min_{x \in X} \|x\|_2$. Such x^* is called the least-norm solution (i.e. least-squares solution).

In other words, if A has rank n, then X has a unique element, while if A has a rank lower than n then X has a unique element of least-Euclidean norm. Several methods can be used for the solution of the overdetermined systems; for example, if A is a full rank matrix the solution of the overdetermined system is equivalent to find the solution of the system of normal equations. details can be found in [94].

The problem defined in Eq. 6.9 is characterized by a Green matrix G with full rank, representing the number of currents in the active coils of the RFX-mod shaped tokamak configuration (i.e. 14 currents for the 14 circuits); thus, it follows from *Theorem 1*, that a unique solution exist and that this solution is a minimum Euclidean norm solution (i.e. least-squares solution). Moreover, the solution of the problem in Eq. 6.9, representing a set of active coil currents that can assume only specific values determined by the engineering constraints on the maximum current that can be driven by each active coil and the circuit configuration of the active coils of RFX-mod shaped tokamak. Thus, the problem defined in Eq. 6.9, can be stated as a constrained linear least-squares problem.

The first solution that can be easily computed is the least-square solution computed by using the SVD method on matrix G considering all the singular values. Nevertheless, the need to impose the engineering constraints on the active coils need to find a new constrained least-squares solution. Before going into the method of solution, we need to specify all the constraints and their physical meaning.

In general, the constraints applied to the solution can be classified into two main categories: the upper/lower boundary constraint and the equality constraint. The first is related to the engineering operational window of each coil of the poloidal field active circuits of RFX-mod while the second one is strictly related to the electrical circuit connections of the poloidal field system. Thus, the first class of constraints is related to both the magnetizing winding (MW) and the field shaping winding (FSW) and it involves the maximum operating current that can be driven in each coil; the maximum current that can be driven on each magnetizing winding sector

	LB [kA]	UB [kA]
MW	-50	50
FSW	-6.25	6.25

Table 6.6: Lower and upper boundary for the currents in the active coils of RFX-mod shaped tokamak.

is of $50kA$. On the other hand, he maximum operating current in coils $FS8$ (A and B) is $6.25kA$, while the inner coils have lower currents. Therefore, in order to satisfy these constraints, the upper/lower boundary limits have been set as reported in Tab. 6.6. The second class of constraints involves the up-down asymmetric RFX-mod shaped tokamak circuit configuration: depending on the single null magnetic configuration, it is necessary to impose a null current on the pairs of coils that are physically disconnected, i.e. the $FS4U/L$ and $FS5U/L$.

The constrained linear least-squares minimization problem can be stated as following:

$$\begin{cases} min_x \frac{1}{2}\|Gx - \psi_b^{coils}\|, \\ A_{eq}x = b_{eq}, \\ LB \leq x \leq UB \end{cases} \tag{6.11}$$

where A_{eq} and b_{eq} are, respectevely, a sparse matrix and a known vector, both made of one and zeros, used to impose the equality constraint while the L and B represent the lower and upper bounds on the solution. The constraints are summarized in Tab. 6.6. The solution of the problem defined in Eq. 6.11 is carried out by means of the *lsqlin* function of $MATLAB - optimizationtoolbox$ which uses the interior-point linear least squares algorithm described in details in the *MATLAB optimization toolbox user guide (page 10-6).*

6.8 Statistical methods for vertical stability analysis

The statistical examination of a body of data is similar to the general alternation of inductive and deductive methods throughout science. A hypothesis is conceived and defined with all necessary exactitude; its logical consequences are ascertained by a deductive argument; these consequences are compared with the available observations; if these are completely in accord with the deductions, the hypothesis is justified at least until fresh and more stringent observations are available. It is

not our interest to provide a detailed statistical analysis of data in general, but to provide the reader with the statistical method applied to construe the results obtained for the vertical stability of experimental and theoretical plasma equilibria in the RFX-mod tokamak experiment.

One of the practical need of statistical methods is to reduce the bulk of any given body of data in order to reduce the results of methodical observations to a more convenient bulk. In general, we want to express all the relevant information contained in the mass of data by means of comparatively few numerical values. The discrimination between relevant and irrelevant information is performed as follows: firstly, we define the population under analysis. In general a population can be any kind of measurable observation repeated indefinitely: the aggregate of the results is a population of measurements. Secondly, we define the mathematical parameters used to characterize the population of data such as mean and standard deviation, whose in fact represent the attempt to learn something about the population. Now, we cannot know the parameters exactly, but we can make estimates of their values calculated from observations. Thirdly, once the population of data is established we can apply a statistical hypothesis testing by which we can examine whether or not the data are in harmony with any suggested hypothesis and if this is significant or not.

The system under analysis is the plasma which is characterized by several plasma parameters such as elongation, triangularity, and so on. The plasma system can assume two different states, each one corresponding to different behaviours in terms of vertical stability: the first, in which the vertical instability is stabilized by the effect of the actuators or the second, in which the vertical instability is not stabilized by the effect of the actuators. The two states are mutually exclusive and correspond to two different behaviours of the growth rate under the action of the actuators: the first is the passage of the growthrate from positive values to negative ones, representing a mode that gets stabilized by the actuators, and the second is the saturation of the mode growth rate to a positive value indifferently how big the proportional action of the actuator is. These two conditions can be recognized, in mathematical terms, by the occurrence or not of a positive real zero of the SISO model obtained from the more general CREATE-L model. This is the background; the situation of interest is constituted by two states of the plasma system, each of them characterized by mean values of plasma parameters derived through experimental and/or theoretical plasmas. Here, we want to give a description of the statistical method adopted to compare the mean values of the parameters of plasmas showing different behaviours in terms of vertical stability. In other words, we want to highlight if the unstable

plasmas are characterized by typical values of plasma parameters, for example a particular threshold value of elongation or triangularity and so on; obviously this typical values can be determined only by comparison of the same parameter values associated to the other plasma state in which the vertical instability is suppressed.

Now, each set of plasma parameter data can be treated as a set of population of data that can be analysed with statistical methods. Thus, we have two sets of populations, corresponding to the plasma parameters, for each of the state assumable by the plasma system. The question we want to answer is: is there any significant difference between the mean values of the plasma parameters in the two different system states? If it is so, can it be argued that this significant difference is related to the system state behaviour? These questions can be expressed in terms of two hypothesis that can be verified by means of a statistical hypothesis test.

6.8.1 Statistical hypothesis testing

The statistical hypothesis testing are based on two fundamental concepts. The statement of a statistical null hypothesis (H_0) that can be investigated by mathematical-statistical analysis of a bulk of data and the choice of a test statistic to verify the H_0 hypothesis. A test statistic is a random variable and, as such, can be described by a probability distribution; for example, a commonly used test statistic, which has been used also in our analysis, for testing hypotheses about population means is the t of Student. For detailed information on t Student distribution see [95]. The associated test of hypothesis, also known t-test of Student, is applied to verify a hypothesis on the mean values of data satisfying the conditions of validity. We will describe the hypothesis and the conditions of validity later but before doing that it is necessary to introduce the particular statistical hypothesis test adopted for our case under analysis. A general and accurate description of the statistical hypothesis testing can be found in [96].

We follow an hybrid approach, combining aspects of both Fisherian inference and Neyman-Pearson decision-making to statistical hypothesis testing[96]. The example of such a test is given below in the following steps:

1. Specify the null hypothesis H_0, the alternative hypothesis H_A and the test statistic (e.g. t).

2. Specify a priori significance level (e.g. 0.05), which is the long-run frequency of Type I errors (long-run probability of falsely rejecting H_0, which we denote by α) we are willing to accept.

3. Collect the data by one or more random samples from the population(s) and calculate the test statistic from our sample data.

4. Compare that value of the statistic to its sampling distribution, assuming H_0 true.

5. If the probability of obtaining this value or one greater (i.e. P value) is less than the specified significance level (i.e. α), then conclude that the H_0 is false and reject it ("significant" result).

6. If the probability of obtaining this value is greater than or equal to the specified significance level, then conclude there is no evidence that the H_0 is false and retain it ("non-significant" result).

Before explaining the details of the application of the method adopted, it is important to clarify some of the statistical knowledge used in the following. The P value is a property of the data and can be viewed in many different ways; in our approach, it can be stated as the long-run probability of obtaining our sample test statistic, or one more extreme, if H_0 is true. Therefore, the P value is the probability of observing our sample data, or data more extreme, under the repeated identical experiments if H_0 is true. Equivalently, it can be stated as the probability of a result occurring by chance in the long run if H_0 is true.

In any case, the P value must be compared with another level, called significance level α, representing the probability (of obtaining our sample data or data more extreme if H_0 is true) for rejecting H_0. In many experimental scientific fields such as biology and so on, the significance level is conventionally fixed to a level of 0.05, representing a probability of the 5%. All the values below this threshold are treated as significant results, statistically speaking, meaning that the H_0 can be rejected and it implies that the H_A alternative hypothesis is true. It is important to stress that, in our approach, a statistically non-significant result basically means that we should suspend judgment and we have no evidence to reject the H_0. Furthermore, a statistical significant result does not imply that it is also significant in terms of physics. This final conclusions must be inferred with the help of additional results provided by other analysis or theoretical considerations.

The case of our interest deals with the comparison of the mean values of parameters related to two independent samples, whose are the plasma parameters collected from experiments exhibiting two distinct behaviours in terms of vertical stability. The significance test on two mean values of independent samples is performed by following the previous statistical hypothesis testing scheme on two different series of

observations. In our case, the two observations are determined by the occurrence or not of the saturation of the unstable mode, or equivalently, by the presence or not of the positive real zero in the CREATE-L model of the plasma shot under analysis.

The statistical hypothesis test adopted is a two-tailed test, meaning that we are asking if a significant difference exists between two mean values without knowing if one of them is greater or lower than the other. In other words, in two-tailed test, the zero hypothesis H_0 is defined as follows:

$$H_0 : \mu_1 = \mu_2 \iff \mu_1 - \mu_2 = 0 \tag{6.12}$$

The alternative hypothesis H_A is defined as:

$$H_A : \mu_1 \neq \mu_2 \iff \mu_1 - \mu_2 \neq 0 \tag{6.13}$$

Furthermore, the test adopted is heteroscedastic meaning that the collections of data belong to independent groups and then the variance of both the data are different. The degrees of freedom of the t Student are equal to $(n_1 - 1) + (n_2 - 1)$, where n_1 and n_2 are the number of observations respectively of samples 1 and 2. Then, the t index is computed by means of Eq. 6.14.

$$t = \frac{\bar{y_1} - \bar{y_2}}{s_{\bar{y_1} - \bar{y_2}}} \tag{6.14}$$

where $\bar{y_i}$ is the mean value of the analyzed parameter y of the plasma in state $i = 1, 2$, and $s_{\bar{y_1} - \bar{y_2}}$ is the standard error of the difference between the two means:

$$s_{\bar{y_1} - \bar{y_2}} = \sqrt{\frac{(n_1 - 1)s_1^2 + (n_2 - 1)s_2^2}{n_1 + n_2 - 2} \left(\frac{1}{n_1} + \frac{1}{n_2} \right)} \tag{6.15}$$

Now, in order to establish if there is a significant difference between the mean values of the samples, the value of the t is compared with the critical t value, which is the t two-tailed distribution with $n_1 + n_2 - 2$ degrees of freedom at an established significance level α. These critical values are usually collected in tables for single tail or two-tailed distributions of t. Values of t greater than $+t_c$ or less than $-t_c$ have a less than $\alpha = 0.05$ chance of occurring from this t distribution, which is the probability distribution of t when H_0 is true. Equivalently, if the probability (P value) of obtaining our sample t value or one larger is less than 0.05 (our α), then we reject H_0 and the alternative hypothesis H_A is accepted. In other words, the two samples differ significantly in their mean values. Thus, the function $test.t$ of EXCEL provides directly the P value of the sample under analysis. Since we can

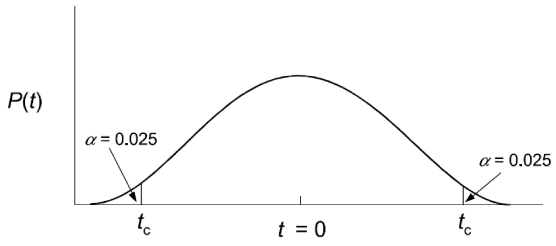

Figure 6.16: Probability distributions of t for a two-tailed, showing critical t values.

reject H0 in either direction, large values of the test statistic at either end of the sampling distribution will result in rejection of H0 as shown in Fig. 6.16 [96]. To do a test with alpha 0.05, then we reject H_0 if our t value falls in the regions where $P = 0.025$ at each end of the sampling distribution ($0.025 + 0.025 = 0.05$). If the probability (P value) of obtaining our t value or one larger is ≥ 0.05, then we do not reject the H_0.

6.8.2 Conditions of validity of the test

The statistical hypothesis test previously described is based on the specification of a probability distribution for the populations of the variable from which our samples came (i.e. parametric test). Since the Student's distribution t is used in these hypothesis testing, and because it is derived directly from the normal distribution, it is necessary to fulfill the conditions of validity required for parametric tests. These conditions of validity are assumptions whose violation would imply that the test statistic (e.g. t) may no longer be distributed as a t distribution, which means that our p-values may not be reliable.

The first assumption is that the samples of data are from normally distributed populations of data. The second assumption is that the observations are collected independently. The first assumption is the most important in terms of statistical investigation, while the second one depends on how you organize your data collection. For example, the observations are not independent if, in an experiment on the electrical conductivity of a metal at different temperatures, they use different metal samples but each of them is measured several times. Considering the first condition of validity, the significance tests based on the t test are usually robust to violations of this assumption. In other words, the test remains roughly valid even when data distributions do not strictly respect the condition of normality. The normality distribution of data can be easily checked graphically by applying a normal probability plot (also called "normal plot").

Chapter 7

Results

This chapter shows the results achieved in the electromagnetic modelling activity of the RFX-mod tokamak device.

7.1 Low-β reference plasma results

The equilibrium data of the open loop LSN and USN low-β reference plasmas reported in Tab. 6.1 have been used to produce the linearized plasma response model of each plasma magnetic configuration by means of CREATE-L code. This provides a dynamical model of both USN and LSN configurations is characterized by 195 states corresponding to the currents of the active circuits (10 Field Shaping Winding, 4 Magnetizing Winding sectors, 2 MHD saddle coil null currents), the passive structures (60 Inconel vessel, 59 copper shell, 59 toroidal support structure) and the plasma. The presence of poloidal and inner equatorial cuts in the shell have been implicitly taken into account by imposing that their total current be null. This model has been successfully used to design and implement the plasma shape feedback control system [1]. A comparison between the reference plasma equilibrium parameters obtained with the CREATE-L and MAXFEA 2D equilibrium code is presented in Tab. 7.1; thus, the plasma USN and LSN equilibria are correctly

	LSN		USN	
	MAXFEA	CREATE-L	MAXFEA	CREATE-L
β_p	0.111	0.1066	0.111	0.1059
l_i	1.0649	1.0401	1.064	1.0412
$R_{\text{X-point}}$ [m]	1.8267	1.822	1.821	1.823
$Z_{\text{X-point}}$ [m]	-0.3841	-0.3871	0.394	0.3898

Table 7.1: Plasma equilibrium values computed by CREATE-L and MAXFEA for both LSN and USN magnetic configurations.

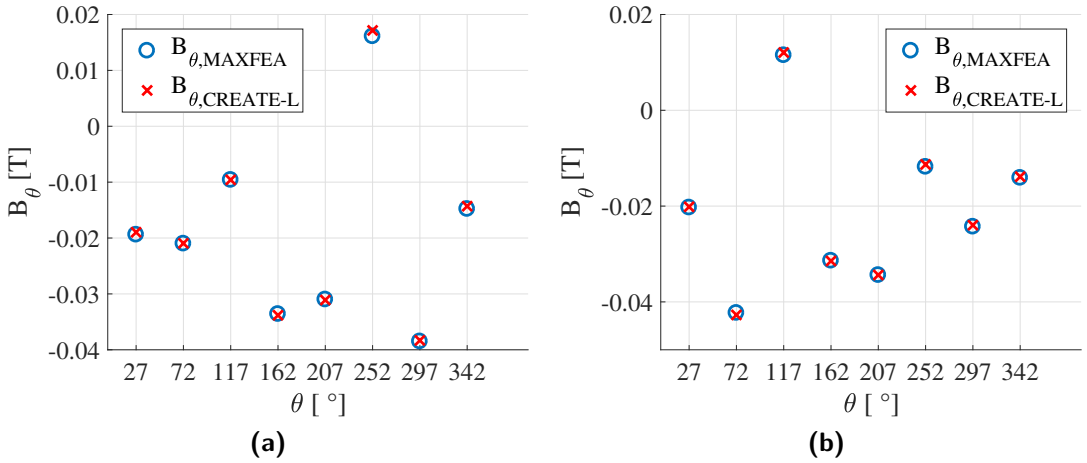

Figure 7.1: LSN **(a)** and USN **(b)** equilibrium poloidal magnetic fields at magnetic pickup coils location computed by CREATE-L and MAXFEA.

	CREATE-L	CarMa0 (3D axisymmetric)	CarMa0 (3D realistic)
γ_{tot} [s^{-1}]	7.36	7.33	8.59
γ_{vessel} [s^{-1}]	335.4	334.2	-

Table 7.2: LSN comparison of growth rates.

reproduced. The model outputs include the direct estimate of the gaps and the magnetic measurements (i.e. poloidal magnetic fluxes and poloidal magnetic field components at pickup coil sensors location). An excellent agreement in the comparison of equilibrium values of the poloidal magnetic fields computed by CREATE-L and MAXFEA is shown in Fig. 7.1 **(a)** and **(b)** respectively for the LSN and USN plasma configurations. A vertical instability $n = 0$ RWM is exhibited by both the models with a slow growth rate ($< 10s^{-1}$), consistent with the experimental evidences [97]. Considering the LSN shot, the growth rate has been computed neglecting the effect of the toroidal support structure (TSS). Thus, the RFX-mod 3 mm thick shell, clamped over the vacuum vessel, provides the main stabilizing contribution as shown in Tab. 7.2. The shell is characterized by poloidal and inner equatorial gaps, which have been reproduced in the 3D realistic mesh adopted in the CarMa0 model production. In addition, a fictitious 3D axisymmetric mesh has been generated and used in computations in order to provide a reference and a cross-check with axisymmetric models for the entire procedure. In this case, the modified inductance matrix computed over the 3D axisymmetric mesh by CarMa0 has been compared with the CREATE-L results, providing a relative error around 1% and an excellent agreement on growth rates as shown in Tab. 7.2. Furthermore, we notice that the introduction of the gaps in the shell has a small destabilizing effect. The same considerations still hold for the USN plasma configuration. Finally, the toroidal support

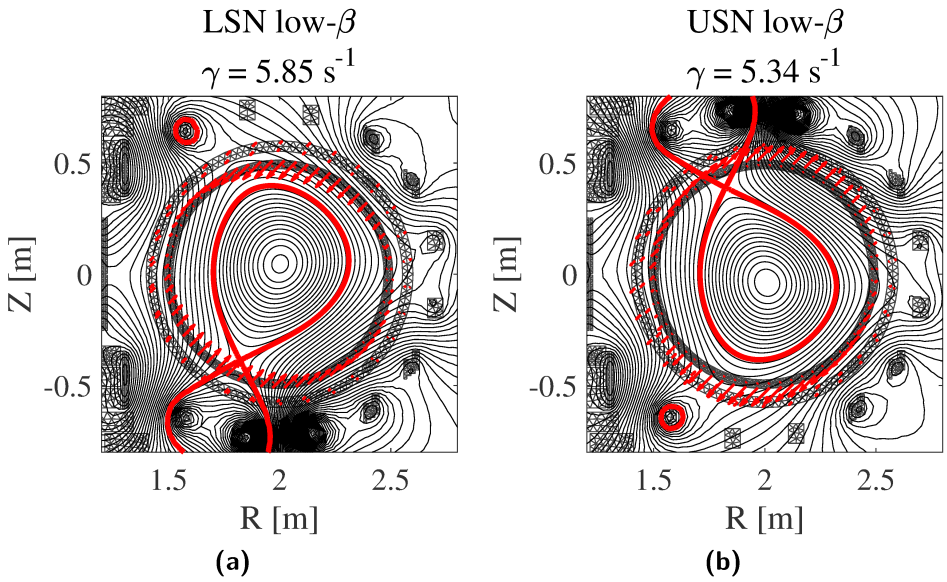

Figure 7.2: LSN **(a)** and USN **(b)** CREATE-L reference plasma equilibrium: poloidal magnetic flux topology, plasma boundary (red line) and current density pattern on passive conductors (red arrows) associated to the vertical instability.

structure (TSS) has been considered in the computation of the growth rates for both configurations, whose values are slowed down as expected. These growth rates are reported for the LSN and USN magnetic configurations in Fig. 7.2, where also the plasma boundary and poloidal flux topology at equilibrium are shown. Furthermore, the pattern of the induced current density distribution in passive conductors, which is representative of a typical vertical instability mode structure, is shown with red arrows, in Fig. 7.2. The same pattern can be considered in the 3D analysis with CarMa0 code, revealing the shell gaps effect on the induced current distribution as shown in Fig. 7.3(a). Finally, a fictitious linear plasma current quench event has been considered with CarMa0NL with a typical current density pattern and the corresponding plasma configuration reported in Fig. 7.3(b). A detailed analysis of the key phenomena ruling the $n = 0$ RWM vertical instability has been performed for USN experimental plasma equilibria, as we will see in the following sections.

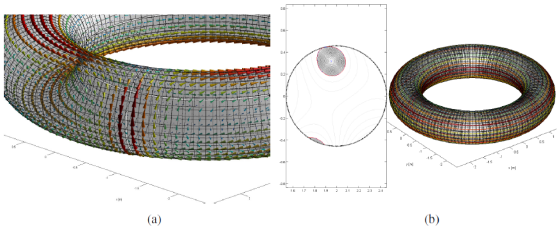

Figure 7.3: LSN Current density patterns and plasma configurations: (a) unstable mode; (b) plasma current quench.

7.2 Iterative procedure results

The iterative procedure described in Sect. 6.4 leads to lower values of $\bar{\chi}^2$ with respect to the basic case of experimental plasmas obtained by following the preliminary phase described in Sect. 6.4.1. In order to quantify the improvement effect of the procedure, we define a relative percentage variation factor, which will be used as relative percentage error for many physical quantities compared to their experimental measurements:

$$\epsilon_V = \frac{V - V^*}{V^*} 100 \tag{7.1}$$

where V is the quantity considered (e.g. B_θ, $\bar{\chi}^2$) and V^* is the reference quantity used as comparison (e.g. the experimental value, the reference case). For example, the V quantity can be a model computed value, or, in the particular case described later, it can be the best $\bar{\chi}^2$ result of the iteration procedure of different runs (see Tab. 6.4). Defining the ϵ parameter leads us to show the improvements obtained in terms of lower values of $\bar{\chi}^2$ by the iterative procedure with respect to the basic case obtained from the preliminary phase. Eq. 7.1 will be used also to compare some physical quantities computed by the CREATE-L model with respect to experimental values, such as the poloidal magnetic field and also later for other comparisons involving the total plasma current.

Before showing the results of the procedure, it is important to define the results of the preliminary phase for two typical cases, constituting a subset of the overall experimental plasma shots analyzed and reported previously in Tab. 6.3: the low-β plasma discharge #36922 and the intermediate-β plasma discharge #39068. The two related plasma linearized models have been produced by following the preliminary phase, and both have shown several mismatches with the experimental data. Firstly, the poloidal magnetic fields computed by the CREATE-L model were characterized by relative percentage errors up to 30% with respect to the pickup coil measurements as shown in Fig. 7.4. This would inevitably be revealed by high values of the $\bar{\chi}^2$, as shown in Tab. 7.3. Secondly, the plasma boundary computed by the CREATE-L model is not in agreement with the one reconstructed from experimental measurements as clearly visible from Fig. 7.5. Thirdly, and maybe the most important thing in terms of the set up of the iterative procedure, these CREATE-L models revealed a clear sensitivity on total plasma current variations as shown in Fig. 7.6. This result led to inevitably set the total plasma current as an additional degree of freedom for the iterative procedure with the possibility of assuming values up to +10% of the experimental one (i.e. the total plasma current measured

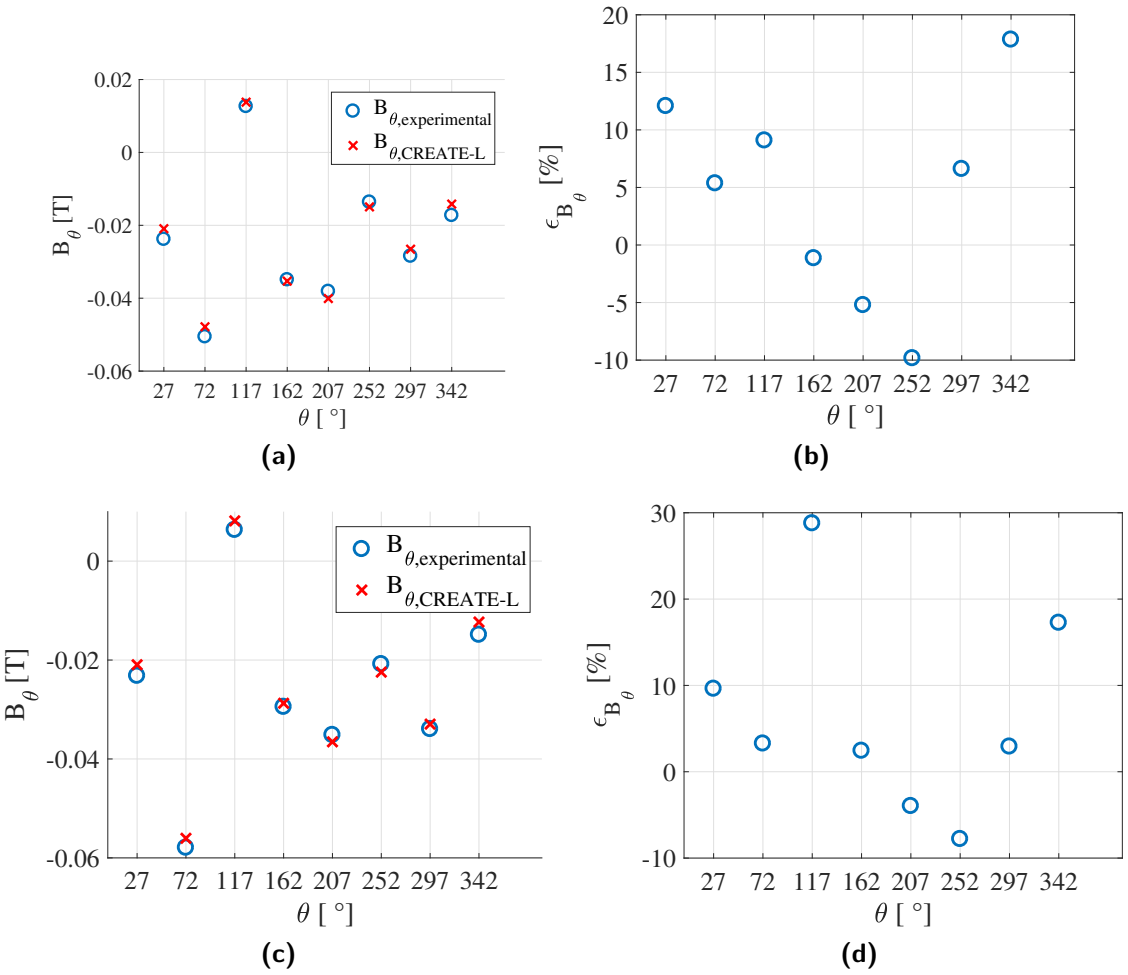

Figure 7.4: # 36922 **(a-b)** and # 39068 **(c-d)** preliminary phase equilibrium poloidal magnetic fields at sensors location and relative percentage error with respect to the measured experimental values

by the Rogowski coil, with the appropriate filtering and subtraction of undesired contributions). It is important to stress that these three results are valid for all the experimental plasmas analyzed, meaning that a simple and general approach, as the preliminary phase is, does not model correctly the experimental plasma equilibrium and therefore do not lead to the production of accurate linearized plasma response models. In particular, the sensitivity on total plasma current has a favorable effect, meaning it leads to lower values of $\bar{\chi}^2$ (i.e. a better agreement with experimental data) only for increments with respect to the Rogowski coil measured value. This is the reason why the iterative procedure allows only increments of the total plasma current.

	$\bar{\chi}^2$		
shot no.	basic case	iterative procedure	$\epsilon_{\bar{\chi}^2}$ [%]
36922	1.5148	0.1224	-91.92
39036	2.7048	0.4905	-81.87
39039	6.4457	1.2414	-80.74
39040	0.3981	0.1963	-50.69
39068	1.4717	0.1529	-89.61
39084	1.2914	0.4451	-65.53
39122	0.6725	0.1810	-73.09
39123	3.3476	0.7169	-78.58
39135	1.3329	0.0775	-94.19
39136	1.3963	0.3226	-76.90

Table 7.3: Iterative procedure results for experimental plasmas in terms of $\bar{\chi}^2$

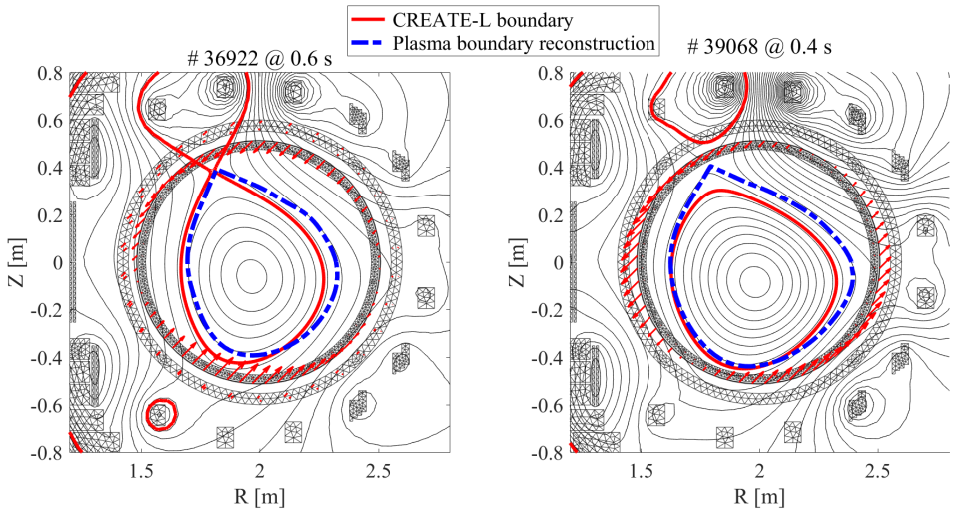

Figure 7.5: # 36922 (a) and # 39068 (b) preliminary phase plasma computed boundary and reconstructed one

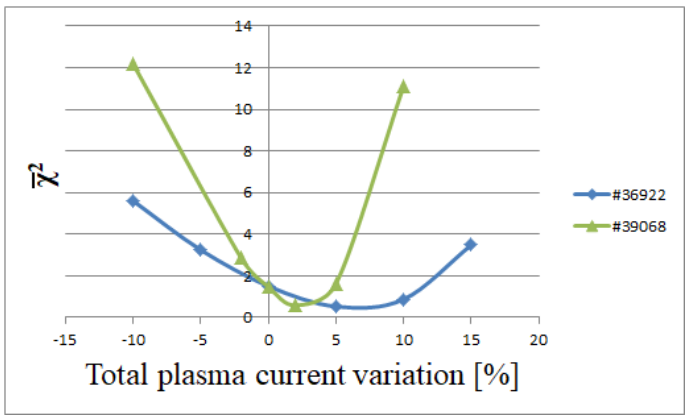

Figure 7.6: # 36922 (a) and # 39068 (b) preliminary phase total plasma current sensitivity

Tab. 7.3 shows the improvements reached by applying the iterative procedure to all the experimental shots under analysis: the best solution reached by the procedure (i.e. the plasma linearized model characterized by the minimum value of $\bar{\chi}^2$) is very accurate in terms of poloidal magnetic field with respect to the experimental values for all the discharges except the plasma discharge #39039. The improvements achieved by using the procedure are clearly evident in Tab. 7.3: all the linearized models of all plasma shots under analysis have a much lower value of normalized chi-square with respect to the reference basic cases; the relative percentage reduction goes from 50% up to the 95%. The accuracy of the CREATE-L model so produced is shown in Fig. 7.7 **(a)-(d)** and Fig. 7.7 **(e)-(j)**, where the match between the experimental and the computed poloidal magnetic fields at sensors locations is clearly evident.

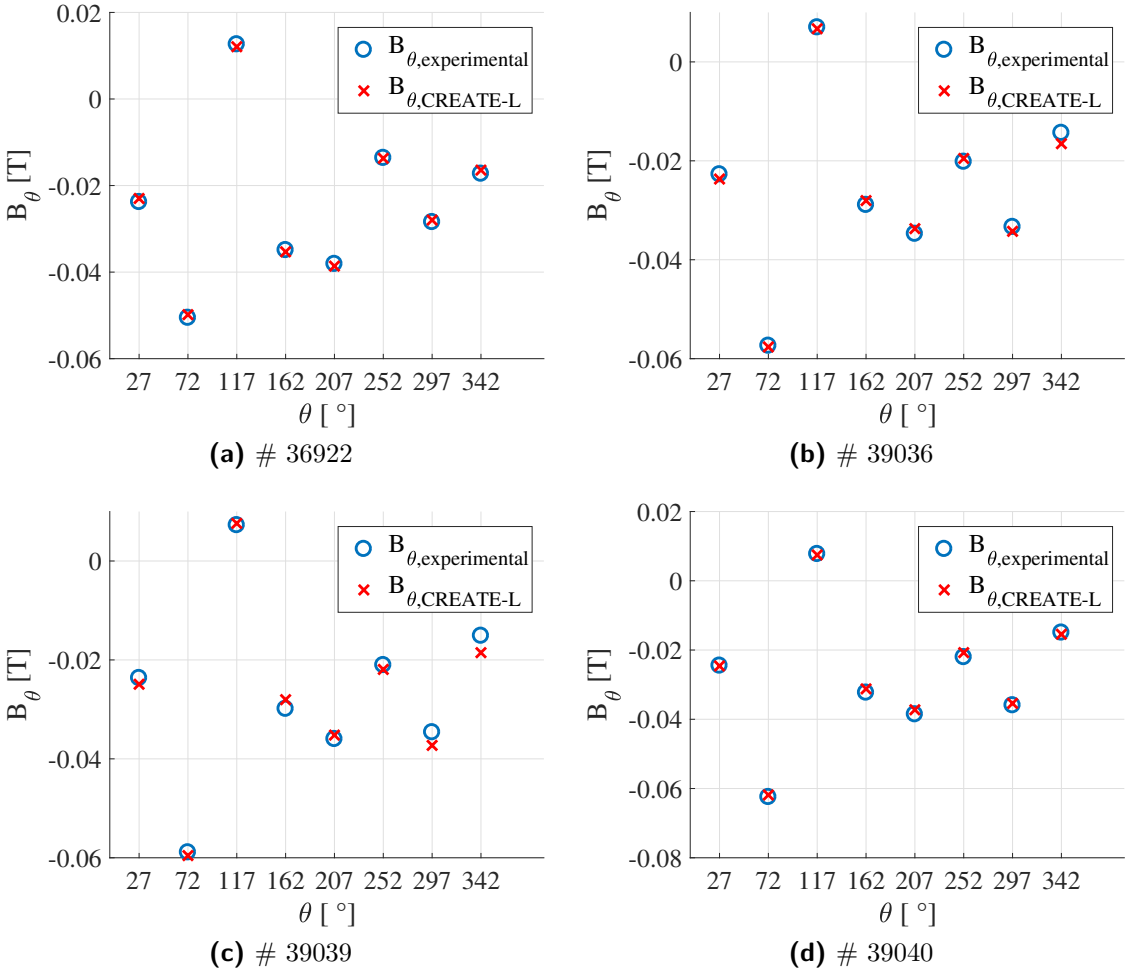

(a) # 36922 **(b)** # 39036

(c) # 39039 **(d)** # 39040

Figure 7.7: CREATE-L and experimental poloidal magnetic fields at sensors location for all shots under analysis **(a) - (d)**

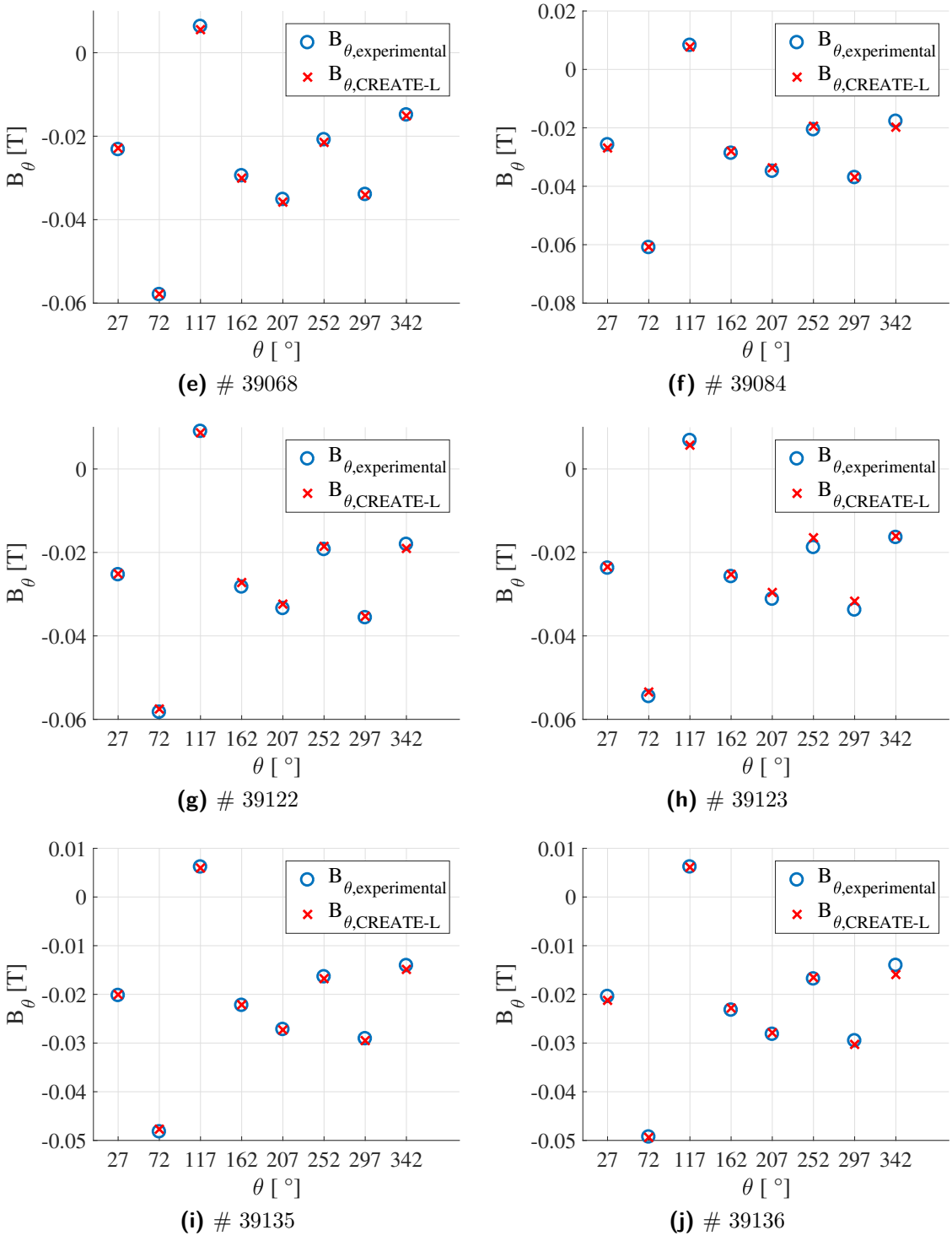

(e) # 39068 **(f)** # 39084

(g) # 39122 **(h)** # 39123

(i) # 39135 **(j)** # 39136

Figure 7.7: CREATE-L and experimental poloidal magnetic fields at sensors location for all shots under analysis **(e) - (j)**

The associated relative percentage error for each sensor measurement is, for the majority of the produced models around the ±5% as shown in Fig. 7.8 **(a)-(d)** and Fig. 7.8 **(e)-(j)**. Even in the worst case (i.e. shot no. 39039), it is always below 30% that is the value previously obtained in the preliminary phase. Some exceptions could involve the values related to the pickup coils located in proximity of the X-point (where the poloidal magnetic field goes to zero); in any case, the iterative procedure leads to very accurate linearized plasma response models.

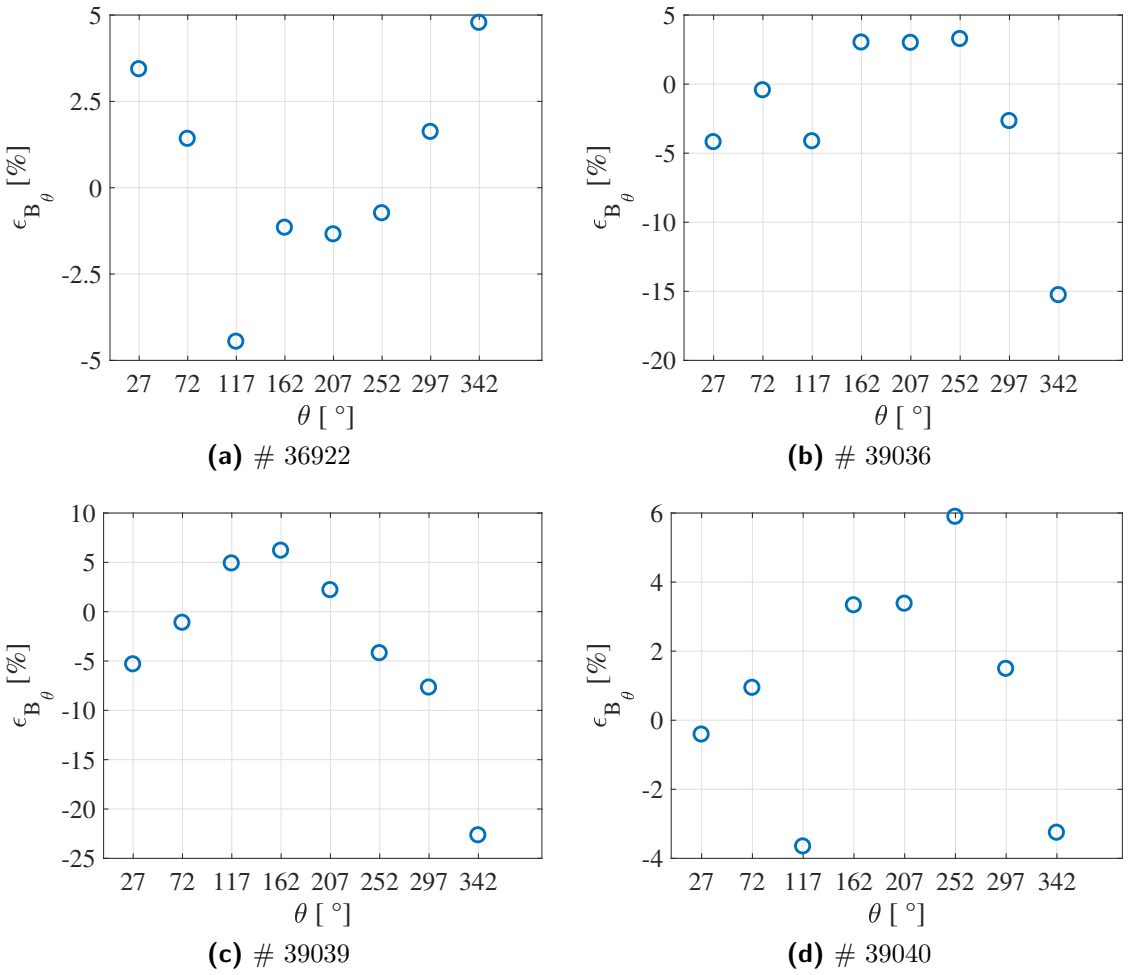

(a) # 36922 **(b)** # 39036

(c) # 39039 **(d)** # 39040

Figure 7.8: CREATE-L relative percentage error with respect to the measured poloidal magnetic fields at sensors location for all shots under analysis **(a) - (d)**

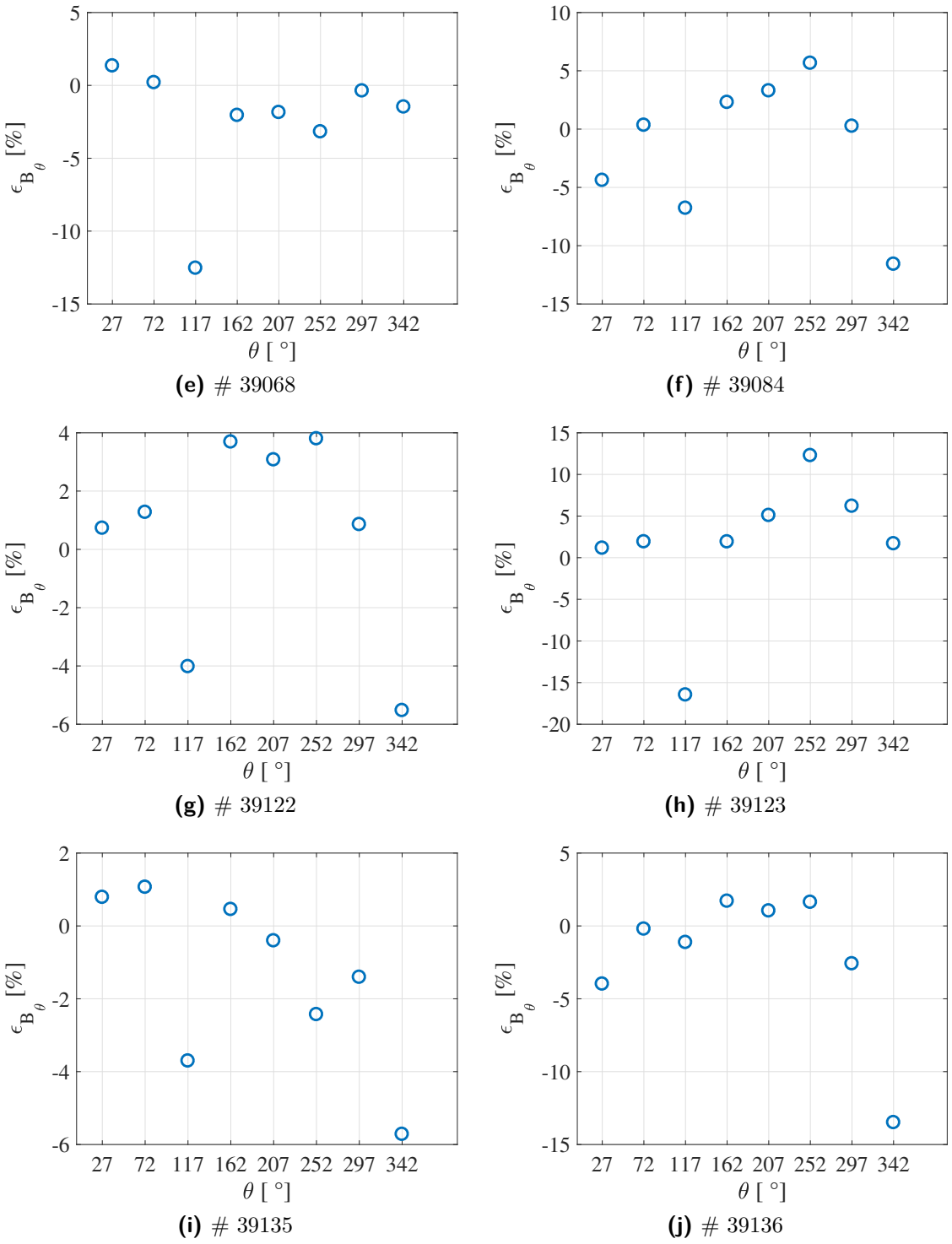

(e) # 39068 **(f)** # 39084

(g) # 39122 **(h)** # 39123

(i) # 39135 **(j)** # 39136

Figure 7.8: CREATE-L relative percentage error with respect to the measured poloidal magnetic fields at sensors location for all shots under analysis **(e) - (j)**

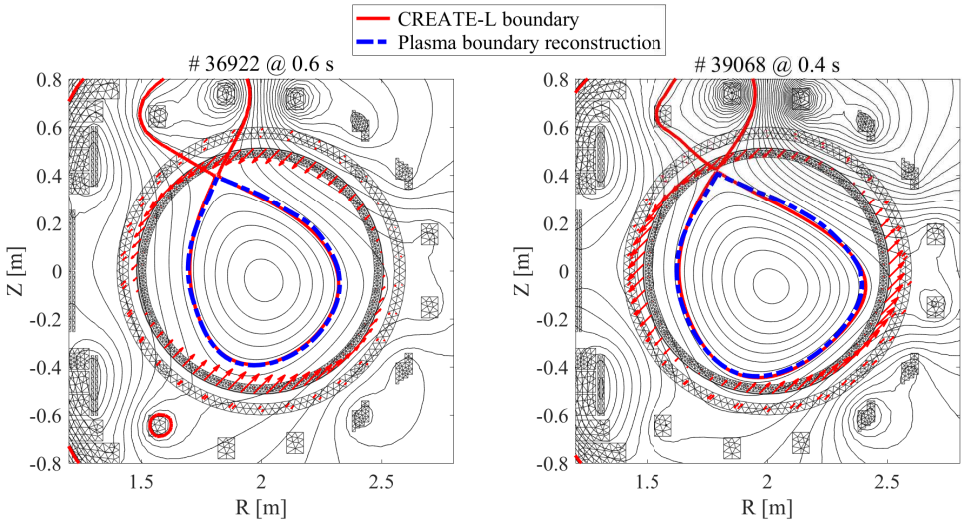

Figure 7.9: # 36922 (a) and # 39068 (b) iterative procedure result in terms of plasma computed boundary and reconstructed one

It is important to stress that lower values of $\bar{\chi}^2$ lead also to a better match between the CREATE-L computed plasma boundary and the reconstructed one. Considering the two previous basic cases, shot no. #36922 and #39068, the new plasma linearized models obtained for these two shots are clearly better in terms of plasma boundary agreement compared to the basic case, as shown in Fig. 7.9. By analyzing all the runs of the iterative procedure for all the shots, it is clear that the solution is always reached with an increased value of total plasma current. Now, since the previous analysis already revealed this kind of sensitivity, we compared the experimental value of the plasma current, i.e. the one measured by the Rogowski coil, to the value obtained by performing the discrete line integral of the poloidal magnetic fields measured by the eight pick-up coils at inner surface of the stabilizing shell. We considered the low-β shot no. #36922, the intermediate-β shot no. #39068, and the H-mode shot no. #39123, which can be considered three typical cases. It has been found a relative percentage error (with respect to the Rogowski value) between the two values of plasma current of the order of 10% as stated by Tab. 7.4. This discrepancy has to be considered as a sort of "experimental uncertainty" which is present for all the duration of the plasma discharges.

The results of the iterative procedure also revealed a clear dependence of the plasma equilibrium on variations of the total plasma current with respect to the Rogowski experimental value. Since this sensitivity has been revealed in all the shots analyzed (Tab. 7.5), it is possible to say that it involves all the plasma regimes under analysis. The new plasma linearized models revealed a clear sensitivity of the equilibrium on the total plasma current: increased values from 1 to 7% with respect

Shot no.	$I_{p,rogowski}[A]$	$I_p(B_\theta)$	$\epsilon_{I_p(B_\theta)}[\%]$	$\epsilon_{I_{p,CREATE-L}}[\%]$
36922	56108.77	61663	9.90	3.80
39068	60912.74	66435	9.07	5.12
39123	56886.88	62699	10.22	1.21

Table 7.4: Comparison of total plasma current values for three typical shots and their associated relative percentage variations with respect to the Rogowski measurement

Shot no.	$I_{p,Rogowski}[kA]$	$I_{p,CREATE-L}[kA]$	$\epsilon_{I_{p,CREATE-L}}[\%]$
36922	56.11	58.24	3.80
39036	59.37	62.47	5.22
39039	61.84	65.94	6.64
39040	64.84	66.11	1.96
39068	60.91	64.03	5.12
39084	63.63	65.83	3.46
39122	60.94	62.42	2.43
39123	56.89	57.57	1.21
39135	49.51	52.16	5.35
39136	51.01	53.86	5.58

Table 7.5: Comparison between total plasma current values of the best CREATE-L model for all shots and the Rogowski coil experimental measurement

to the measured value were necessary to fit the experimental data in terms of poloidal magnetic fields and plasma boundary reconstruction. It can be noticed also that the sensitivity level is always lower than the level of experimental uncertainty (i.e. $\sim 10\%$).

The possibility of a double uncertainty on the magnetic diagnostics, in particular on the calibration of the Rogowski coil and on the measurements of the magnetic pickup coils, should be taken into account. The Rogowski coil has been always calibrated considering only the RFP configuration, which means with a simple subtraction of a constant related to the poloidal voltage loop integral, i.e. the toroidal magnetic flux. This simple correction provided good results in the RFP configuration, in which once the plasma current is fixed, also the flux will be fixed. This relation does not hold in the Tokamak configuration because the toroidal field is produced by the external coils and it dominates the configuration. In fact, the Rogowski coil is subjected to the stray toroidal magnetic field. In the circular tokamak, this discrepancy can be corrected with a simple constant, but in the case of the shaped tokamak the problem is complicated by the asymmetric geometrical configuration of the field shaping coils. Furthermore, the unbalanced magnetomotive force due

to the disconnection of the upper/lower couple of FS coils could lead to local magnetic fields that are not desired. This would affect also the magnetic pickup coils whose calibration is made one by one. Nevertheless, the Rogowski coil should be considered a more accurate measurement in the shaped tokamak operations, since it performs correctly the line integral compared to the circuitation of the poloidal field measured by the pickup coils; in fact, this is a discrete line integral which, because of the discreteness, could be more influenced by the "undesired" contributions (i.e. asymmetric active field shaping coils, X-point, ...). An accurate correction should be performed by using an overall circuit model with the coupling between any active or passive winding and the measurement device written in terms of mutual inductances.

Improvement on the plasma linearized models of USN experimental plasmas has an impact on many physical aspects involved in the control purposes; one of these is the vertical stability which is the subject of next section.

7.3 Open loop stability analysis

The new accurate plasma linearized models of experimental plasmas allowed further investigations on vertical stability, including 3D wall effects, in three different plasma regimes (i.e. low-β, intermediate-β, H-mode). We will consider for a detailed analysis of the vertical instability three previously adopted typical cases (i.e. low-β #36922, intermediate-β #39068, H-mode #39123), constituting a subset of the overall experimental plasma shots analyzed as reported previously in Tab. 6.3. All

Shot no.	γ $[s^{-1}]$
36922	5.09
39036	9.95
39039	6.99
39040	2.79
39068	2.56
39084	11.33
39122	3.49
39123	4.45
39135	8.90
39136	9.08

Table 7.6: Computed growth rates in 2D (vessel, shell, tss) for all the experimental shots under analysis

the plasma models exhibit a slow $n = 0$ vertical instability growth rate ($< 10s^{-1}$) which is consistent with the experimental evidences in RFX-mod [97]. The computed growth rates for the three typical cases take into account different numbers and descriptions of the passive surrounding conducting structures, as summarized in Tab. 7.7. All the other shots have been considered in the $2D$ wall approximation, by using the CREATE-L model for the computation of the growth rate; the overall results of the growth rate computations for all the shots are summarized in Tab. 7.6. It can be noticed that by introducing the toroidal support structure (TSS), the growth rate is slowed down by a factor up to 18% with respect to the case with only the vessel and shell as passive conductors. The comparison between 2D and

	γ [s^{-1}]			
Shot no.	2D (vessel,shell)	3D (vessel,shell)	2D (vessel,shell,tss)	3D (vessel,shell,tss)
36922	6.17	7.36	5.09	6.48
39068	3.12	3.55	2.56	3.11
39123	5.42	6.18	4.45	5.39

Table 7.7: Computed growth rates for different descriptions of the surrounding passive conductors (vessel, shell and toroidal support structure tss

3D results (Tab. 7.7) shows that the poloidal and inner equatorial shell gaps have a destabilizing effect with an increasing of the mode growth rate up to 16% compared to the 2D case. Beyond the decreasing values of growth rate for plasmas with increased values of β_p, it is interesting to note that the structure of the unstable mode, represented by a pattern of current on the passive conductors, is significantly different for the three shots as shown in Fig. 7.10. In particular, the low-β plasma (i.e. #36922) has a typical antisymmetric pattern of currents on the upper and lower passive conductors with respect to the equatorial plane, representing a vertical instability [98]. Instead, the intermediate-β plasma (i.e. #39068) is characterized by a pattern spanning the conductors in all the poloidal angles, involving in particular the conductors on the outer and inner sides of the equatorial plane. This feature is more evident in the H-mode plasma (i.e. #39123) where the up-down antisymmetric components are smaller, while the one related to the outer and inner sides are stronger. The outer-inner pattern is typically associated to horizontal instability which may be possible in these plasmas with strong shaping also along the equatorial plane, as shown in Fig. 7.10. This result will be recalled in section Sect. 7.7.1 when the the statistical results will be discussed. In addition, it is reasonable to think that a more uniform distribution of the mode along the poloidal angle (Fig. 7.10), leads to a slower instability growth rate. The same considerations can be extended to all the experimental shots analyzed, as it can be seen from Fig. 7.11. Finally, the 3D mode structure has been computed with CarMa0 code for each of the three typical shots confirming the 2D CREATE-L analysis; the patterns are represented in Fig. 7.12, where the passive induced current patterns are represented by arrows with colors of increasing level of intensity.

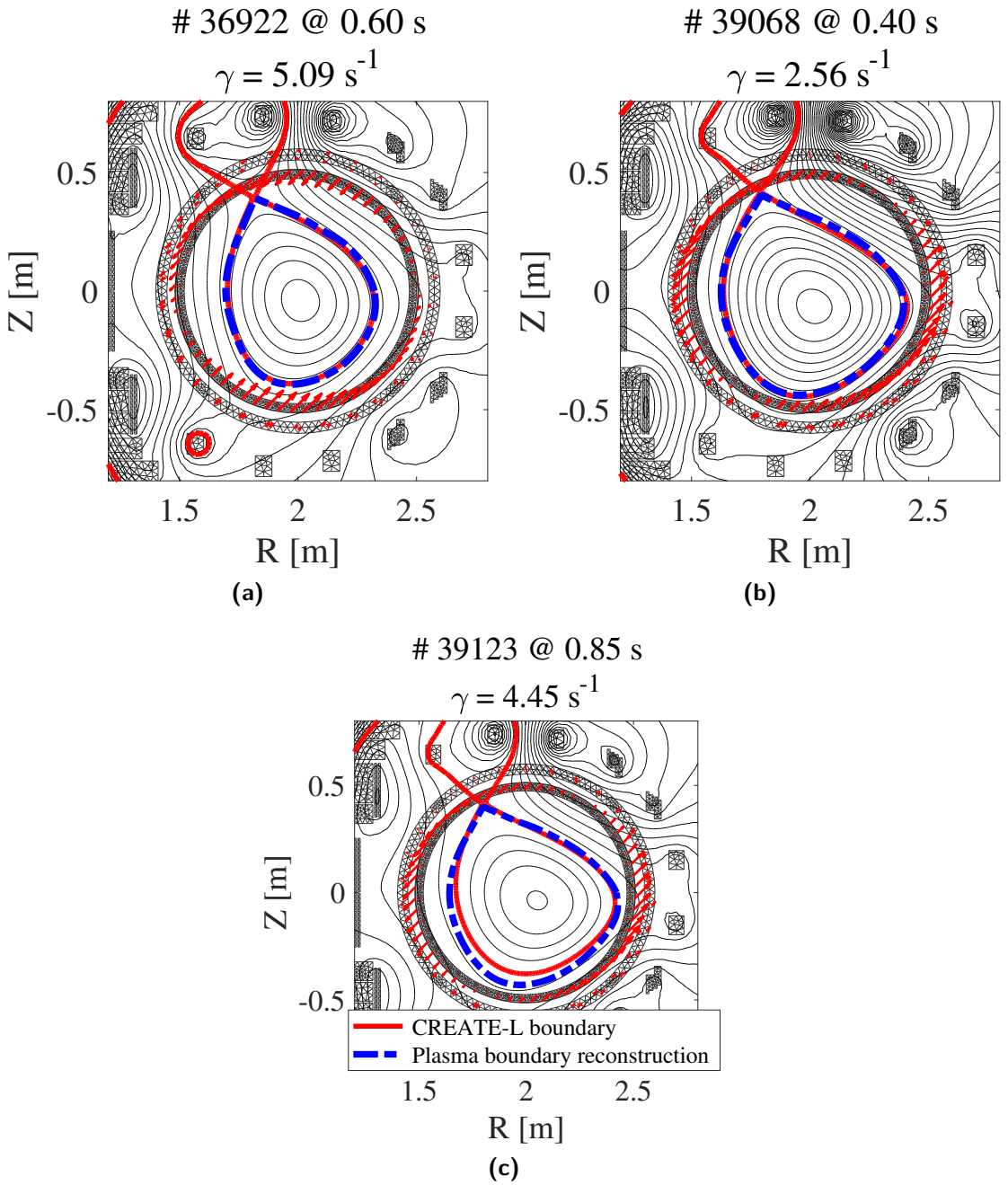

Figure 7.10: # 36922 **(a)**, # 39068 **(b)**, # 39123 **(c)** plasma equilibrium computed boundary (red) and reconstructed (blue), with current density pattern on passive conductors (red arrows) associated to unstable mode structure for each experimental shot

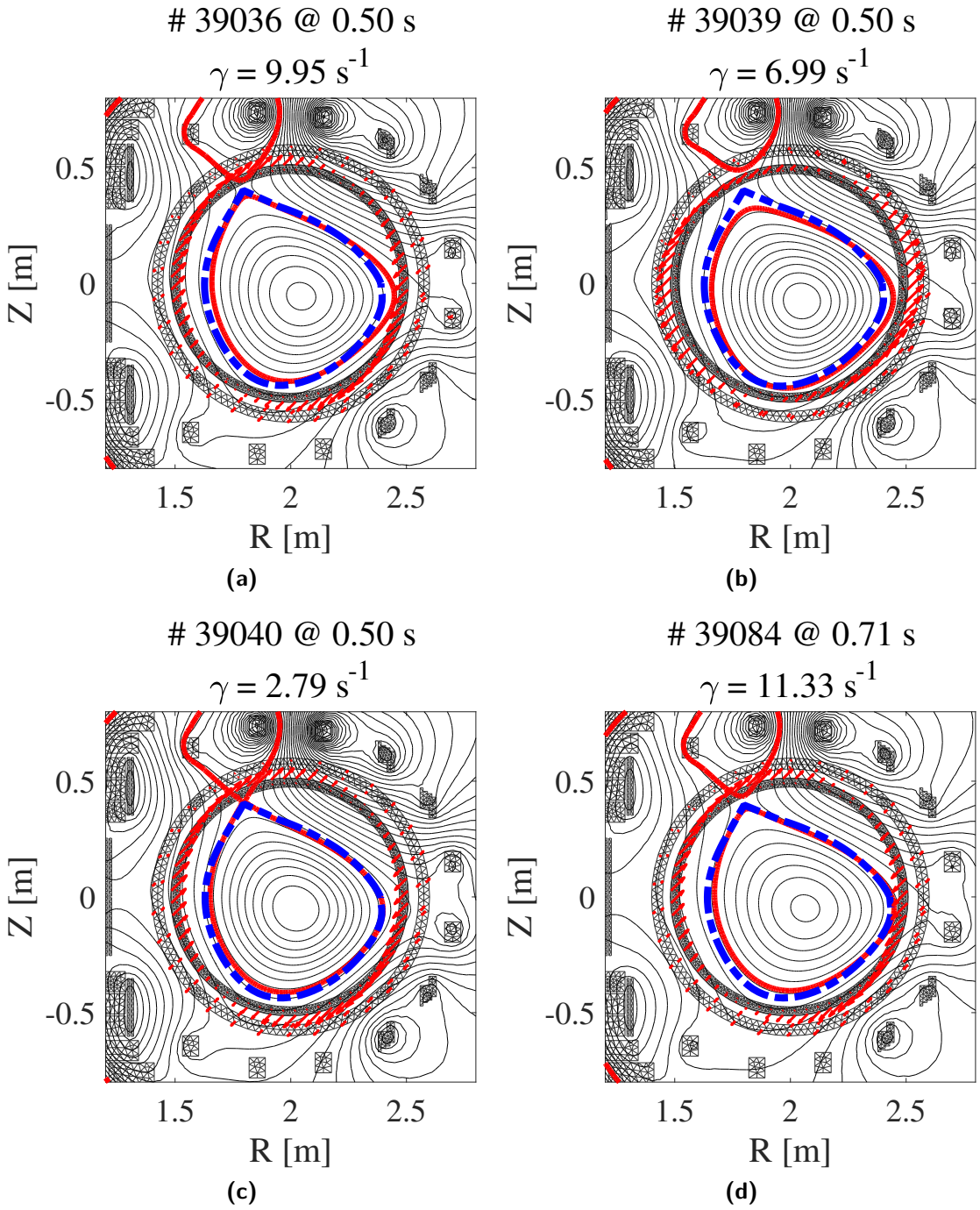

Figure 7.11: Plasma equilibrium computed boundary (red) and reconstructed (blue), with current density pattern on passive conductors (red arrows) associated to unstable mode structure for each experimental shot **(a)-(d)**

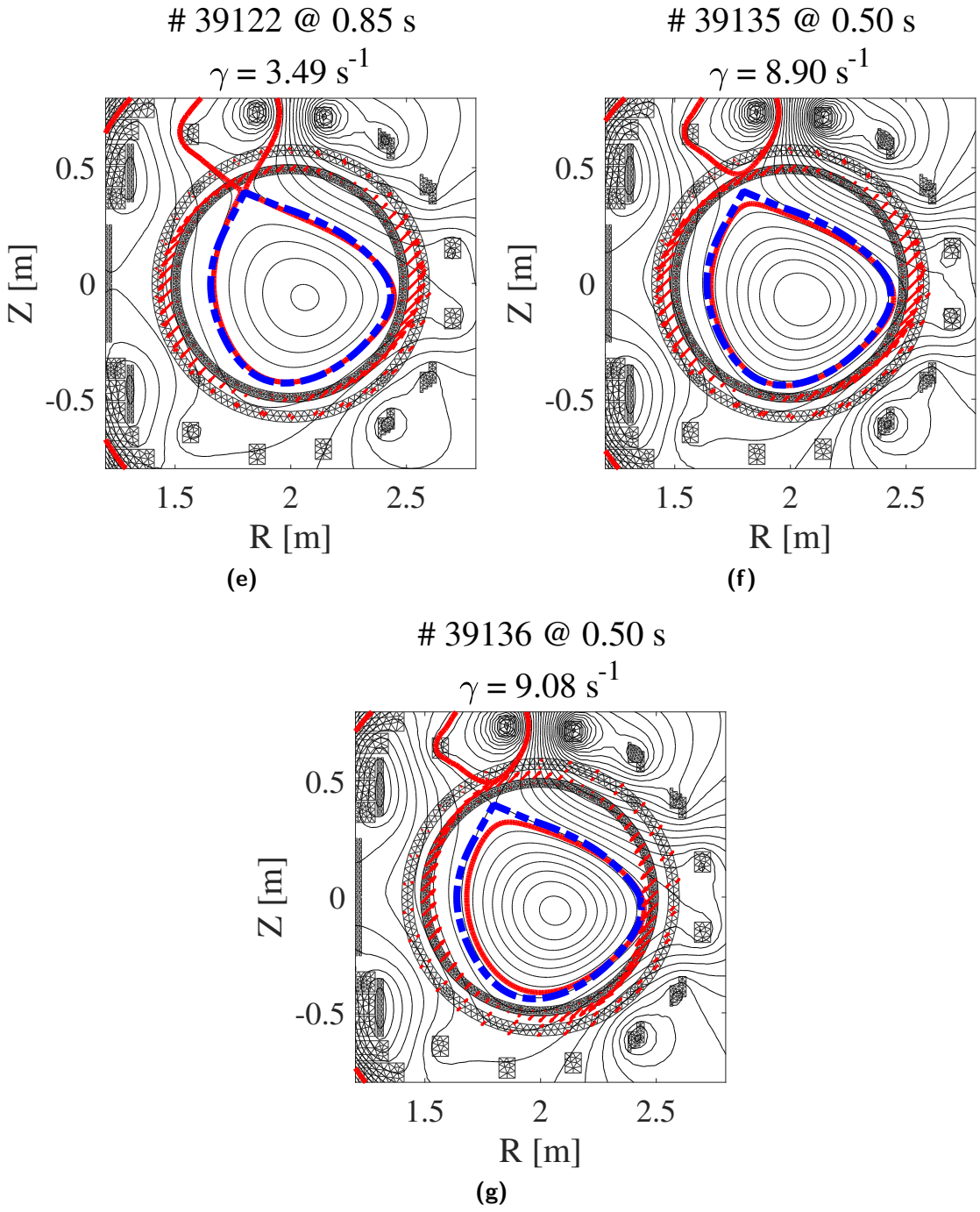

Figure 7.11: Plasma equilibrium computed boundary (red) and reconstructed (blue), with current density pattern on passive conductors (red arrows) associated to unstable mode structure for each experimental shot **(e)-(g)**

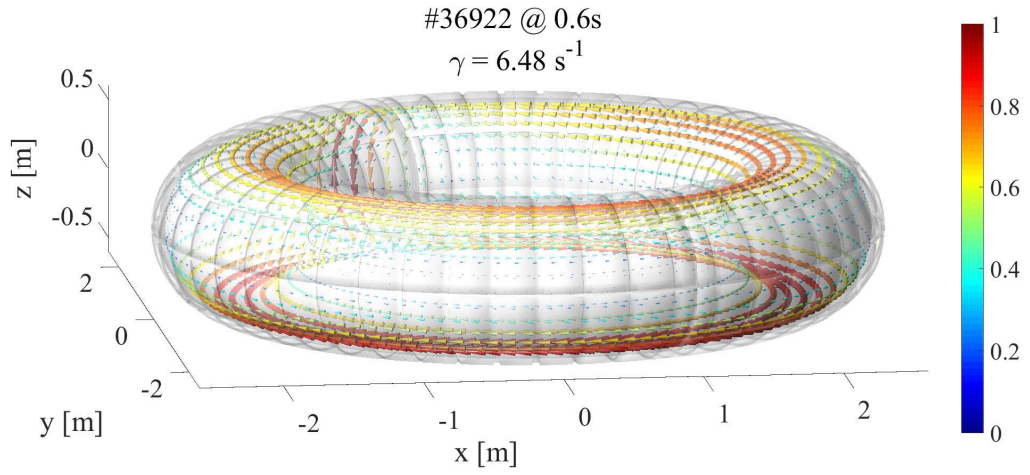

(a)

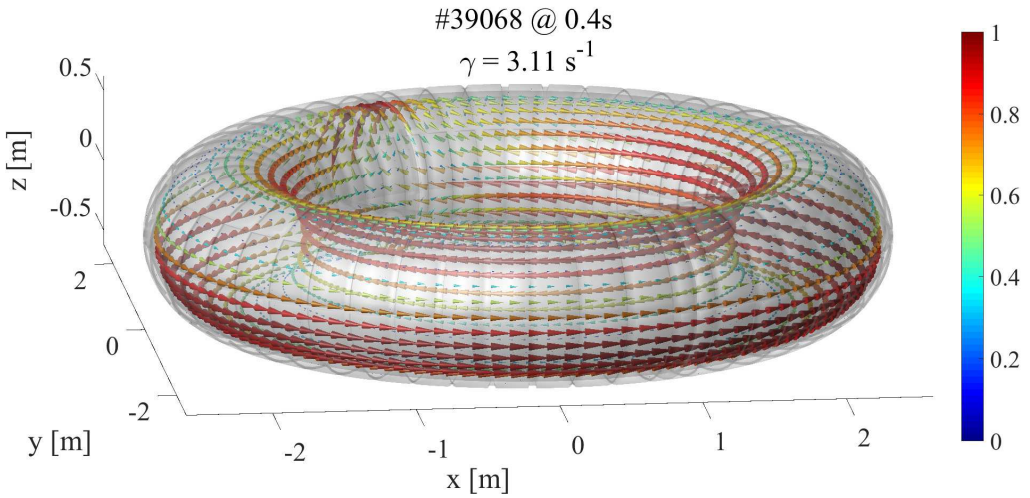

(b)

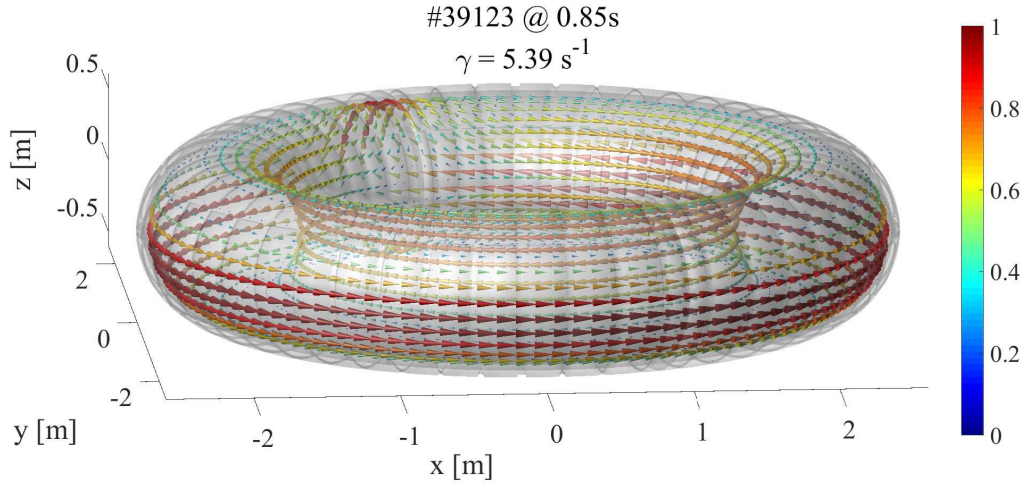

(c)

Figure 7.12: 3D current density pattern on passive conductors (red arrows) associated to unstable mode structure for each of the three typical experimental shot

7.4 Closed loop stability analysis

The SISO models related to the control of the vertical position have been used for the closed loop stability analysis. Firstly, the CREATE-L model reproducing the low-β experimental plasma shot no. 36922 has been used to verify the CREATE-L model of the numerically generated low-β plasma adopted for the control system design. This reference model perfectly matches the one obtained from experimental data, as it can be seen from open loop Bode plot in Fig. 7.13 **(a)**-**(b)**.

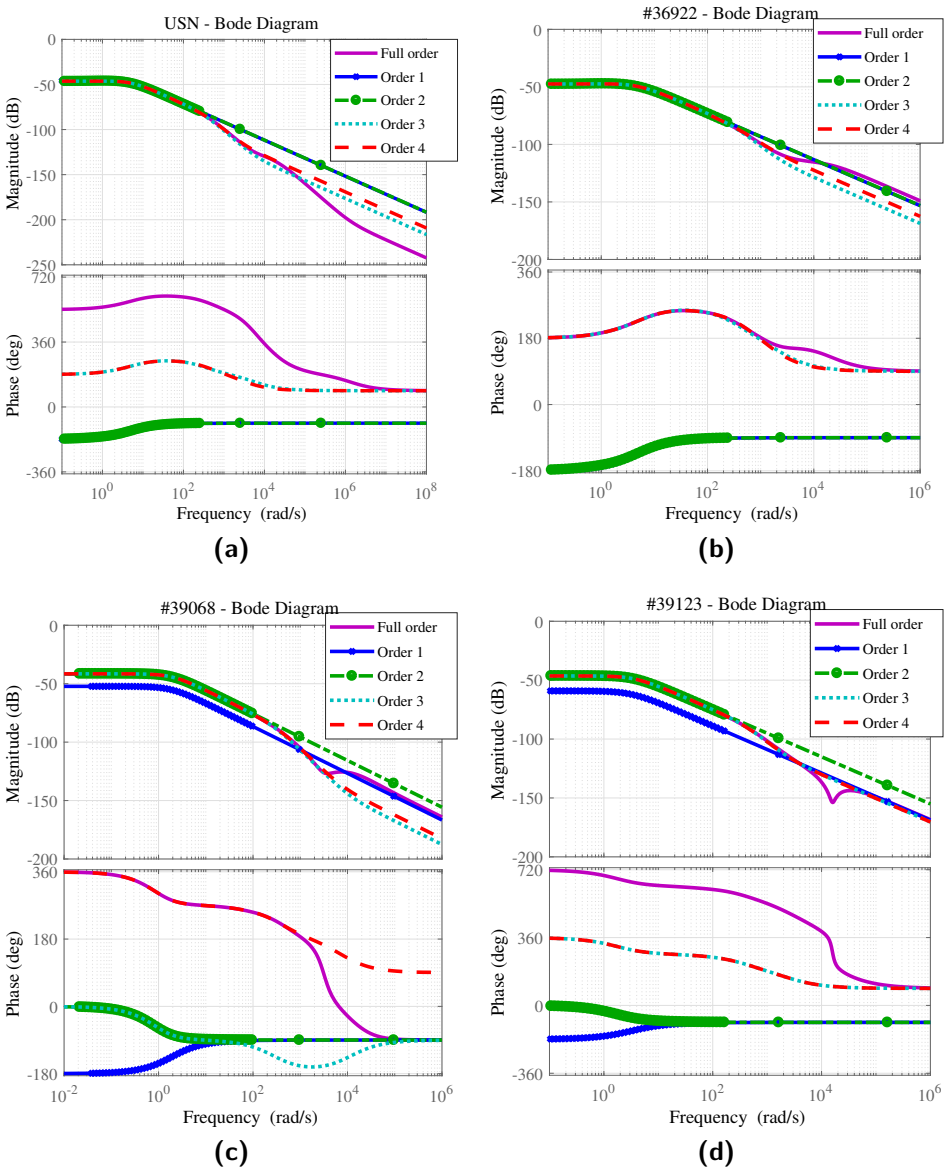

Figure 7.13: Bode diagram of the four typical plasma models **(a)** USN low-β reference, **(b)** # 36922 low-β, **(c)** # 39068 intermediate-β, **(d)** # 39123 H-mode

It can be stated following [1], that for the low-β plasma the higher order dynamics are negligible for the vertical position control design. It is important to remind that the vertical position control has been developed by stabilizing a reduced order system obtained from the full order CREATE-L model of a numerically generated low-β plasma configuration. The reduced order adopted (i.e. first order model, see [1]) was obtained by the truncation of the state space model, meaning that all the states from 4 to 188 were eliminated. The comparison between this reference model and its counterpart obtained from the experimental data of shot no. 36922, which was itself obtained thanks to the mentioned control system so designed, validates the use of such reduced order models for low-β plasmas.

Now, it is interesting to note that the SISO models of the intermediate-β and H-mode plasma revealed to be non-minimum phase systems, this means that they are characterized by a different behaviour with respect to the previously analyzed low-β models. For these systems, the transfer functions have zeros in the right-hand s-plane contrary to the minimum phase systems. This puts a serious limitation on the robust stability of the feedback system since a simple proportional gain is not able to stabilize the unstable mode. In fact, all the intermediate-β and H-mode plasma models report an interesting common feature: the asymptotic independence of the growth rates from the gain applied by the control system. Fig. 7.14 shows that by increasing the value of the gain, the mode slows down but not enough to be stabilized because it saturates at the value of the positive zero. In this picture, the zero works as a center of attraction for the unstable pole, preserving its position on the right half of the s-plane or equivalently on its unstable condition. It is important to highlight that the saturation phenomenon has not be seen experimentally, reasonably because

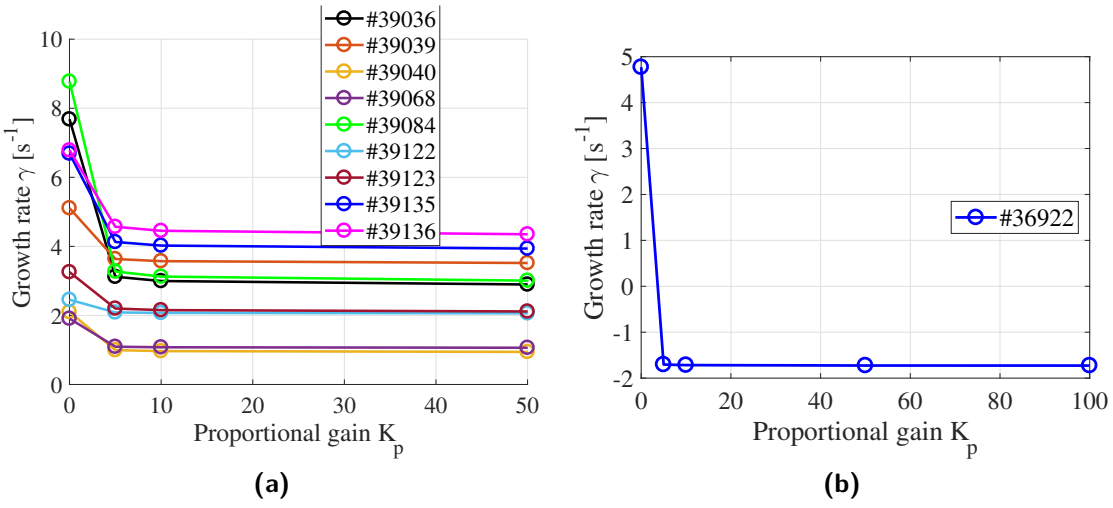

Figure 7.14: Asymptotic independence of the growth rates from the gain **(a)** and stabilization of the growthrate **(b)**

of the slow values of the growth rates that lead the instability to behave on a time scale much longer than the time interval of the plasma discharge. Nevertheless, these models exhibit a different behaviour with respect to the one of the low-β plasmas, and it cannot be explained as a numerical effect. The dynamic of the behavior of these new systems is not the topic of this section which will be investigated in the final section of the chapter. What is important to underline is the effects of these new models representing the new experimental data, and the control system through which these data were produced, remembering that the design of this control system has been based on the old low-β models. It means that we have to analyze the non-minimum phase systems representing this new class of linearized plasma response models.

The presence of the positive zero cannot be explained as the effect of the derivation of the SISO system from the full CREATE-L model previously described in Sect. 6.5.2 (e.g. reconnection matrix, balanced reduction, ...). In fact, the full SISO model, which was obtained by just applying the circuit reconnection matrix, exhibits this positive real zero even by applying to it a simple balanced reduction (i.e. *balreal* MATLAB function), in which if the system is unstable its stable part is isolated, balanced, and added back to the unstable part. Both full-order and reduced order models exhibit positive real zeros. In particular, the position of the smaller zero, which attracts the unstable pole, does not change when the reduction procedure is applied. In fact, more real positive zeros can be present in the original SISO models, usually at very high values (e.g. 10^3), or also complex conjugate couple of zeros with a real positive part at high values too. In all the cases, there is always one positive real zero at a significant value, which means at a value in proximity of the unstable pole and able to attract the pole. For each plasma equilibrium, this zero is always present at the same value in all the models: full-order, balanced reduced or truncated reduced order models. What does a positive zero mean for a system? A transfer function is called a minimum phase transfer function if all its zeros lie in the left-hand s-plane, instead if it has zeros in the right-hand s-plane it is called a non-minimum phase transfer function [99]. The meaning of the terms minimum or non-minimum phase is illustrated in Fig. 7.15, see [99] for details.

The range of phase shift of a minimum phase transfer function is the least possible or minimum corresponding to a given amplitude curve, whereas the range of the non-minimum phase curve is the greatest possible for the given amplitude curve. This is evident looking at the comparison between the phase diagrams of shot # 36922 and # 39068 represented in Fig. 7.13, where the first is a minimum phase system while the second not. Non-minimum phase systems have a markedly different phase in

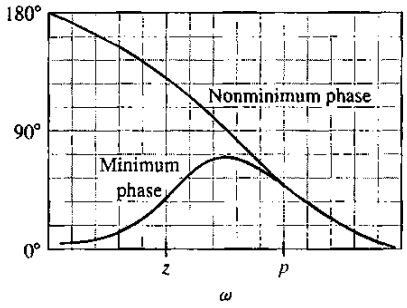

Figure 7.15: The phase characteristics for the minimum phase and nonminimum phase transfer function

the limit $\omega \rightarrow$ inf, as can be seen from Fig. 7.13, when compared to a corresponding minimum phase system (i.e. a similar system with no zeros in the right-half s-plane). This usually results in an unacceptable transient response; in fact, non-minimum phase systems with only one right-half plane zero (or odd number of them) result in a transient response that has opposite sign when compared to the input [88], which is the typical "undershoot" behaviour.

All the SISO models of the new linearized plasma response models produced from the experimental data are non-minimum phase systems. From their frequency response analysis, it turns out that the reduced order models previously adopted, i.e. models of first or second order, are not able to reproduce the behaviour of the analyzed experimental plasmas. Thus, the previous assumption of negligible high order dynamics used for the control system design, does not hold anymore for these types of plasma. This can be easily verified comparing the Bode diagrams of the non-minimum phase systems (shot no. # 39068 and # 39123 in Fig. 7.13**(c)-(d)**) with the minimum phase one (i.e. #36922 and USN in Fig. 7.13 **(a)-(b)**); it can be seen that a first or second order reduced model is compatible with the full order for the low-β plasmas while a third order at least is needed for the shaped tokamak models # 39068 - # 39123. As shown in Fig. 7.16, the same considerations can be made by analyzing the step response of these systems. It is interesting that the new plasma linearized models, in which the SISO model exhibits at least one positive real zero in the proximity of the unstable pole, are all related to the same experimental champaign; in addition, they are all non-minimum phase systems. The investigation of the causes of the presence of such positive zero, that leads to the saturation of the growthrate under the action of the controller will be treated in the final section of the chapter.

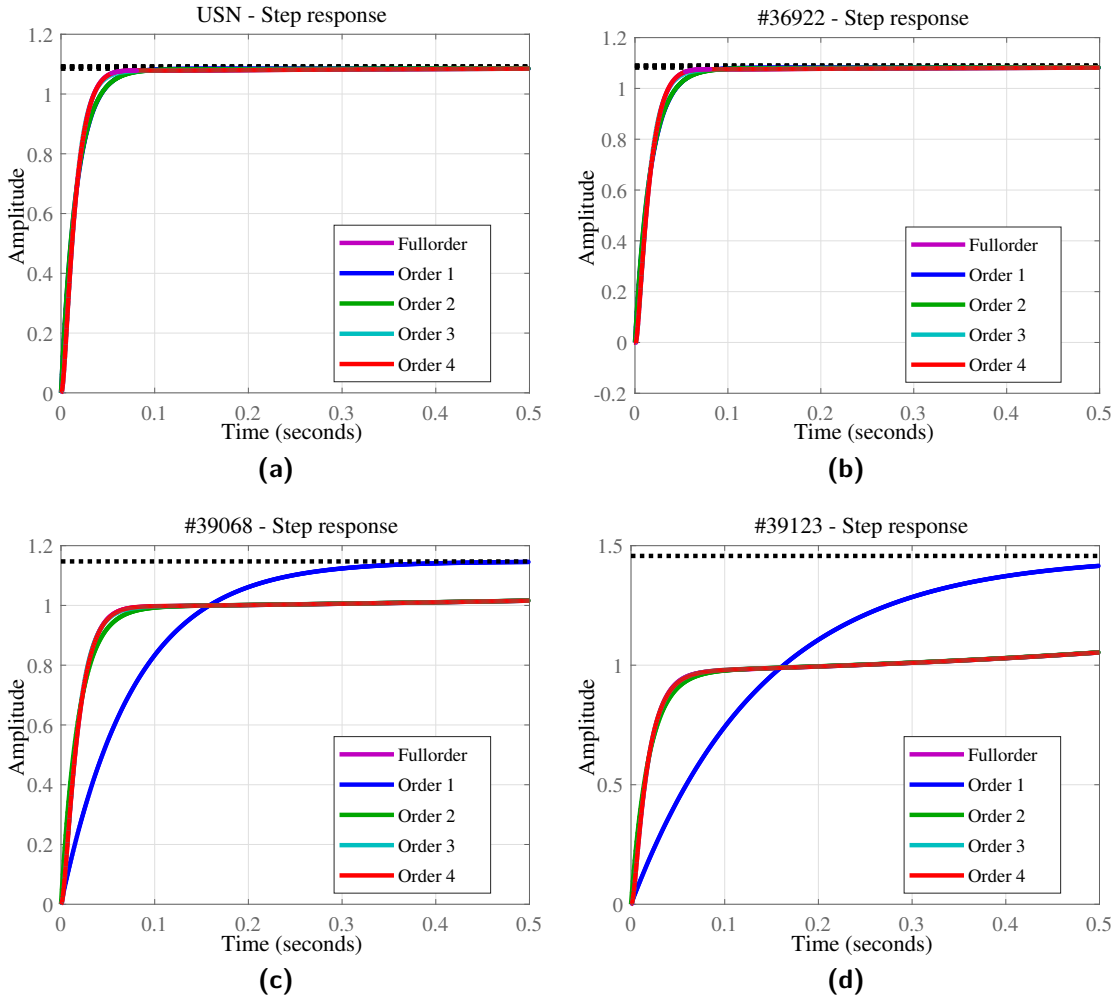

Figure 7.16: Step response of the four typical plasma models **(a)** USN low-β reference, **(b)** # 36922 low-β, **(c)** # 39068 intermediate-β, **(d)** # 39123 H-mode

7.5 Plasma shape control test results

The simulations described in Sect. 6.6 aim to investigate the nature of the plasma-wall gaps oscillations seen in the experiments. We have seen that two different approaches are used, leading to two distinct simulations: the first approach involves oscillating noise on the gaps while the second concerns the additional input representing a perturbation on the plasma β_p. Despite the results shown in Sect. 7.4 related to the saturation of the $n = 0$ growth rates, we assume that the plasma is vertically stable for the intermediate-β plasma shot # 39068 under analysis. The assumption is justified by the fact that the growth rate of the vertical instability is extremely small, so small that a VDE has not been seen in the experiments. However, this assumption is necessary because the shape controller is designed assuming a vertically stable system.

The results of the first simulation are shown in Fig. 7.17, where the noise oscillating signals lead to oscillations on the plasma-wall gaps; this has to be intended as a preliminary and qualitative results since it can be argued that we are in some way confusing the cause with the effect. This is the reason why the second approach on simulation is needed by defining the additional input on the model related to the β_p disturbances, as defined in Eq. 6.5 of Sect. 6.6. The signal applied as poloidal beta disturbance to the model is in fact used as β_0 disturbance, since in the CREATE-L model the poloidal beta is represented by the parameter β_0. The time behaviour of β_0 disturbance has been derived from the one of $\beta_p(t)$ by the following scaling

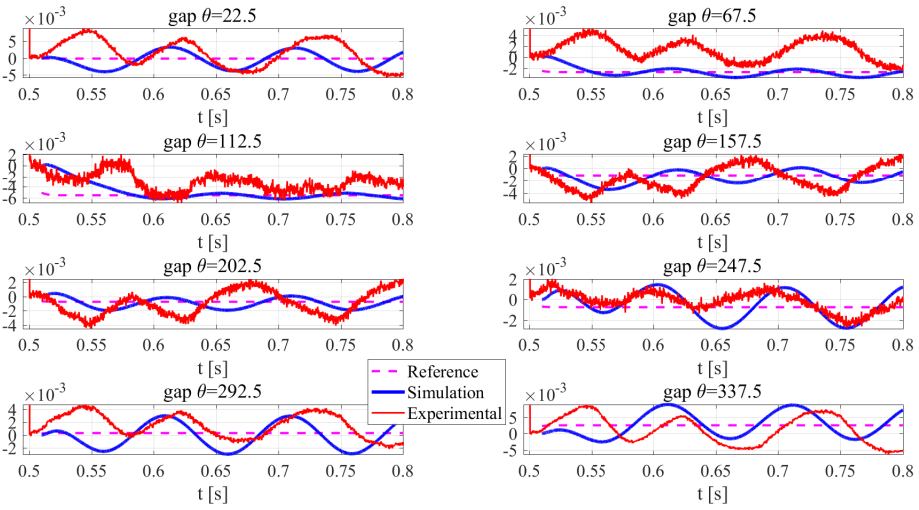

Figure 7.17: Shot no. 39068, oscillations of the eight gaps from the first simulation with oscillating noise signals

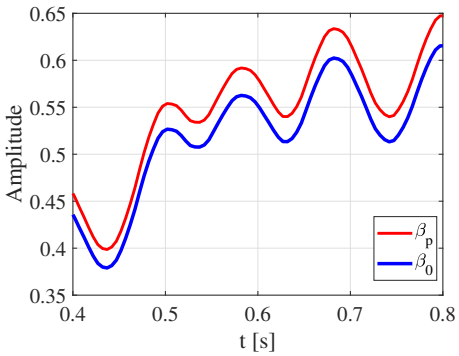

Figure 7.18: Shot no. 39068, β_0 and β_p oscillating disturbance signals

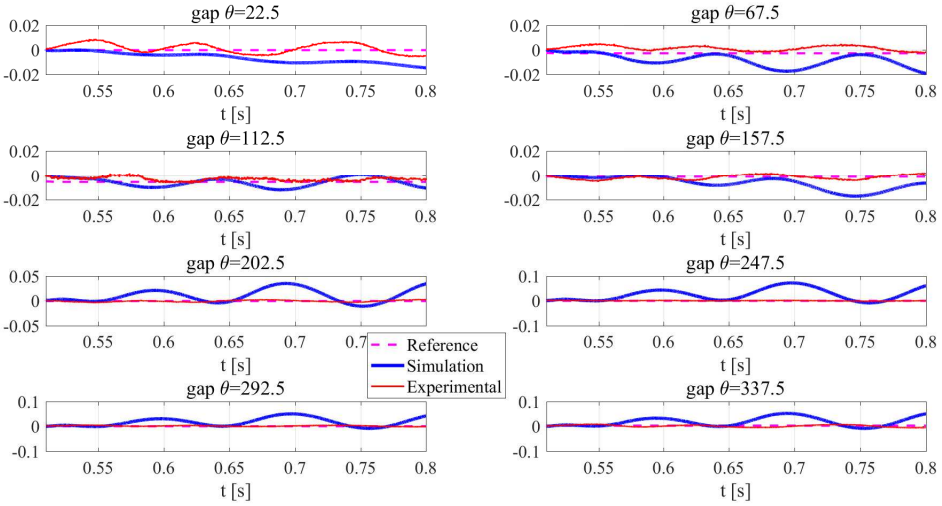

Figure 7.19: Shot no. 39068, oscillations of the eight gaps from the second simulation with oscillating β_0 disturbance as additional input

relation:

$$\beta_0(t) = \frac{\beta_p(t)}{\beta_p(t_{eq})}\beta_0(t_{eq}) \tag{7.2}$$

where $t_{eq} = 0.4$ is the time instant of the plasma equilibrium at which the plasma linearized model has been derived. The time behaviour of the β_0 and β_p quantities is shown in Fig. 7.18. The results of this second simulation on shot # 39068 are consistent with the previous one in the sense that oscillations on the eight plasma-wall gaps occur as shown in Fig. 7.19. Now, it is clearly evident that the simulations do not match the experimental values of the oscillating gaps; on the other hand, oscillations exist both in the experimental data and in the simulations. A particular property of the simulation is the radial asimmetry of the model results highlighted by the clear difference in terms of amplitude between the first four gaps (from $\theta = 22.5°$ to $\theta = 157.5°$) and the second four(from $\theta = 202.5°$ to $\theta = 337.5°$). The first four

gaps are located in the upper part of the machine (positive values of the $z-$axis), while the second four gaps are located in the lower part. The oscillations should be considered as reflections of the pulsed gas puffing control. In fact, the gas puffing has a time scale comparable with the one of the oscillations, as shown previously in Fig. 6.10. In addition, all the experimental plasma discharges with a pulsed gas puffing control exhibit oscillating plasma-wall gaps while the others do not.

7.6 Nonlinear modelling of RFX-mod tokamak plasmas

The nonlinear time evolution of plasma equilibrium was focused to reproduce the experimental plasma discharges in terms of magnetic flux topology and poloidal magnetic fields in agreement with experimental data. The analysis takes into account a 3D volumetric description of the passive conducting structures (i.e. vessel and shell) and it has been carried out by means of the CarMa0NL code [55]. The time evolution of the plasma equilibrium is determined by solving a non-linear set of equations [55] in which the values of the total plasma current and the active coil current variations (with respect to the equilibrium) are imposed from experimental values at each time instant. It is assumed the same plasma current density parametrization as the CREATE-L code, with three parameters associated to physical quantities (i.e. internal inductance, poloidal beta and safety factor on axis). The nonlinear analysis treats these parameters as time varying disturbances. As shown in Fig. 7.20, the β_0 parameter related to the poloidal beta is computed by imposing a fit to the experimental time behaviour of β_p. The other two parameters α_M and α_n have been kept constant during the whole time evolution, and they are equal to the values of the plasma linearized model determined with the iterative procedure.

The selected shot is the low-β experimental plasma # 36922. The time instant at which the nonlinear analysis starts is the one previously determined (Sect. 7.2), i.e. $t_i = 0.6s$. The final time instant is the one at which the plasma current vanish $t_f = 1.2$, which means at the end of the discharge. The time step adopted is $dt = 6.6741\ 10^{-4}s = 0.6674\ ms$, corresponding to 900 iterations in time. For each time instant, a maximum number of 50 Newton-Raphson iterations have been set. Reminding that a remarkable sensitivity on total plasma current exists for

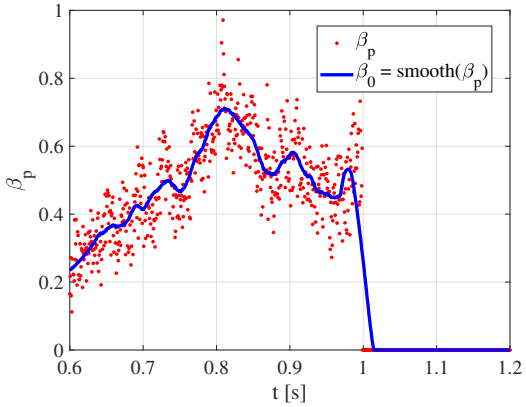

Figure 7.20: Shot no. 36922, time evolution of β_p and the associated β_0 parameter

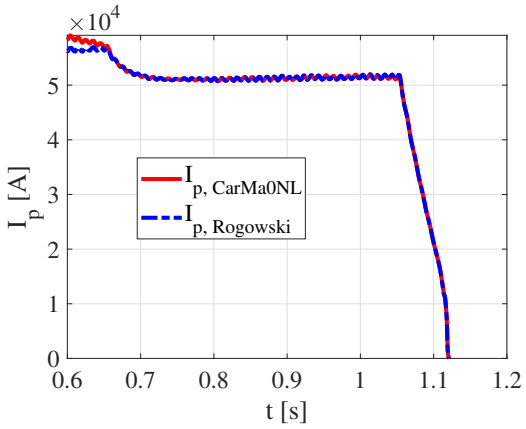

Figure 7.21: Shot no. 36922, time evolution of the experimental total plasma current and the one imposed as input in the simulation

the plasma linearized models obtained from experimental data, since the nonlinear analysis has the CREATE-L linearized model of the equilibrium at t_i as a starting point, it is necessary to consider this sensitivity also in the time evolution. The problem is that since the nature of this sensitivity is not clear, we have to assume a time evolution also for it. In the case under analysis, this sensitivity is quantified by an increment of 3.8% on the total plasma current with respect to the value measured by the Rogowski coil. It has been assumed that this increased value of total plasma current does not hold for all the plasma discharge, and in particular that it would vanish in a time scale of $100dt$, equivalently at $t_2 = 0.66s$. This assumption is based on a previous nonlinear time evolution analysis in a 3D axisymmetric mesh, in which a better agreement in terms of magnetic flux topology was evident for the simulations without a constant value of increased total plasma current kept constant for all the time of the discharge. The time behaviour of the total plasma current used in the analysis and the value measured by the Rogowski are shown in Fig. 7.21 where, as assumed, the percentage increment vanishes in the first 100 time instants of the discharge. It is important to remind that the vertical control system is not considered in this analysis, meaning that there is no active control on the plasma position.

The CarMa0NL code allowed us to compute the eight poloidal magnetic field values considering the contribution of both the plasma and the eddy currents induced in the 3D volumetric wall; thus the poloidal magnetic fields have been computed for the entire time evolution in correspondence of the magnetic pickup coils location meaning at 8 poloidal angles and at 4 toroidal angles. The experimental mean values of these fields have been compared with the CarMa0NL simulated ones, and a mean value on the 4 toroidal sections has been considered for each poloidal angle

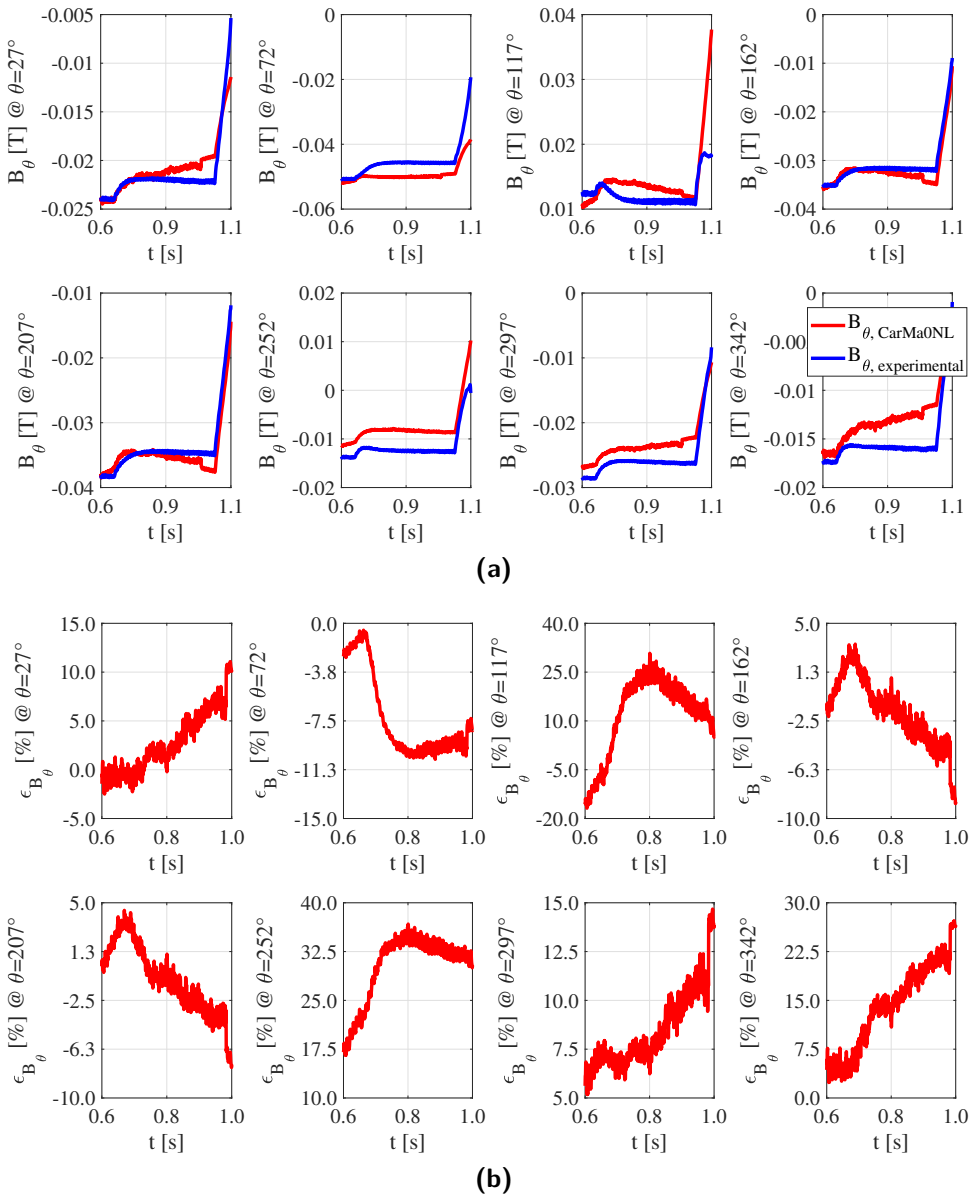

Figure 7.22: Shot no. 36922, time evolution of the poloidal magnetic fields **(a)** and relative perccentage errors **(b)** at different sensor locations

as shown in Fig. 7.22. The behaviour is not well reproduced for all the poloidal angle positions as shown by the relative percentage error with respect to the experimental values for each poloidal angle in Fig. 7.22; the error at positions $\theta = 117°, 252°, 342°$ reaches values up to 30%, while at all the other poloidal locations it is in the range of 10%. In terms of boundary the agreement between the non-linear computation and the plasma boundary reconstruction based on experimental data decreases as time evolves; this can be seen from Fig. 7.23 where a clear deviation in the position of the plasma from the reconstructed boundary can be recognized $200ms$ after the instant of equilibrium. This vertical position deviation can be due to the missing

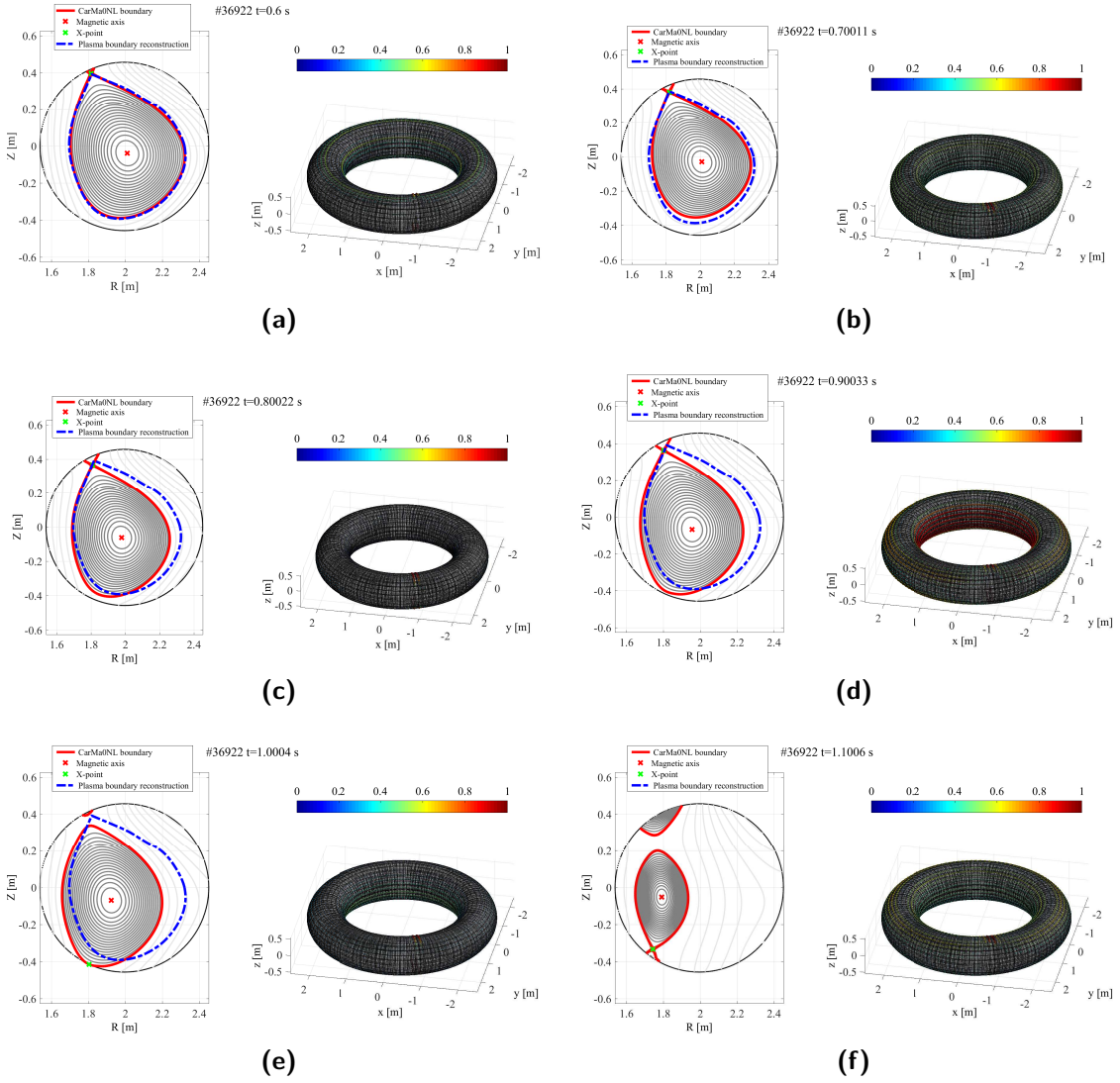

Figure 7.23: Shot no. 36922, time evolution of the magnetic flux topology and eddy current pattern on passive conductors

control system in the nonlinear modelling activity. A similar analysis have been carried out for a circular experimental plasma discharge, during the L-H transition [100].

7.7 Vertical stability of shaped plasmas in RFX-mod tokamak

In this section we present the results obtained in the investigation of the possible conditions for the occurrence of the $n = 0$ vertical instability growth rate saturation under the action of the proportional gain controller. This behaviour was shown previously in the closed loop stability analysis in Sect. 7.4, where it was highlighted that the only CREATE-L plasma model that does not show the saturation phenomena is the one referred to the low-β shot # 36922. All the other models presenting the saturation of the growth rate are related to experimental plasmas with two main common features: the increased values of β_p and the strong plasma shaping. The latter involves several plasma shape parameters that are defined in Eq. 7.3 - Eq. 7.10 and they can be represented as shown in Fig. 7.24.

It is important to remind also that the saturation has not be seen experimentally, reasonably because of the slow values of the growth rates that lead the instability to behave on a time scale much longer than the time interval of the plasma discharge. Therefore, in order to investigate the cause of this phenomenon, it was necessary to extent the available experimental data with new numerically generated equilibria produced by solution of the inverse equilibrium problem (see Sect. 6.7.1). The results that we will present are obtained through the investigation of the whole bulk of data which includes the already presented CREATE-L plasma linearized models obtained from experimental data and the new set of plasma linearized models obtained from the numerically generated plasma equilibria.

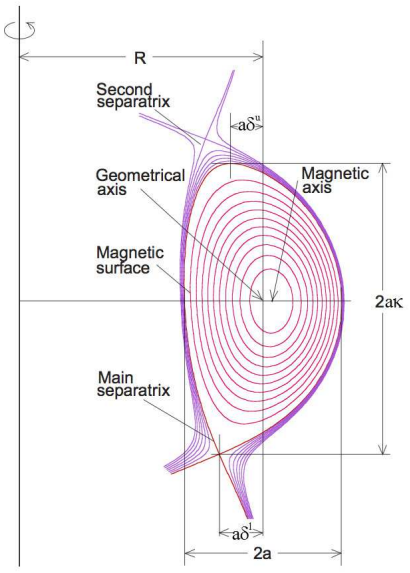

Figure 7.24: Plasma shape with main plasma parameters

- Geometrical center:

$$R_{geo} = \frac{R_{outer} + R_{inner}}{2} \tag{7.3}$$

$$Z_{geo} = \frac{Z_{outer} + Z_{inner}}{2} \tag{7.4}$$

- Minor radius:

$$a = \frac{R_{outer} - R_{inner}}{2} \tag{7.5}$$

- Upper elongation:

$$\kappa_u = \frac{Z_{upper} - Z_{geo}}{R_{outer} - R_{geo}} = \frac{Z_{upper} - Z_{geo}}{a} \tag{7.6}$$

- Lower elongation:

$$\kappa_l = \frac{Z_{geo} - Z_{lower}}{R_{outer} - R_{geo}} = \frac{Z_{geo} - Z_{lower}}{a} \tag{7.7}$$

- Elongation:

$$\kappa = \frac{Z_{upper} - Z_{lower}}{R_{outer} - R_{inner}} = \frac{Z_{upper} - Z_{lower}}{2a} = \frac{\kappa_u + \kappa_l}{2} \tag{7.8}$$

- Upper Triangularity:

$$\delta_u = \frac{R_{geo} - R_{upper}}{R_{geo} - R_{inner}} = \frac{R_{geo} - R_{upper}}{a} \tag{7.9}$$

- Lower Triangularity:

$$\delta_l = \frac{R_{geo} - R_{lower}}{R_{geo} - R_{inner}} = \frac{R_{geo} - R_{lower}}{a} \tag{7.10}$$

- Triangularity:

$$\delta = \frac{R_{geo} - \frac{R_{upper}}{2} - \frac{R_{lower}}{2}}{R_{geo} - R_{inner}} = \frac{\delta_u + \delta_l}{2} \tag{7.11}$$

These new class of numerically generated plasma linearized models represent variations on real experimental plasma equilibria, which means that they are derived from models related to experimental plasma by combining different plasma parameters from different plasma regimes. This combination has been addressed by defining and imposing three different boundary conditions, each one derived from the experimental data representative of the conditions that we want to impose. The

first boundary condition is the definition of the plasma domain, which means that if we want to study the effect of a strong shaped plasma we have to use the boundary reconstruction obtained from an experimental plasma shot with strong shaping, for example shot # 39068. The second boundary condition is the definition of the degrees of freedom of the direct equilibrium solver, i.e. the three parameters related to the plasma current density profile parametrization (α_M,α_N,β_0) plus the total plasma current value I_p. The third boundary condition is the imposition of the poloidal magnetic flux at the plasma boundary which is the sum of the flux due to the unknown currents flowing in the external active coils and of the proper flux of the current flowing through the plasma. In particular, the distribution of the total equilibrium poloidal magnetic flux depends on the distribution of the plasma pressure and the density of the longitudinal current in the plasma column [52]. Thus, this boundary condition on the poloidal flux at the plasma boundary must be imposed consistently with the second boundary condition involving the plasma parameters (α_M,α_N,β_0,I_p) since the poloidal magnetic flux at the plasma boundary changes with a change in the plasma current density profile, meaning a change in (α_M,α_N,β_0), or with a change on total plasma current I_p. Therefore, the third boundary condition is a function of the second one:

$$\Psi_b = \Psi_b(\alpha_M, \alpha_N, \beta_0, I_p) \tag{7.12}$$

where with Ψ we denote the total poloidal flux, $\Psi = 2\pi\psi$. A simple relation of the dependence expressed in Eq. 7.12 can be found by the reader in [52] at section 2.4. The importance of this consistent imposition of these two boundary conditions can be seen by explaining one of the numerically generated plasma equilibria produced for the investigation of the growth rate saturation phenomena. Consider that we want to obtain a plasma equilibrium characterized by the standard plasma shape of the USN low-β plasmas in RFX-mod, for example the shape of plasma shot # 36922, but with an increased value of β_p; this will be, for example, a plasma equilibrium similar to the experimental shot no # 39068, which is an intermediate-β plasma, but without the strong shaping that characterize it. In order to obtain such a plasma equilibrium we impose properly the three boundary conditions previously described. Firstly, we use the standard plasma shape of shot # 36922. Secondly, in order to obtain a correct plasma with increased β_p, we impose the second boundary condition by imposing the values of (α_M,α_N,β_0,I_p) equal to the one of shot # 39068. Finally, the third boundary condition is consistently imposed by using the values of poloidal flux at the boundary of shot # 39068. Then, by solving the inverse equilibrium problem a numerically generated intermediate-β plasma with a typical USN plasma

Typical case	BC#2: $(\alpha_M, \alpha_N, \beta_0, I_p)$	BC#3: Ψ_b
36922	(1.2846,0.9985,0.3,58240.09)	-1.078
39068	(2,1.1,0.5116,64030.37)	-0.6836
39123	(1.5927,0.9911,0.8939,57573.56)	-1.2427

Table 7.8: Boundary conditions values derived from the three typical cases

shape for RFX-mod is obtained (Fig. 7.25 **(b)**). This allows us to investigate for example the effect of only the β_p in the saturation phenomena, removing the possible effect of the plasma shaping. With the same procedure we can compute low-β plasma equilibria with strong shaping, which experimentally do not exist in the data of RFX-mod. The boundary conditions assume the values of the three typical experimental plasmas previously analyzed (i.e. #36922,#39068,#39123), each representative of different regimes determined by the β_p value (i.e. low-β,intermediate-β and H-mode) and also by different plasma shaping as already seen in Sect. 7.2; the values of the second and the third boundary conditions are summarized in Tab. 7.8.

The procedure described above allowed us to produce a set of linearized plasma response models as variations on the experimental data equilibria: once the equilibrium active coils currents have been found, we slightly change the plasma shape of the new equilibrium by modifying the values of currents in both the external-internal and up-down saddle coils circuits without affecting the equilibrium global parameters. This allowed us to investigate, for example, the effect of only the β_p in a plasma with a standard USN plasma shape (e.g. #36922) or vice versa the effect of a strong plasma shape (e.g. #39068, #39122) in a low-β plasma. The equilibria so produced are summarized in Tab. 7.9 where the boundary conditions are specified in numerical values in Tab. 7.8. Fig. 7.25 shows the magnetic flux topology of all these new class of plasmas.

Case	BC#1 Plasma boundary	BC#2	BC#3	β_p	Plasma regime
36922_psib39068_1	36922	39068	39068	~ 0.5	intermediate-β
36922_psib39068_2	36922	39068	39068	~ 0.5	intermediate-β
36922_psib39123_1	36922	39123	39123	~ 0.85	increased-β/H-mode
36922_psib39123_2	36922	39123	39123	~ 0.9	increased-β/H-mode
39068_psib36922_1	39068	36922	36922	~ 0.3	low-β
39068_psib36922_2	39068	36922	36922	~ 0.3	low-β
39068_psib36922_3	39068	36922	36922	~ 0.3	low-β
39068_psib36922_4	39068	36922	36922	~ 0.3	low-β
39068_psib36922_5	39068	36922	36922	~ 0.3	low-β
39068_psib36922_6	39068	36922	36922	~ 0.3	low-β
39068_psib36922_7	39068	36922	36922	~ 0.3	low-β
39068_psibUSN_1	39068	USN	USN	~ 0.1	low-β

Table 7.9: New numerically generated class of plasmas obtained by inverse equilibrium solutions with proper boundary conditions defined from experimental typical plasma cases

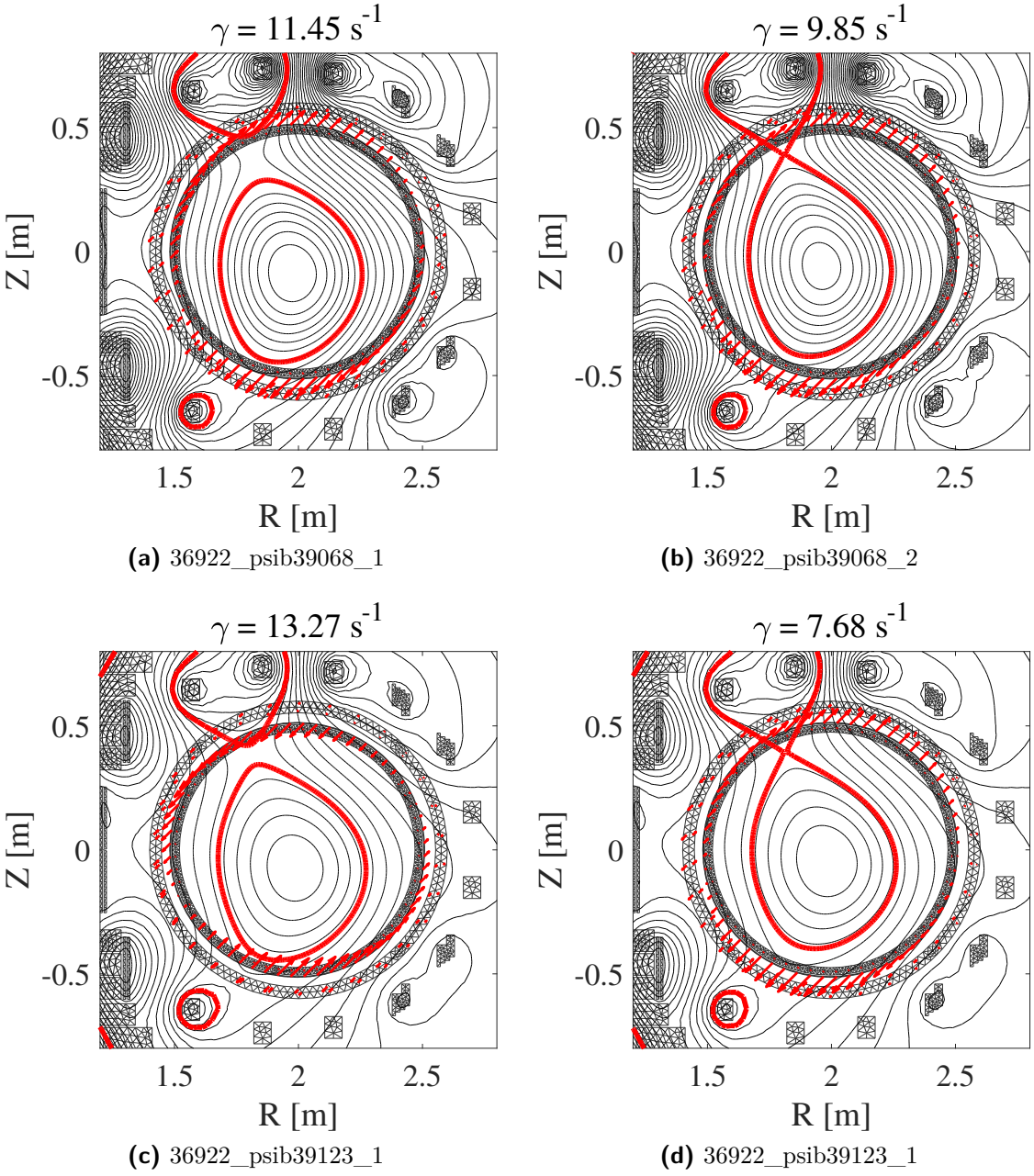

(a) 36922_psib39068_1 **(b)** 36922_psib39068_2

(c) 36922_psib39123_1 **(d)** 36922_psib39123_1

Figure 7.25: CREATE-L poloidal magnetic flux topology of the new class of plasmas obtained as variations on the experimental data equilibria **(a) - (d)**

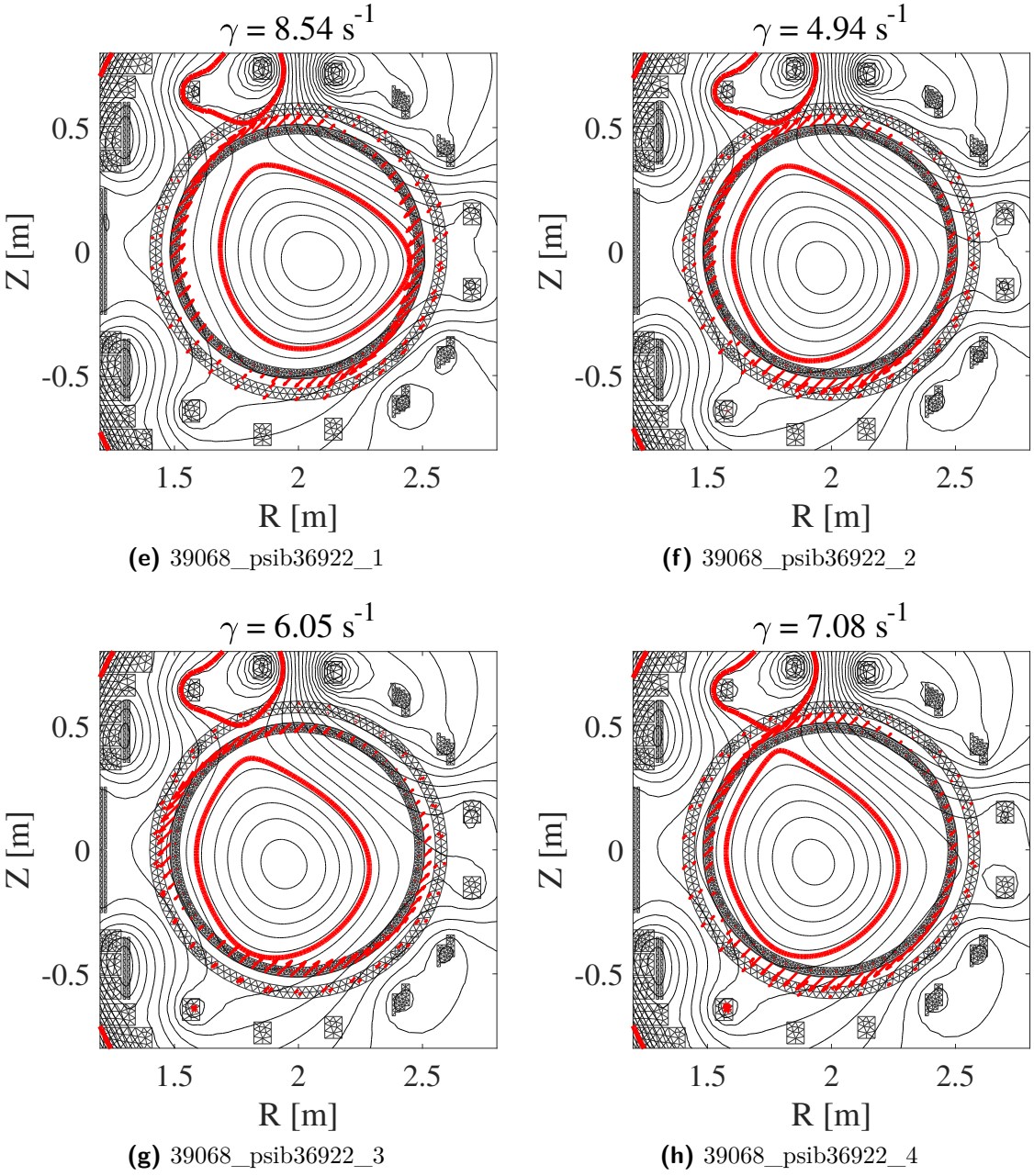

(e) 39068_psib36922_1 **(f)** 39068_psib36922_2

(g) 39068_psib36922_3 **(h)** 39068_psib36922_4

Figure 7.25: CREATE-L poloidal magnetic flux topology of the new class of plasmas obtained as variations on the experimental data equilibria **(e)** - **(h)**

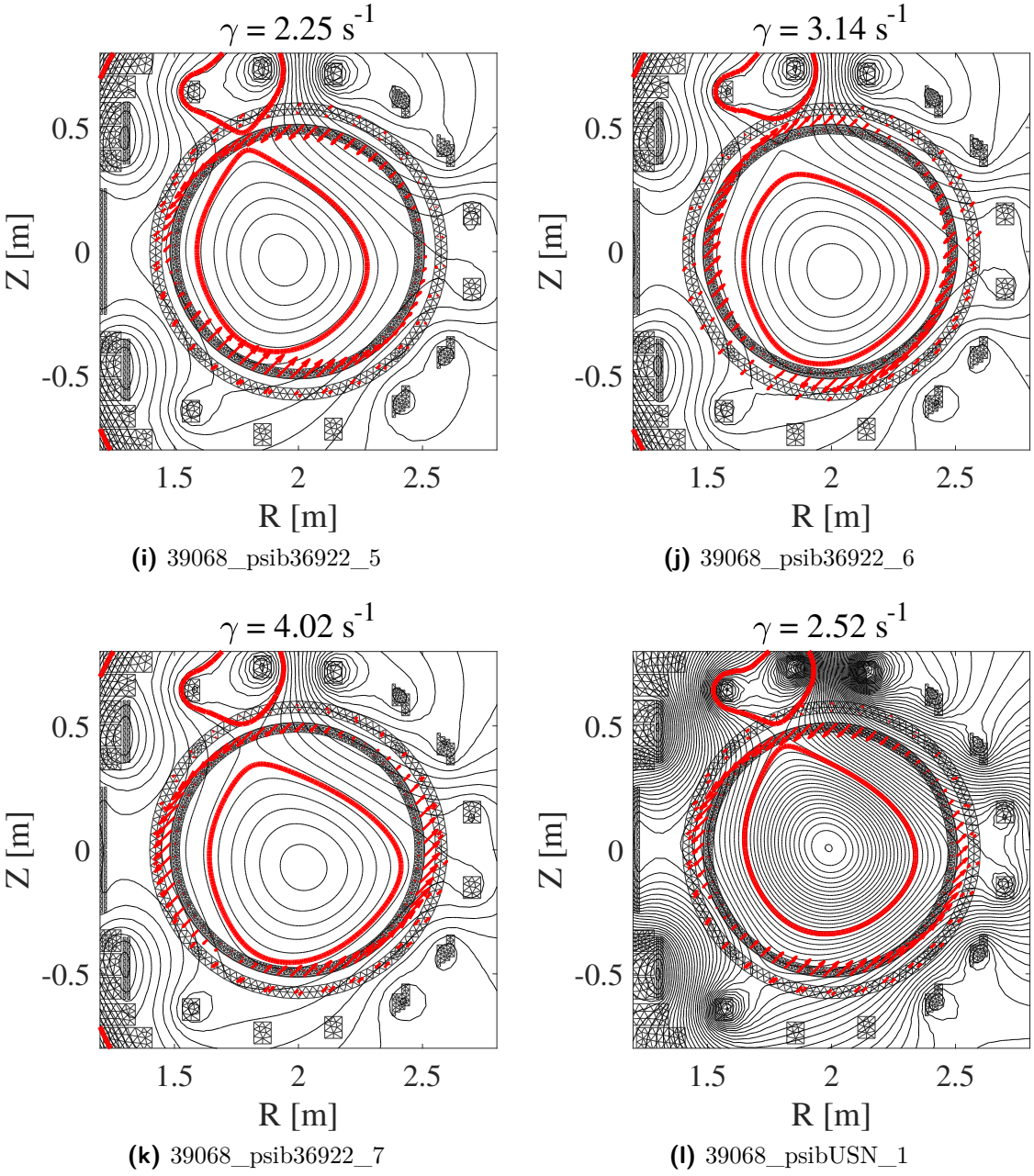

(i) 39068_psib36922_5 **(j)** 39068_psib36922_6

(k) 39068_psib36922_7 **(l)** 39068_psibUSN_1

Figure 7.25: CREATE-L poloidal magnetic flux topology of the new class of plasmas obtained as variations on the experimental data equilibria **(i) - (l)**

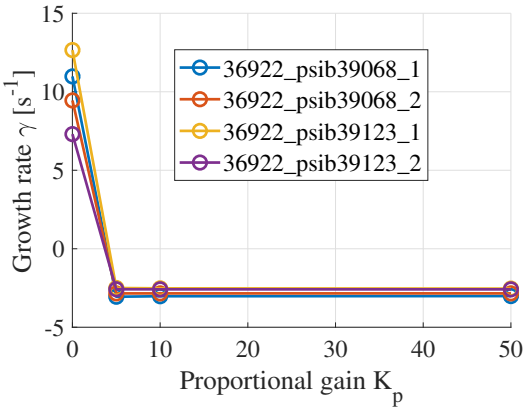

Figure 7.26: Stabilization of the growthrate for numerically generated equilibria characterized by standard shape and increased β_p.

In fact, one of the first hypothesis was that the saturation occurred only in plasmas with increased values of β_p (e.g. #39068, #39122). This hypothesis can be rejected by analyzing the numerically generated intermediate-β and H-mode plasmas, which are characterized by a "standard" USN shape (like the shot # 36922, which does not present saturation) but with increased values of β_p (see the first four rows of Tab. 7.9). These plasmas do not present the saturation of the unstable mode to a positive value, as it can be seen from Fig. 7.26; in fact there is no presence of positive real zeros in their associated SISO models. Therefore, it is not the increased value of β_p that determine the saturation phenomenon. This class of four plasma equilibria is represented in Fig. 7.25 **a** - **d**.

On the other hand, the two numerically generated equilibria that show the saturation (Fig. 7.27) belong to the class of low-β plasmas but they both have a plasma shaping similar to experimental plasmas characterized by the saturation of the un-

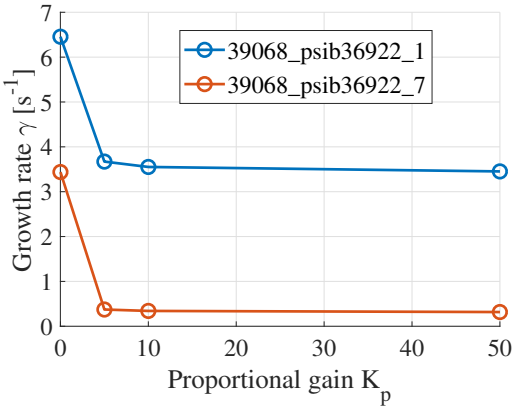

Figure 7.27: Asymptotic independence of the growth rates from gain for the numerically generated equilibria characterized by low-β and strong plasma shape.

stable mode (e.g. #39068). These are collected in the last 8 rows of Tab. 7.9, where it can be recognized the low-β imposed boundary conditions (BC#2 and BC#3), and the one related to have a plasma shape similar to the experimental plasmas characterized by the saturation (e.g. BC#1 #39068). The closed loop analysis shows that only few of these plasma linearized models revealed the presence of a positive real zero able to exhibit a saturation of the vertical instability growth rate as shown in Fig. 7.27; these are just 2 of the whole 12 plasmas in Tab. 7.9, and both belong to the class of low-β plasmas. In particular we are referring to the plasma equilibiria: 39068_*psib*36922_1 and 39068_*psib*36922_7, which are represented in Fig. 7.25 **e** and **k**.

Thus, the phenomenon could be related to the strong plasma shaping that characterizes these experimental plasmas. This is the road that leads us to the application of the statistical hypothesis test to the whole set of plasma linearized models, including the one produced numerically and the one related to experimental data. The results on plasma shape conditions for the occurrence of such behaviour are reported in the next section.

7.7.1 Statistical testing results

As already described in Sect. 6.8, the plasma system can assume two different states, each one corresponding to a different behaviour in terms of vertical stability: the first, in which the vertical instability is stabilized by the effect of the actuators (i.e. state 1); the second, in which the vertical instability is not stabilized by the effect of the actuators (i.e. state 2). The two states are mutually exclusive and correspond to two different behaviours of the growth rate under the action of the actuators: the first is the passage of the growthrate from positive values to negative ones and the second is the asymptotic independence of the growth rates from the proportional gain action. Each of the two states is characterized by mean values of plasma parameters derived through experimental and numerically generated plasmas.

Now we present the results of the statistical hypothesis test of the whole bulk of data which is constituted by 23 CREATE-L plasma models (i.e. 10 referred to experimental shots while 13 numerically generated); 12 of these are in state 1 while the others are in state 2. The statistical hypothesis test adopted is a two tailed t-test of Student for independent groups of collection of data (i.e. *heteroscedastic*); this involves the shape parameters defined previously in Eq. 7.3 - Eq. 7.10 and also other plasma parameters including the global plasma parameters (i.e. β_p, l_i, q_0). Since we are interested in the plasma shape parameters, which are related to our hypothesis on the condition of occurrence of the state 2, in this section we will

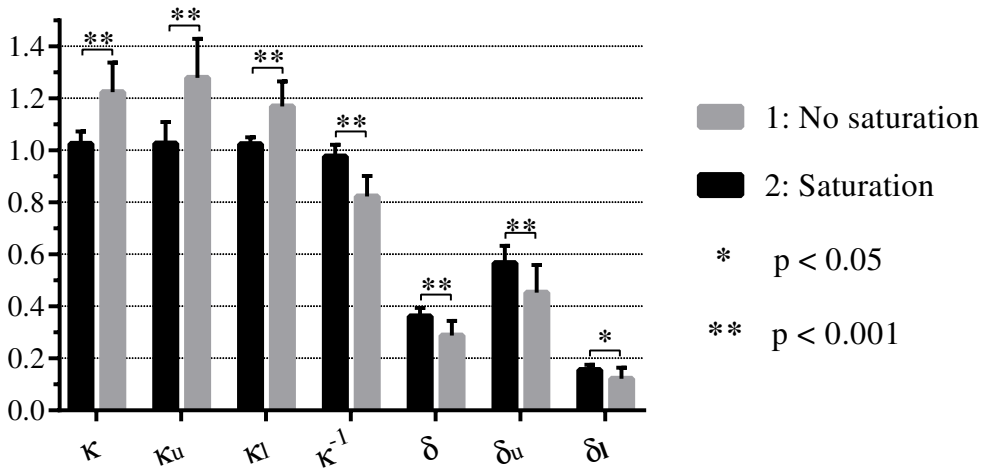

Figure 7.28: Comparison between the mean values of plasma shape parameters in state 1 and state 2

	State 1		State 2		
Parameters	Mean	Std. deviation	Mean	Std. deviation	P value
κ	1.224	0.1144	1.025	0.04808	6.041E-05
κ_u	1.279	0.1497	1.026	0.08361	8.926E-05
κ_l	1.169	0.09625	1.025	0.02541	2.639E-04
κ^{-1}	0.8237	0.07793	0.9771	0.04534	1.629E-05
δ	0.288	0.05697	0.3616	0.03278	1.220E-03
δ_u	0.4536	0.1056	0.5672	0.06614	5.763E-03
δ_l	0.1223	0.04256	0.156	0.01997	2.541E-02

Table 7.10: Statistical hypothesis testing results on plasma shape parameters for both the plasma state 1 and 2

focus our attention only on these. The results on other plasma parameters can be found in Appendix A. It is important to remind that the conditions of validity of the statistical hypothesis test previously defined in Sect. 6.8.2, must be satisfied. Therefore in Appendix A, we show that all the data fulfill the normality distribution condition, as it can be seen from the normality plot in Fig. A.2 - Fig. A.3; moreover, the normality condition has been additionally verified with the D'Agostino-Pearson normality test (Appendix A).

The statistical hypothesis test results are summarized in the diagram in Fig. 7.28 where a significant difference between the mean values of the plasma shape parameters for the two different plasma states are highlighted by extremely low values of the P value (see also Tab. 7.10). This means that there are significant differences in the plasma shape parameters of the plasmas with the saturation behaviour (state 2) with respect to the one without the occurrence of it (state 1). In fact, Fig. 7.28

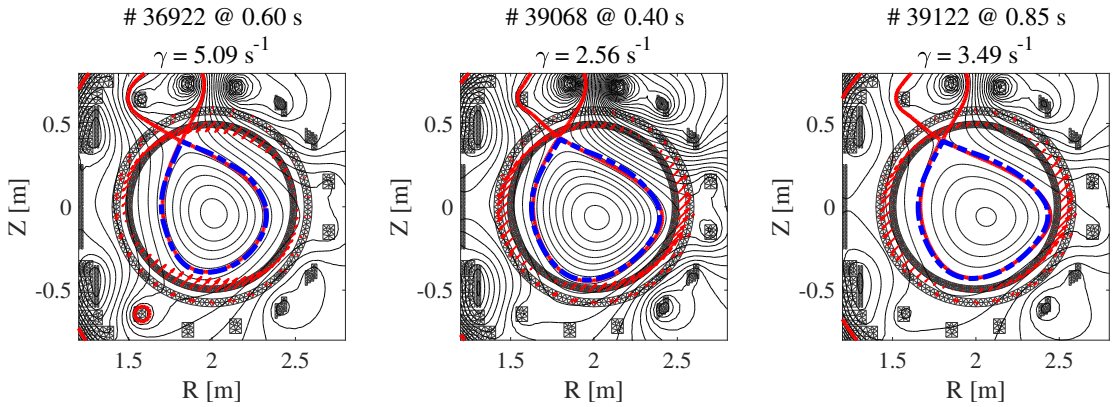

Figure 7.29: # 36922 , # 39068, # 39122 plasma equilibrium computed boundary (red) and reconstructed (blue), with current density pattern on passive conductors (red arrows) associated to unstable mode structure for each experimental shot

shows that the saturation phenomenon occurs in plasmas much more horizontally elongated and with higher positive triangularity. Both the parameters play a role but, while the one related to triangularity is difficult to be explained, the other due to elongation can be interpreted using the results of the vertical stability analysis. In fact, the impression is that the loss of stabilization with a more strong horizontal shaping, see parameter k^{-1} in Fig. 7.28, could be connected with a horizontal $n = 0$ mode destabilization.

A clear difference of current density pattern exists between the plasmas in state 1 (e.g. # 36922, Fig. 7.29) and the plasmas in state 2 (e.g. #39068 and #39122, Fig. 7.29). Reminding that the current density pattern is associated to the mode structure, the plasma shot #36922 has a typical antisymmetric pattern on the upper-lower passive conductors with respect to the equatorial plane, representing a vertical instability [101]; instead, the plasma shots # 39068 and # 39122 are characterized by a pattern spanning the conductors along the poloidal circumference, involving in particular the conductors on the outer and inner side of the equatorial plane [101].

These results can be extended to all the plasmas under analysis since all of them with strong shaping have the same mode structure spanning the conductors in all the poloidal angles. In particular, the outer-inner pattern is typically associated to horizontal displacement events and it can be recognized in all the plasmas presenting the saturation of the unstable mode. Nevertheless, this appears to be just a necessary condition since many numerically generated plasmas, obtained with the solution of the inverse equilibrium problem, do not exhibit the saturation behaviour even with a current density pattern involving also conductors in the outer-inner side of the equatorial plane. The mode structure can be viewed as an additional feature useful

to provide a physical interpretation of the saturation phenomena. Thus, following this line, a superposition of an $n = 0$ horizontal instability with an $n = 0$ vertical instability may be possible in the plasmas of state 2 since they present an evident strong shaping also along the equatorial plane.

In conclusion, the statistical analysis revealed that all the plasma shape parameters are significantly different for the plasmas in state 2 with respect to the one in state 1. Significant differences in elongation, triangularity and horizontal elongation, i.e. the inverse of the elongation, have been verified by extremely low values of the P value, see Tab. 7.10. Therefore, the plasma shape parameters have to be considered as the main set of conditions for the occurrence of the $n = 0$ unstable growth rate saturation, preserving it from being stabilized by the actual proportional control system.

Chapter 8

Conclusions

An iterative procedure for the production of accurate linearized plasma response models has been developed and tested successfully. These new linearized plasma response models of shaped experimental plasmas characterized by different regimes (i.e. from low-β to H-mode) and strong shaping conditions, showed a wide class of aspects for further investigations. The procedure revealed for all of them a peculiar sensitivity on total plasma current, suggesting an experimental uncertainty on the magnetic diagnostics. Regarding the actual vertical position control system, the new models suggest that a global performance improvement could be achieved by further tuning of the control parameters; in fact, the previous adopted assumption of negligible high order dynamics does not hold anymore for these new plasma linearized models. In addition, the controller is not able to achieve vertical stability on the new linearized models, leading to a saturation phenomenon of the growth rate as the gain factor increases. The phenomenon has been mathematically recognized in the presence of a positive real zero in the SISO system derived from these new plasma linearized models. The causes of this saturation have been investigated by extending the available experimental data with new numerically generated equilibria. It has been found that the increased value of β_p has no influence in this phenomenon while the plasma shape parameters have it. The statistical hypothesis test suggests that the conditions of occurrence of the saturation have to be searched in the plasma shaping: a significant difference exists between the mean values of the shape parameters of these two class of plasmas. The saturation phenomenon occurs in plasmas much more horizontally elongated and with higher positive triangularity. These considerations give the impression that a $n = 0$ horizontal instability could be superposed to the $n = 0$ vertical instability, leading the actuators to be ineffective on the growth rate which in fact saturates at the positive real zero value.

Appendix A

Additional results

We present the normality plot for all the plasma parameters of both plasma states involved in the statistical analysis, represented in Fig. A.2 and Fig. A.3. In addition to the normality plots, all the plasma parameters have passed successfully the D'Agostino-Pearson normality test (i.e. "omnibus K2" test). It first computes the skewness and kurtosis to quantify how far the distribution is from Gaussian in terms of asymmetry and shape; then, it calculates how far each of these values differs from the value expected with a Gaussian distribution, and computes a single P value from the sum of these discrepancies. The null hypothesis associated to the test is that all the values were sampled from a population that follows a Gaussian distribution. Thus, if the P value is higher than the traditional 0.05 cut off value, the data successfully pass the normality test. This condition has been fulfilled for all the parameters adopted in the statistical analysis as it can be seen from Tab. A.1. The statistical hypothesis test numerical results are summarized in Tab. A.2, where the mean values and standard deviations of the two sets of plasma data are reported with the computed P value of the statistical hypothesis test of significance. The plasma shape parameters test has been already discussed in Sect. 7.7.1, while the results related to the plasma global parameters are presented in Fig. A.1. It can be seen from both Fig. A.1 and Tab. A.2 that there are no significant differences except for the internal inductance. This is consistent with our remarks, since we argue that these parameters have no role in the occurence of the saturation behaviour. The internal inductance result has to be considered not significant in a more physical sense, since its computation is determined by the plasma current density parametrization adopted in the CREATE-L code. In addition, H-mode plasma conditions are not properly modeled since the code does not allow non-monotonic profiles. Nevertheless, a non-monotonic version of the CREATE-L code exists but the RFX-mod device does not provide experimental plasma current density profiles

(no dedicated diagnostics) or kinetic quantities ones, since the plasma density is too low for the diagnostics to work properly.

	D'agostino-Pearson normality test					
	State 1			State 2		
Parameters	$K2$	P value	Passed?	$K2$	P value	Passed?
κ	0.3469	0.8408	Yes	1.017	0.6015	Yes
κ_u	0.1069	0.9480	Yes	1.708	0.4256	Yes
κ_l	1.41	0.4940	Yes	0.5405	0.7632	Yes
κ^{-1}	0.9832	0.6117	Yes	0.4379	0.8034	Yes
δ	1.768	0.4132	Yes	0.695	0.7065	Yes
δ_u	1.688	0.4300	Yes	0.394	0.8212	Yes
δ_l	0.0129	0.9936	Yes	0.8542	0.6524	Yes
β_p	3.689	0.1581	Yes	0.7919	0.6730	Yes
l_i	5.966	0.0506	Yes	2.308	0.3154	Yes
q_a	1.452	0.4838	Yes	1.894	0.3879	Yes
q_0	5.868	0.0532	Yes	0.8223	0.6629	Yes
γ	1.17	0.5571	Yes	2.781	0.2490	Yes

Table A.1: D'Agostino Pearson normality test results

	State 1		State 2		
Parameters	Mean	Std. deviation	Mean	Std. deviation	P value
β_p	0.3997	0.2657	0.6045	0.2188	5.593E-02
l_i	0.8912	0.06703	0.9686	0.09071	3.276E-02
q_a	3.105	0.3608	3.313	0.2705	1.327E-01
q_0	1.459	0.1838	1.356	0.3196	3.653E-01
γ	6.155	3.42	4.967	2.439	3.462E-01

Table A.2: Statistical hypothesis testing results on other plasma parameters for both the plasma state 1 and 2

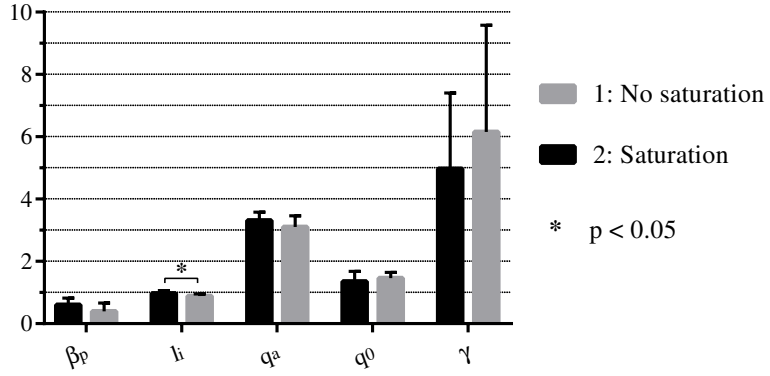

Figure A.1: Comparison between the mean values of plasmas global parameters in state 1 and state 2

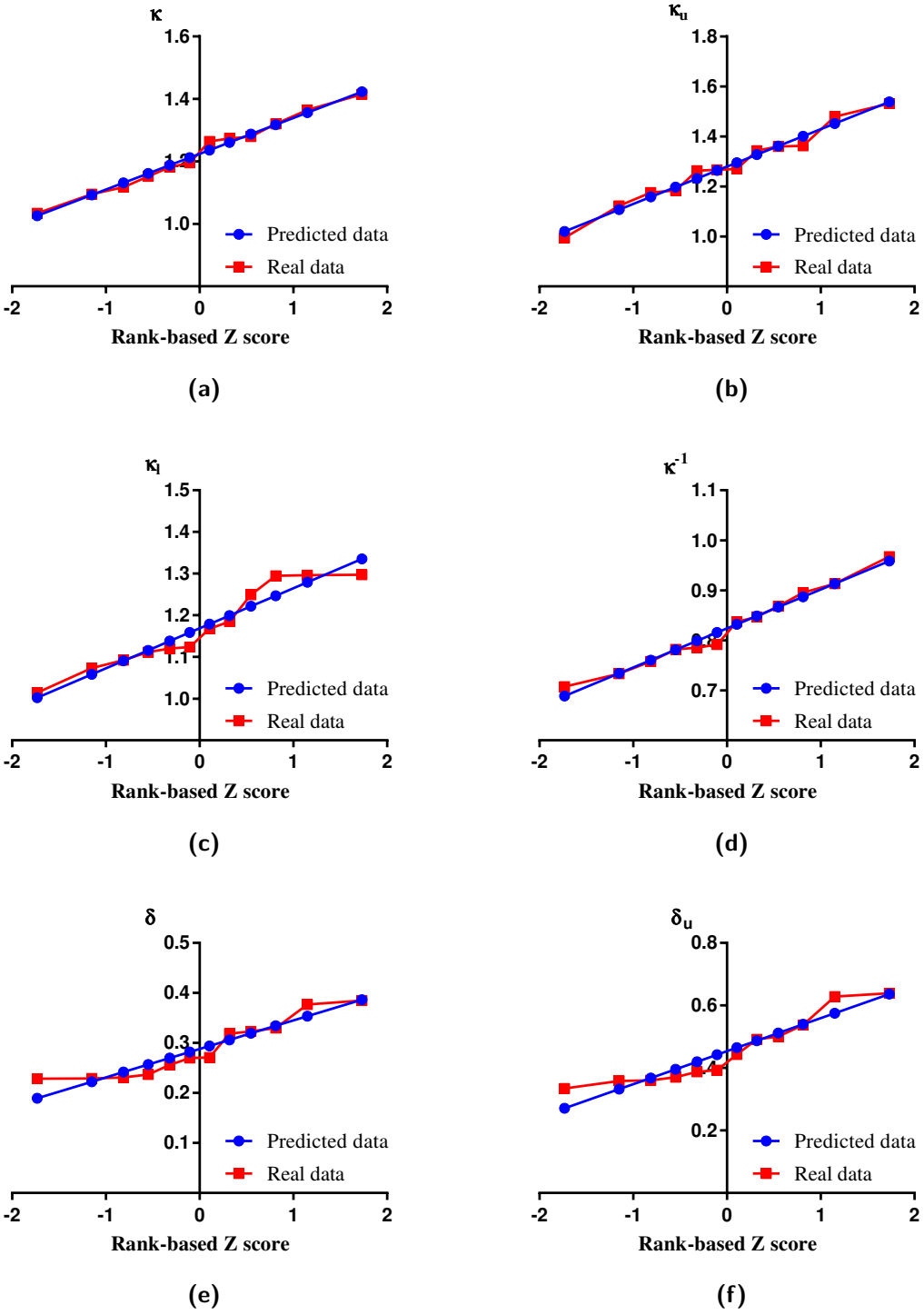

Figure A.2: Normality plot for the state 1 parameters

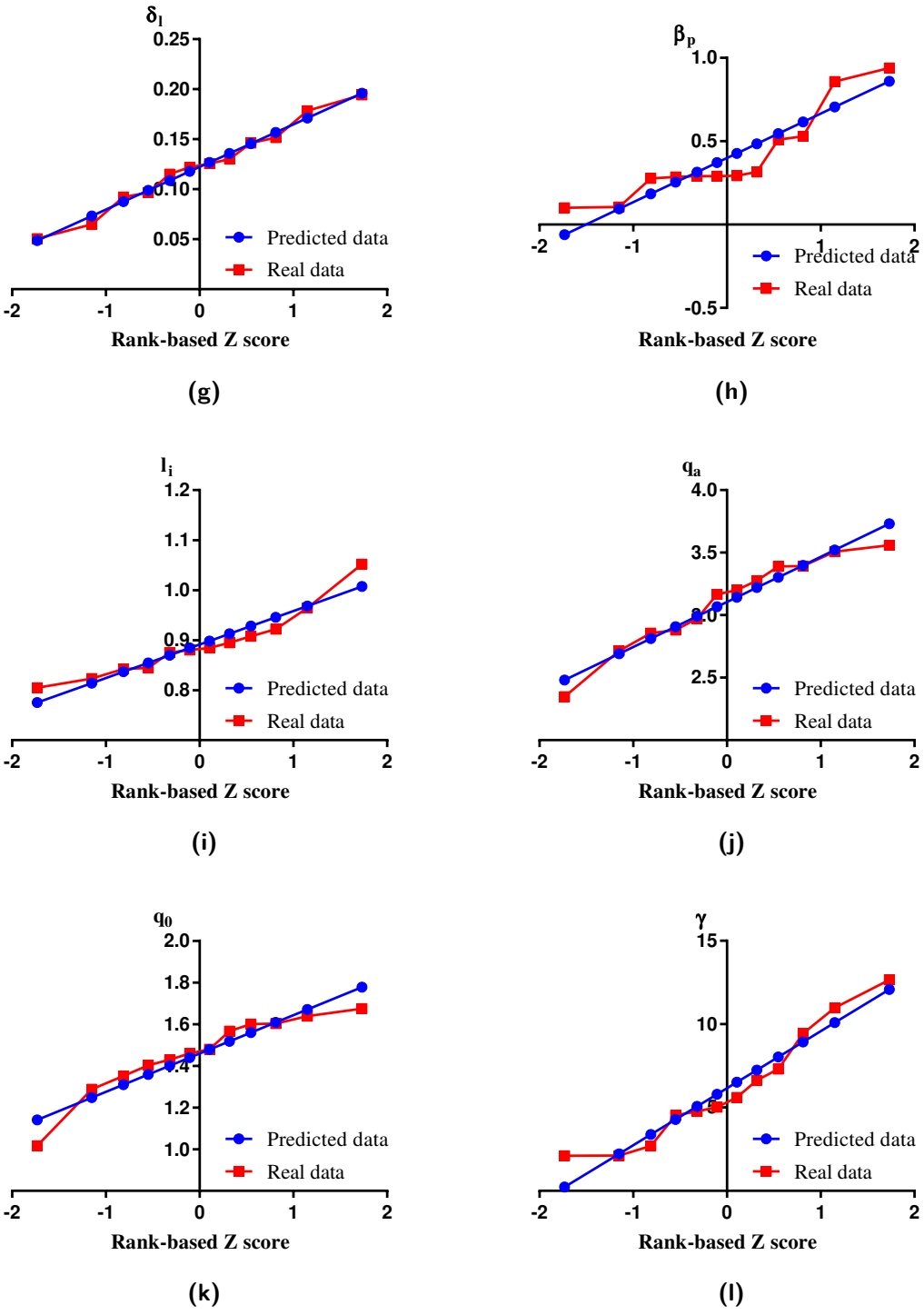

Figure A.2: Normality plot for the state 1 parameters

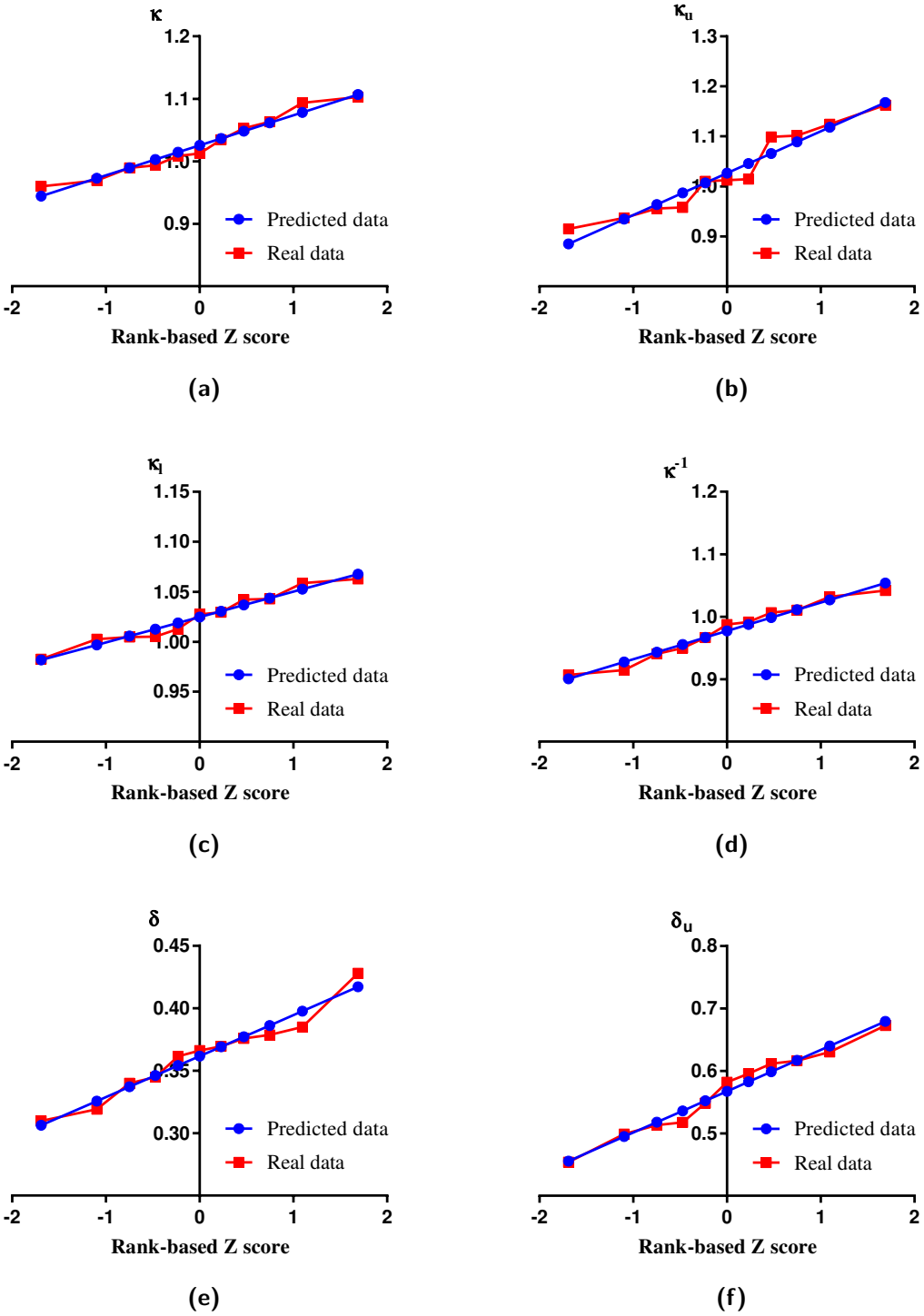

Figure A.3: Normality plot for the state 2 parameters

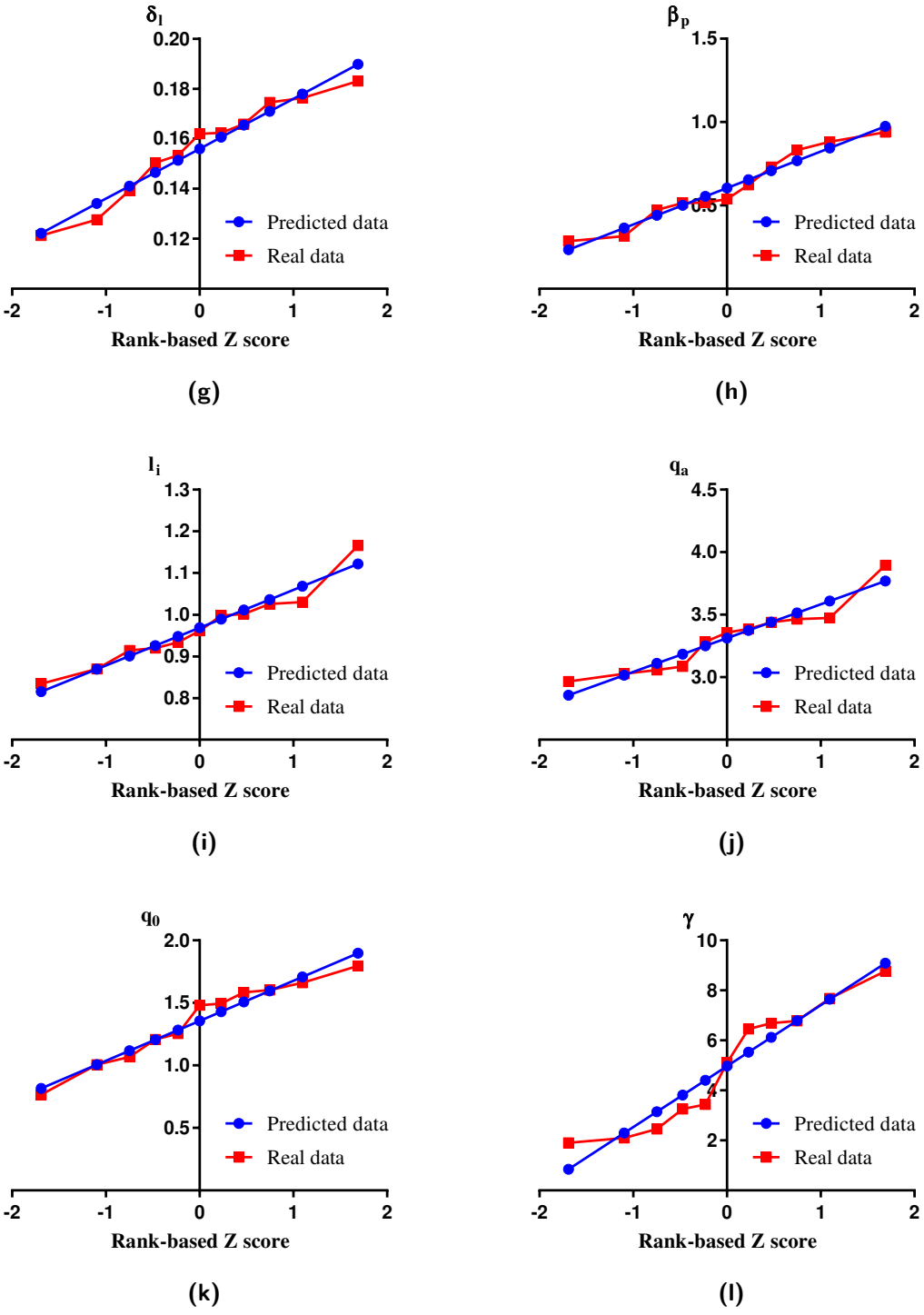

Figure A.3: Normality plot for the state 2 parameters

Bibliography

[1] Marchiori, G., Finotti, C., Kudlacek, O., Villone, F., Zanca, P., Abate, D., Cavazzana, R., Jackson, G., Luce, T., and Marrelli, L., "Design and operation of the RFX-mod plasma shape control system," *Fusion Engineering and Design*, Vol. 108, 2016, pp. 81–91.

[2] Shafranov, V. D., "The initial period in the history of nuclear fusion research at the Kurchatov Institute," *Physics-Uspekhi*, Vol. 44, No. 8, 2001, pp. 835–843.

[3] Gamow, G., "My World Line: An Informal Autobiography. Viking Adult," *New York, USA*, 1970.

[4] Jacquinot, J., "Fifty years in fusion and the way forward," *Nuclear Fusion*, Vol. 50, No. 1, 2009, pp. 014001.

[5] Lawson, J. D., "Some criteria for a power producing thermonuclear reactor," *Proceedings of the Physical Society. Section B*, Vol. 70, No. 1, 1957, pp. 6.

[6] "Oleg Lavrentiev a top secret physicist," *Izvestia Nauka*, 2003.

[7] Smirnov, V., "Tokamak foundation in USSR/Russia 1950–1990," *Nuclear fusion*, Vol. 50, No. 1, 2009, pp. 014003.

[8] Carruthers, R., *Plasma Physics and Controlled Fusion*, Vol. 30, 1988, pp. 11993.

[9] S W Cousins and A A Ware, *Proc. Phys. Soc. London Ser. B*, Vol. 64, No. 159, 1951.

[10] A D Sakharov, I E Tamm, M. A. L., *Plasma Physics and the Problem of Controlled Thermonuclear Reactions*, London Pergamon, 1961.

[11] L Spitzer, D J Grove, W E Johnson, L Tonks, and W F Westendorp, "Problems of the Stellarator as a Useful Power Source," Tech. rep., 1954.

[12] Bohm, D., *The Characteristics of Electrical Discharges in Magnetic Fields*, McGraw Hill - New York, 1949.

[13] Bennett, W. H., *Phys. Rev.*, Vol. 45, No. 890, 1934.

[14] Mukhovatov, V. S., "Tokamaki," *Itogi Nauki i Tekhniki Ser. Fizika Plazmy*, Vol. 1, 1980, pp. 6.

[15] Bernstein, I. B., *Proc. R. Soc. A*, Vol. 244, No. 17, 1958.

[16] Meade, D., *Nuclear Fusion*, Vol. 50, No. 1, 2010, pp. 014004.

[17] Y V Gott, M S Ioffe, and Tel'kovsky], V. G., "Proc. Conf. Plasma Physics and Controlled Nuclear Fusion Research," 1961.

[18] M S Ioffe and R I Sobolev, *J. Nuclear Energy*, Vol. C 7, No. 501, 1965.

[19] E hinnov and A S Bishop, *Phys. Fluids*, Vol. 9, No. 195, 1966.

[20] T Ohkawa and D W Kerst, *Phys. Rev. Lett.*, Vol. 7, No. 41, 1961.

[21] T Ohkawa and et al, *Phys. Rev. Lett.*, Vol. 24, No. 95, 1970.

[22] A Gibson and et al, *Plasma Phys.*, Vol. 9, 1967, pp. 1–12.

[23] Taylor, J. B., *Phys. Rev. Lett.*, Vol. 33, 1974, pp. 1139.

[24] Rose, D. J., *Nucl. Fusion*, Vol. 9, No. 183, 1969.

[25] A Galeev and et al, *Zh. Eksp. Teor. Fiz.*, Vol. 53, No. 348, 1967.

[26] R J Bickerton, J W Connor, and J B Taylor, *Nature Phys. Sci.*, Vol. 229, No. 110, 1971.

[27] H Eubank and et al, *Phys. Rev. Lett.*, Vol. 43, No. 270, 1979.

[28] V M Leonov and et al, *Nucl. Fusion (Suppl.)*, Vol. 1, No. 393, 1980.

[29] A Gondhalekar and et al, *proc. 7th Int. Conf. on Plasma Physics and Controlled Nuclear Fusion Research*, Vol. 1, 1978, pp. 199.

[30] M Murakami and et al, *proc. 9th Int. Conf. on Plasma Physics and Controlled Nuclear Fusion Research*, Vol. 1, 1982, pp. 61.

[31] Goldston, R., *Plasma Phys. Control. Nucl. Fusion*, Vol. 26, 1984, pp. 87.

[32] L A Artsimovich and V D Shafranov, *Soviet Phys. - JETP Lett.*, Vol. 13, No. 72, 1972.

[33] F Wagner and et al, *Phys. Rev. Lett.*, Vol. 49, 1982, pp. 1408.

[34] Basis, I. P., *Nucl. Fusion*, Vol. 39, 1999, pp. 2137.

[35] T. Ohkawa and H G Voorhies, *Phys. Rev. Lett.*, Vol. 22, 1969, pp. 1275.

[36] M Greenwald and et al, *Nucl. Fusion*, Vol. 28, 1988, pp. 2199.

[37] F Troyon and et al, *12th European Conf. on Plasma Physics and Controlled Fusion*, Vol. 26IA, 1984.

[38] M C Zarnstorff and et al, *Phys. Rev. Lett.*, Vol. 60, 1988, pp. 1306.

[39] G L Schmidt and et al, *Proc. 11th Int. Conf. on Plasma Physics and Controlled Nuclear Fusion Research*, Vol. 1, 1986.

[40] Team, J., *Proc. 11th Int. Conf. on Plasma Physics and Controlled Nuclear Fusion Research*, Vol. 1, 1986, pp. 31.

[41] Team, J., *Proc. 12th Int. Conf. on Plasma Physics and Controlled Nuclear Fusion Research*, Vol. 1, 1988, pp. 41.

[42] Goedbloed, J. P. and Poedts, S., *Principles of magnetohydrodynamics: with applications to laboratory and astrophysical plasmas*, Cambridge university press, 2004.

[43] Artsimovich, L., "Research on controlled thermonuclear reactions in the USSR," *Physics-Uspekhi*, Vol. 1, No. 2, 1958, pp. 191–207.

[44] Albanese, R. and Villone, F., "The linearized CREATE-L plasma response model for the control of current, position and shape in tokamaks," *Nuclear Fusion*, Vol. 38, No. 5, 1998, pp. 723.

[45] Ariola, M. and Pironti, A., *Magnetic control of tokamak plasmas*, Vol. 187, Springer, 2008.

[46] Igochine, V. et al., *Active control of magneto-hydrodynamic instabilities in hot plasmas*, Springer, 2015.

[47] Freidberg, J. P., *Ideal MHD*, Cambridge University Press, 2014.

[48] Kruskal, M. and Tuck, J., "The instability of a pinched fluid with a longitudinal magnetic field," *Proceedings of the Royal Society of London A: Mathematical, Physical and Engineering Sciences*, Vol. 245, The Royal Society, 1958, pp. 222–237.

[49] Shafranov, V., "The stability of a cylindrical gaseous conductor in a magnetic field," *Atomic Energy*, Vol. 1, No. 5, 1956, pp. 709–713.

[50] Goedbloed, J. P., Keppens, R., and Poedts, S., *Advanced magnetohydrodynamics: with applications to laboratory and astrophysical plasmas*, Cambridge University Press, 2010.

[51] Shafranov, V., "Plasma equilibrium in a magnetic field," *Reviews of Plasma Physics*, Vol. 2, 1966, pp. 103.

[52] Mukhovatov, V. and Shafranov, V., "Plasma equilibrium in a tokamak," *Nuclear Fusion*, Vol. 11, No. 6, 1971, pp. 605.

[53] Luxon, J. and Brown, B., "Magnetic analysis of non-circular cross-section tokamaks," *Nuclear Fusion*, Vol. 22, No. 6, 1982, pp. 813.

[54] Albanese, R., Coccorese, E., and Rubinacci, G., "Plasma modelling for the control of vertical instabilities in tokamaks," *Nuclear Fusion*, Vol. 29, No. 6, 1989, pp. 1013.

[55] Villone, F., Barbato, L., Mastrostefano, S., and Ventre, S., "Coupling of nonlinear axisymmetric plasma evolution with three-dimensional volumetric conductors," *Plasma Physics and Controlled Fusion*, Vol. 55, No. 9, 2013, pp. 095008.

[56] Portone, A., Villone, F., Liu, Y., Albanese, R., and Rubinacci, G., "Linearly perturbed MHD equilibria and 3D eddy current coupling via the control surface method," *Plasma Physics and Controlled Fusion*, Vol. 50, No. 8, 2008, pp. 085004.

[57] Villone, F., Chiariello, A., Mastrostefano, S., Pironti, A., and Ventre, S., "GPU-accelerated analysis of vertical instabilities in ITER including three-dimensional volumetric conducting structures," *Plasma Physics and Controlled Fusion*, Vol. 54, No. 8, 2012, pp. 085003.

[58] Lackner, K., "Computation of ideal MHD equilibria," *Computer Physics Communications*, Vol. 12, No. 1, 1976, pp. 33–44.

[59] Takeda, T. and Tokuda, S., "Computation of MHD equilibrium of tokamak plasma," *Journal of computational physics*, Vol. 93, No. 1, 1991, pp. 1–107.

[60] Blum, J., "Numerical simulation and optimal control in plasma physics," 1989.

[61] Jardin, S., *Computational methods in plasma physics*, CRC Press, 2010.

[62] Jardin, S. and Larrabee, D., "Feedback stabilization of rigid axisymmetric modes in tokamaks," *Nuclear fusion*, Vol. 22, No. 8, 1982, pp. 1095.

[63] Martin, P., Adamek, J., Agostinetti, P., Agostini, M., Alfier, A., Angioni, C., Antoni, V., Apolloni, L., Auriemma, F., Barana, O., et al., "Overview of the RFX fusion science program," *Nuclear Fusion*, Vol. 51, No. 9, 2011, pp. 094023.

[64] Stella, A., Guarnieri, M., Bellina, F., Campostrini, P., Chitarin, G., Trevisan, F., and Zaccaria, P., "The RFX magnet system," *Fusion Engineering and Design*, Vol. 25, No. 4, 1995, pp. 373–399.

[65] Gnesotto, F., Guarnieri, M., and Santagiustina, A., "Dynamic control of the equilibrium field configuration in RFX," *Fusion engineering. Vol. 1*, 1983.

[66] Peruzzo, S., Agostini, M., Agostinetti, P., Bernardi, M., Bettini, P., Bolzonella, T., Canton, A., Carraro, L., Cavazzana, R., Dal Bello, S., et al., "Design concepts of machine upgrades for the RFX-mod experiment," *Fusion Engineering and Design*, 2017.

[67] Cavinato, M. and Marchiori, G., "Design of the new RFX equilibrium active control system," *Fusion engineering and design*, Vol. 74, No. 1, 2005, pp. 567–572.

[68] Zanca, P., Marrelli, L., Paccagnella, R., Soppelsa, A., Baruzzo, M., Bolzonella, T., Marchiori, G., Martin, P., and Piovesan, P., "Feedback control model of the mÂ =Â 2, nÂ =Â 1 resistive wall mode in a circular plasma," *Plasma Physics and Controlled Fusion*, Vol. 54, No. 9, 2012, pp. 094004.

[69] Zanca, P., Marchiori, G., Marrelli, L., Piron, L., et al., "Advanced feedback control of magnetohydrodynamic instabilities: comparison of compensation techniques for radial sensors," *Plasma Physics and Controlled Fusion*, Vol. 54, No. 12, 2012, pp. 124018.

[70] Spolaore, M., Cavazzana, R., Marrelli, L., Carraro, L., Franz, P., Spagnolo, S., Zaniol, B., Zuin, M., Cordaro, L., Dal Bello, S., et al., "H-mode achievement and edge features in RFX-mod tokamak operation," *Nuclear Fusion*, 2017.

[71] Kudlacek, O., Zanca, P., Finotti, C., Marchiori, G., Cavazzana, R., and Marrelli, L., "Real time measurement of plasma macroscopic parameters on RFX-mod using a limited set of sensors," *Physics of Plasmas*, Vol. 22, No. 10, 2015, pp. 102503.

[72] Taylor, R., Brown, M., Fried, B., Grote, H., Liberati, J., Morales, G., Pribyl, P., Darrow, D., and Ono, M., "H-mode behavior induced by cross-field currents in a tokamak," *Physical review letters*, Vol. 63, No. 21, 1989, pp. 2365.

[73] Kikuchi, M., Lackner, K., and Tran, M. Q., "Fusion physics," 2012.

[74] Martin, Y., "Threshold power and energy confinement for ITER," *Proc. 16th IAEA International Conference on Fusion Energy*, Vol. 2, 1997.

[75] Albanese, R. and Rubinacci, G., "Finite element methods for the solution of 3D eddy current problems," *Advances in Imaging and Electron Physics*, Vol. 102, 1997, pp. 1–86.

[76] Albanese, R. and Rubinacci, G., "Integral formulation for 3D eddy-current computation using edge elements," *IEE Proceedings A (Physical Science, Measurement and Instrumentation, Management and Education, Reviews)*, Vol. 135, No. 7, 1988, pp. 457–462.

[77] Barabaschi, P., "The MAXFEA code," *Plasma Control Technical Meeting*, 1993.

[78] Crotinger, J. A., LoDestro, L., Pearlstein, L. D., Tarditi, A., Casper, T., and Hooper, E. B., "Corsica: A comprehensive simulation of toroidal magnetic-fusion devices. final report to the ldrd program," Tech. rep., Lawrence Livermore National Lab., CA (United States), 1997.

[79] Abate, D., Marchiori, G., and Villone, F., "Non-linear evolution of RFX-mod tokamak equilibria during LH transition including 3D wall effects," *43rd EPS Conference on Plasma Physics*, 4 - 8 July 2016.

[80] Kuznetsov, A., Shchepetov, S., and Sychugov, D. Y., "Is it possible to extract information on the plasma pressure profile from magnetic measurements in stellarators?" *Nuclear fusion*, Vol. 34, No. 2, 1994, pp. 185.

[81] Shchepetov, S. and Kuznetsov, A., "Equilibrium magnetic fields and currents in a nonaxisymmetric torus: external magnetic fields in stellarators," *Nuclear fusion*, Vol. 36, No. 9, 1996, pp. 1097.

[82] Kuznetsov, A. and Shchepetov, S., "Method of magnetic analysis for stellarator equilibria," *Nuclear fusion*, Vol. 37, No. 3, 1997, pp. 371.

[83] Gutarev, Y. V., Kuznetsov, Y. K., Pashnev, V., and Ponomarnenko, N., "Fiz. Plazmy, 14, 286–291 (1988)," *English translation: Sov. J. Plasma Phys*, Vol. 14, 1988, pp. 164–167.

[84] Pashnev, V. and Nemov, V., "Use of magnetic diagnostics in stellarators," *Nuclear fusion*, Vol. 33, No. 3, 1993, pp. 435.

[85] Pustovitov, V., "Magnetic diagnostics: General principles and the problem of reconstruction of plasma current and pressure profiles in toroidal systems," *Nuclear fusion*, Vol. 41, No. 6, 2001, pp. 721.

[86] Vladimirov, V. S., "Equations of mathematical physics," *Moscow Izdatel Nauka*, 1976.

[87] Stratton, J., *Electromagnetic Theory, McGrow-Hill, New-York*, London, 1941.

[88] Tewari, A., "Modern control design," *NY: John Wiley & sons*, 2002.

[89] Kailath, T., *Linear systems*, Vol. 156, Prentice-Hall Englewood Cliffs, NJ, 1980.

[90] Abate, D., "Multiobjective optimization techniques for the solution of free-boundary plasma equilibrium inverse problems," 2014.

[91] Luce, T., "An analytic functional form for characterization and generation of axisymmetric plasma boundaries," *Plasma Physics and Controlled Fusion*, Vol. 55, No. 9, 2013, pp. 095009.

[92] Tonti, E., *The mathematical structure of classical and relativistic physics*, Springer, 2013.

[93] Williams, G., "Overdetermined systems of linear equations," *The American Mathematical Monthly*, Vol. 97, No. 6, 1990, pp. 511–513.

[94] Marcuzzi, F., "Analisi dei dati mediante modelli matematici," *CLEUP sc Padova*, 2011.

[95] Student, "The probable error of a mean," *Biometrika*, 1908, pp. 1–25.

[96] Quinn, G. P. and Keough, M. J., *Experimental design and data analysis for biologists*, Cambridge University Press, 2002.

[97] Marchiori, G. et al., "41st EPS Conference on Plasma Physics," *Berlin, June 2014, paper P5*, Vol. 40, 2014.

[98] Abate, D. et al., "42nd EPS Conference on Plasma Physics," *Lisbon, June 2015, paper P4.159*, 2015.

[99] Dorf, R. C. and Bishop, R. H., *Modern control systems*, Pearson, 2011.

[100] Abate, D., Marchiori, G., and Villone, F., "43rd EPS Conference on Plasma Physics," *Leuven, July 2016, paper P5.013*, 2016.

[101] Abate, D., Marchiori, G., and Villone, F., "44th EPS Conference on Plasma Physics," *Belfast, June 2017, paper P4.137*, 2017.